Theses and Dissertations--Chemistry                                     Chemistry

2023

# DEVELOPMENT OF AN EFFECTIVE Au:Pd BIMETALLIC HETEROGENEOUS CATALYST FOR OXIDATIVE LIGNIN DEPOLYMERIZATION TO LOW MOLECULAR WEIGHT AROMATICS

Gayan P. Karunasinghe
*University of Kentucky*, gpkarunasinghe@gmail.com
Author ORCID Identifier:
 https://orcid.org/0000-0002-1535-558X
Digital Object Identifier: https://doi.org/10.13023/etd.2023/474

Right click to open a feedback form in a new tab to let us know how this document benefits you.

STUDENT AGREEMENT:

I represent that my thesis or dissertation and abstract are my original work. Proper attribution has been given to all outside sources. I understand that I am solely responsible for obtaining any needed copyright permissions. I have obtained needed written permission statement(s) from the owner(s) of each third-party copyrighted matter to be included in my work, allowing electronic distribution (if such use is not permitted by the fair use doctrine) which will be submitted to UKnowledge as Additional File.

I hereby grant to The University of Kentucky and its agents the irrevocable, non-exclusive, and royalty-free license to archive and make accessible my work in whole or in part in all forms of media, now or hereafter known. I agree that the document mentioned above may be made available immediately for worldwide access unless an embargo applies.

I retain all other ownership rights to the copyright of my work. I also retain the right to use in future works (such as articles or books) all or part of my work. I understand that I am free to register the copyright to my work.

REVIEW, APPROVAL AND ACCEPTANCE

The document mentioned above has been reviewed and accepted by the student's advisor, on behalf of the advisory committee, and by the Director of Graduate Studies (DGS), on behalf of the program; we verify that this is the final, approved version of the student's thesis including all changes required by the advisory committee. The undersigned agree to abide by the statements above.

<div align="right">

Gayan P. Karunasinghe, Student

Prof. Mark Meier, Major Professor

Prof. Kenneth Graham, Director of Graduate Studies

</div>

DEVELOPMENT OF AN EFFECTIVE Au:Pd BIMETALLIC HETEROGENEOUS
CATALYST FOR OXIDATIVE LIGNIN DEPOLYMERIZATION TO LOW
MOLECULAR WEIGHT AROMATICS

_____

DISSERTATION
_____

A dissertation submitted in partial fulfillment of the
requirements for the degree of Doctor of Philosophy in the
College of Arts and Sciences
at the University of Kentucky

By

Gayan Karunasinghe

Lexington, Kentucky

Co- Directors: Dr. Mark Meier, Professor of Chemistry and

Dr. Mark Crocker, Professor of Chemistry

Lexington, Kentucky

2023

ABSTRACT OF DISSERTATION

DEVELOPMENT OF AN EFFECTIVE Au:Pd BIMETALLIC HETEROGENEOUS
CATALYST FOR OXIDATIVE LIGNIN DEPOLYMERIZATION TO LOW
MOLECULAR WEIGHT AROMATICS

The principal concept behind biorefining involves the transformation of lignocellulosic biomass into valuable products and energy resources. Historically, biorefinery strategies for lignocellulosic biomass have primarily focused on improving the conversion of cellulose into ethanol, often neglecting the underutilized lignin component. Lignin consists of phenolic subunits, from which it follows that value-added products can be obtained from lignin depolymerization. Unfortunately, lignin utilization is particularly challenging due to its high structural irregularity and recalcitrance. The goal of this study was to develop an AuPd/Li-Al layered double hydroxide (LDH) bimetallic catalyst for efficient lignin depolymerization, resulting in the production of high-value aromatic compounds. The structural complexity of lignin renders the study of individual reactions in lignin difficult. Therefore, model compounds were used to evaluate catalyst performance. Initially, we prepared AuPd bimetallic nanoparticles with varying molar ratios supported on a basic Li-Al LDH using a sol-immobilization method. Subsequently, we characterized the synthesized catalysts and evaluated them in aerobic oxidation reactions of 1-phenylethanol and simple benzylic alcohols at atmospheric pressure to identify the most effective catalyst configurations. Those catalysts demonstrating promising performance were further examined in the aerobic oxidation of lignin model dimers containing $\beta$-O-4 linkages. Remarkably, these model compounds underwent sequential oxidation, ultimately leading to the cleavage of the $\beta$-O-4 bonds. Subsequently, we evaluated the catalysts in the oxidative deconstruction of $\gamma$-valerolactone (GVL) extracted from maple lignin at 120 °C, again using $O_2$ as the oxidant. These results highlight the potential of the AuPd/Li–Al LDH catalyst system as an eco-friendly approach for lignin depolymerization under mild conditions, offering a promising avenue for valorizing lignin in biorefining processes.

KEYWORDS: Lignin, Biomass, Depolymerization, Bimetallic, Catalyst

Gayan Karunasinghe
*(Name of Student)*

12/15/2023
Date

DEVELOPMENT OF AN EFFECTIVE Au:Pd BIMETALLIC HETEROGENEOUS
CATALYST FOR OXIDATIVE LIGNIN DEPOLYMERIZATION TO LOW
MOLECULAR WEIGHT AROMATICS


By
Gayan Karunasinghe


| | |
|---|---|
| Prof. Mark Meier | |
| Co-Director of Dissertation | |
| Prof. Mark Crocker | |
| Co-Director of Dissertation | |
| Prof. Kenneth Graham | |
| Director of Graduate Studies | |
| 12/15/2023 | |
| Date | |

## DEDICATION

To *my mom, wife, daughter, and brothers*

ACKNOWLEDGMENTS

I extend my heartfelt gratitude to the individuals who have been involved in the completion of my PhD dissertation. I owe a debt of gratitude to my advisors, Prof. Mark Crocker, and Prof. Mark Meier, for their unwavering guidance, support, and profound expertise. Their mentorship has been the cornerstone of my academic journey, shaping me as a researcher and scholar. I am profoundly thankful for the opportunities they provided me to grow and contribute to our field. I would like to express my sincere appreciation to Prof. Eduardo Santillan Jimenez, Prof. Doo Young Kim, and Prof. Jian Shi for their critical evaluation, constructive feedback, and their persistent encouragement for me to best in my research. Their insights and contributions have been invaluable in shaping this dissertation.

I want to express my special thanks to Dr. Dali Qian, Dr. Robert Pace, Tonya Morgan, and Shelley Hopps for their indispensable roles in analyzing samples and assisting with data analysis. Their dedication and hard work were instrumental in bringing this research to fruition. I also want to thank my teaching supervisors, Dr. Manjari Patwardhan, Dr. April French, and Dr. Allison Soult for their guidance in refining my teaching skills. Their mentorship has been helpful in my growth as an effective educator. Also, I could not succeed as a TA without the support of all Instructional Lab Coordinator, specially, Mr. Michael Kevin Woodrum, and all TAs and lead TAs.

Furthermore, I would like to extend my appreciation to the department managers in the Department of Chemistry, Mr. Daniel Whittaker, Ms. Meagan Looney, Ms. Jenny Owen, Ms. Christine Smothers, Ms. Emily Cheathan, and Ms. Christine Morgan. Their efforts in fostering a welcoming and supportive atmosphere over the past few years have been instrumental in my academic journey.

This work could have never been completed without the support of my amazing family, my wife, Udari Kodithuwakku, and daughter, Dahamdi Karunasinghe, who have

been the bedrock of my strength and resilience. Your unwavering support and understanding have been my driving force. Also, my mother and siblings, your love and encouragement have been the foundation of my life.

I extend my appreciation to my lab colleagues, Julia Parker and Great Umenweke, for their friendship, insightful discussions, and shared experiences. Their collaboration and friendship have been essential to the progress of my work.

This academic journey has been challenging, marked by countless hours of hard work and unwavering determination. I have been fortunate to be surrounded by a network of support, encouragement, and inspiration. Each of you has played a unique and significant role in my success, and I eagerly anticipate carrying the invaluable lessons learned during this journey into the future.

TABLE OF CONTENTS

LIST OF FIGURES

# LIST OF SCHEMES

# CHAPTER 1.    INTRODUCTION AND BACKGROUND

## 1.1    Lignocellulosic Biomass

Escalation of the global energy demand is the main driving force in the search for sustainable supplies of energy and renewable materials.[1] Globally, fossil fuels are mostly consumed to fulfil these energy requirements. However, the utilization of fossil fuels has huge impacts on the Earth due to the emission of greenhouse gases. Today, the main goal is replacement of fossil resources by sustainable alternatives that should be at least renewable, $CO_2$-neutral, widely available, and should not compete with food production. Among available options, lignocellulosic biomass is one of the resources that meets these essential criteria. Lignocellulosic biomass consists of three highly functional biopolymers, namely:[1-3]

I.  Cellulose (~30–50 wt%): a polymer made up of glucose, a six-carbon sugar.
II.  Hemicellulose (~20–35 wt%): a polymer made up of two five-carbon sugars (D-xylose, L- arabinose), and three six-carbon sugars (D-glucose, D-galactose, D-mannose).
III.  Lignin (~15–30 wt%).

Hexose sugars such as glucose are produced from cellulose hydrolysis, glucose mainly being used to produce ethanol, which can be mixed with gasoline for use in fuel motor vehicles.[4, 5] Hemicellulose has been applied as plant gum for thickeners, adhesives, protective colloids, emulsifiers, and stabilizers.[6] Recently, a very promising application is as a biodegradable oxygen barrier film.[4, 7] Hemicellulose is typically depolymerized to form xylose, which is then fermented into ethanol or organic acids. Xylose can also be converted to furfural, which is a solvent used for lubricants, coatings, adhesives, furan resins, etc. It can also be used as a starting material to produce nylon, plastics, motor oil, etc.[4]

The primary products used in the above applications are derived from the carbohydrate fraction. This leaves the lignin part of the biomass, which is mostly regarded as a low-value by-product or a low-grade fuel. Lignin is often present in greater amounts than the hemicellulose component, and occasionally even exceeds the cellulose fraction. Typically, it contains 40% of the energy stored within the biomass, has a high heating value, and contains a variety of aromatic sub-units.[8, 9] Commercial applications of lignin are still limited and are primarily associated with the use of lignosulphonates in concrete admixtures, animal feed pellets and road binders. Lignin is also extensively used as a low-grade fuel to produce heat in pulping processes.

## 1.2    The Structure of Lignin

Lignin is deposited in the cell wall during cell differentiation, and it is necessary for both the structural integrity and stiffness of plants. Lignin is hydrophobic and helps in the transport of water and nutrients throughout the plant, as well as helping to protect plants from pathogens and insects.[1, 2, 10] This amorphous polymer is the only renewable source of aromatic compounds. Unfortunately, lignin is highly underutilized because the structure of lignin is highly recalcitrant and irregular (unlike cellulose). Moreover, its structure varies depending on the source and isolation method.[11]

Lignin is composed of three p-hydroxycinnamyl alcohol monomers (monolignols), namely, p-coumaryl, coniferyl, and sinapyl alcohol (see Figure 1), which are polymerized through an enzyme-mediated dehydrogenation polymerization pathway and bind together by C−C and ether bonds.[2, 12, 13] In the polymer, these monolignols are present as p-hydroxyphenyl (H), guaiacyl (G), and syringyl (S) units (Figure 1). The ratios of these monomers differ based on plant species; normally, grasses contain all three monomers, while coniferyl alcohol is prominent in softwoods (coniferous tree-based), and both coniferyl and sinapyl alcohol are prominent in deciduous tree-based hardwoods.[2]

2
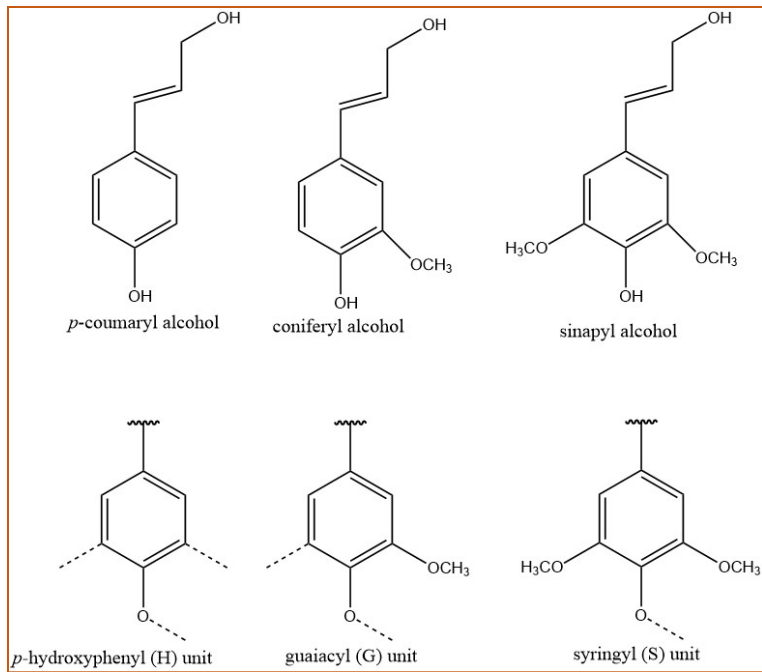
Figure 1.1· Predominant monomers and generic lignin units

In general, oligomer−oligomer or oligomer−monomer couplings are prominent during the lignification process, while fewer linkages are formed from monomer−monomer coupling reactions.[2, 12] During lignification, the most common linkage formed is the alkyl aryl ether unit, which is known as the β-O-4 ether linkage. This linkage typically accounts for ~50% of bonds formed during polymerization and it has the lowest bond dissociation energy when compared with other linkages.[14, 15] Therefore, most studies related to lignin depolymerization target the β-O-4 linkage. Other major linkages formed during lignification are β-5, β-1, β-β and 4-O-5 (Figure 2), which, with the exception of the 4-O-5 linkage, result from carbon−carbon bond formation, and which are difficult to degrade using traditional processing methods.[2, 16]
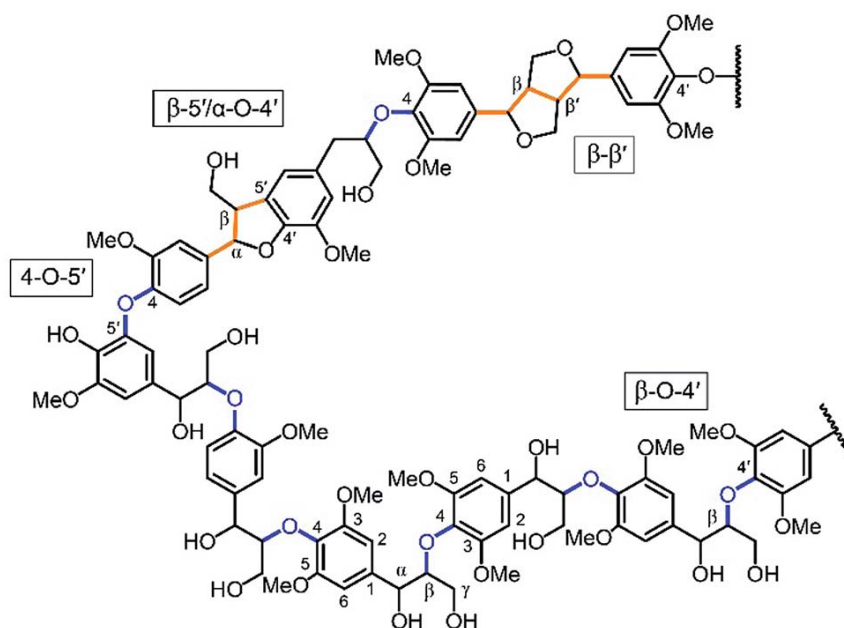
Figure 1.2 Representation of the structure of a hardwood lignin by Luterbacher et al[17]

There are three primary categories of biomass, namely, softwood, hardwood, and grasses. Softwood typically has the highest lignin content, comprising approximately 30% of the biomass. Hardwoods contain the next highest percentage of lignin, ranging from about 20% to 25%.[16, 18-20] Softwood is mainly composed of guaiacyl units (G), accounting for approximately 90% of all units, whereas hardwoods have roughly equal amounts of guaiacyl and syringyl units (G and S).[21] Major monolignol inter-unit linkage distributions in the lignin of softwoods and hardwoods are shown in Table 1.1.[22, 23]

Table 1.1 Percent of inter-unit linkages in softwood and hardwood lignin

| Linkage type | Softwood | Hardwood |
| --- | --- | --- |
| β-O-4 | 45-50% | 60% |
| β-5 | 9-12% | 3-10% |
| β-1 | 2-9% | 1-7% |
| β-β | 2-6% | 3% |
| 5-5 | 9-25% | 0-9% |
| α-O-4 | 6-8% | 6-8% |
| 4-O-5 | 0-7% | 0-9% |
| Others | 13% | 5% |

## 1.3    Isolation of Lignin

Lignin isolation from lignocellulosic feedstock can be accomplished through various methods that involve mechanical, chemical, and biochemical processes.[24-26] These methods aim to separate lignin from the other components of lignocellulosic biomass, such as cellulose and hemicellulose. Treatment conditions, such as temperature, pressure, solvent type, and pH range, play a crucial role in lignin isolation and processing. These factors can significantly impact the efficiency of lignin extraction, the quality of the isolated lignin, and its subsequent applications.[22, 27] The various methods used to isolate or process lignocellulosic biomass inevitably result in modifications to the native structure of lignin. Consequently, the structural variability observed in industrial lignin is further amplified, posing challenges for the development of processes that utilize lignin as a feedstock for chemical production. Depending on the specific isolation methods and conditions employed, lignin derived from the same biomass feedstock can exhibit

5

significant differences in terms of structure and properties.[27] This adds to the existing complications associated with the natural variation in lignin's structure. Lignin is primarily produced from pretreatments employed in the pulp and paper industries, such as the kraft or lignosulfonate processes.[28] Furthermore, novel feedstocks customized for biorefineries also provide additional sources of lignin such as organosolv.[22] Each pretreatment method possesses distinct advantages and disadvantages, which will be further explored below.

The kraft pulping process is the primary method used for lignin isolation, accounting for more than 90% of all chemical pulps produced.[1, 29, 30] Its widespread adoption can be attributed to three key factors: (i) the production of high-quality pulp, (ii) the efficient recovery of pulping chemicals within the process, and (iii) the self-sufficiency in meeting energy requirements.[1, 31, 32] The white pulping process involves the utilization of high pH levels and significant quantities of aqueous sodium hydroxide and sodium sulfide (white liquor) at temperatures ranging from 150 °C-180 °C for approximately 2 hours in a stepwise process.[33] During this process, biomass undergoes delignification, and the lignin undergoes both degradation and condensation reactions.[30, 31] The notable feature of this liquor is the inclusion of hydrosulfide ions ($HS^-$), which improve the selectivity of pulping by promoting delignification and lignin depolymerization while minimizing carbohydrate solubilization.[34] The harsh alkaline environment in kraft lignin processing offers benefits such as efficient delignification, improved lignin solubility, effective recovery of pulping chemicals, and self-sufficiency in energy, making it a widely adopted method in the pulp and paper industry.[31] While kraft lignin processing presents several advantages, it also carries certain drawbacks. The method relies on significant quantities of chemicals, such as sodium hydroxide and sodium sulfide, which can have adverse environmental effects.[35] Additionally, the lignin obtained through kraft lignin processing typically exhibits relatively lower purity compared to alternative isolation methods.[36] The presence of impurities and residual chemicals from the pulping process may limit its direct suitability for certain high-value applications, necessitating additional purification steps to

attain the desired lignin quality. Furthermore, the kraft process lacks precise control over the resulting lignin structure. The rigorous conditions and complex chemical reactions involved in kraft pulping can induce notable modifications and variations in the lignin structure. This structural variability may pose challenges when utilizing kraft lignin as a feedstock for applications that demand a more customized and consistent lignin structure.[36]

The sulfite pulping treatment yielding lignosulfonates is the second most significant chemical pulping process. It is typically carried out within a pH range of 2 to 12, depending on the chosen cation. In alkaline sulfite pulping, calcium or magnesium sulfites (or bisulfite) are employed.[1, 2, 30] The incorporation of sulfonate groups into the resulting products enhances their water solubility.[22, 33] Unlike the kraft process, sulfite pulping does not extensively degrade lignin, resulting in a larger molecular weight of the isolated lignin.[22, 30, 33] However, the lignin obtained from sulfite pulping is heavily contaminated with sulfur, which presents challenges for lignin utilization in chemical and material production.[30] This contamination necessitates increased purification requirements, reduces product quality, and may poison many upgrading catalysts.

The organosolv pulping process has emerged as an alternative to kraft or sulfite pulping, aiming to produce a more suitable lignin by-product for co-utilization and functioning more as a biomass fractionation process. This method involves the use of various organic solvent mixtures, such as 1,4-dioxane, ethanol, acetone, methanol, or organic acids like acetic or formic acid, at elevated temperatures.[33, 37] Instead of reacting lignin with inorganic chemicals, the organosolv pulping relies on organic solvents to dissolve lignin. This faster process allows for the recovery of dissolved lignin in a less degraded and modified form compared to kraft and sulfite pulping. The main advantages of the organosolv process are the formation of distinct streams of cellulose, hemicelluloses, and lignin, enabling the valorization of all components of lignocellulosic biomass.[37] Additionally, the process is generally considered environmentally friendly as it avoids the use of sulfides and the harsh conditions associated with kraft or lignosulfonate processes.

7

Consequently, organosolv lignin typically exhibits low sulfur content and higher purity compared to lignin obtained from other methods. However, it should be noted that the recovery of materials, such as solvents, has not been fully optimized in the organosolv process, resulting in relatively higher costs compared to other methods.

Apart from the methods discussed in detail above, there are several other techniques for isolating lignin including pyrolysis, steam explosion, the use of ionic liquids, organocatalysis and acid hydrolysis.[38]

## 1.4     Sources of Aromatic Compounds

Even though lignin is an attractive renewable resource for the production of bio-based materials, fuels, and chemicals, efficient catalytic depolymerization is required to produce chemicals and fuel additives from lignin because of its structural complexity. In this field, reductive and oxidative depolymerization methods play an important role in the production of chemicals from lignin.

In the chemical industry, benzene, toluene and xylene (BTX) exhibit a significant range of application and represent 60% of all aromatics on the market with a price range of 700-1,500 USD/MT.[39] The main source of BTX is petroleum, although related compounds are available from the reductive depolymerization of lignin. The reductive depolymerization pathway can also provide other major products such as phenol, cyclohexane, etc., although the highest product value does not exceed 2,500 USD/MT.[39, 40]

On the other hand, the oxidative depolymerization process can be used to produce oxygenated aromatic monomers from lignin. These products have relatively high market value. A few well-known lignin products are vanillin, vanillic acid, syringic acid, and aromatic aldehydes. Vanillin is the main component of natural vanilla extract. It is used as a flavoring agent in foods, beverages, pharmaceuticals, and in the fragrance industry.[16, 18]

8

The main source of vanillin in the market is crude oil (representing approximately 80% of the total supply) while only 20% of vanillin in the market is produced from lignin.[41] Vanillin from lignin and crude oil have similar prices of 12,000 USD/MT, which is approximately 10 times higher than the BTX market value. Syringic acid is even more valuable, with prices ranging between 20,000-100,000 USD/MT if obtained from lignin.[39]

In addition to aromatic compounds, lignin may be a source of additional products such as carbon fiber, activated carbons, resins, and hydrogels.[39, 42] The development of an economically viable lignin valorization route would require much more research to optimize the technology. However, the ability of lignin to be a source of aromatic compounds suggests that it has great potential to become an essential feedstock in the future chemical industry, with lignin oxidation affording products with the highest values.

## 1.5    Oxidative Lignin Depolymerization

In early work, oxidative lignin depolymerization was conducted using oxidants alone or with simple transition metal ions such as $Cu^{2+}$, $Mn^{3+}$, $Co^{2+}$, and $Zr^{4+}$.[43-45] Composite metal oxide and metal oxide catalysts containing Co, Fe, Cu, Mn (e.g., CuO, $MnO_2$) were subsequently applied to improve the extent of lignin depolymerization.[43, 46, 47] Other than inorganic metal catalysts, homogeneous organic catalysts and organometallics have been used to effect the oxidative depolymerization of lignin. There are three types of oxidative depolymerization based on lignin structural degradation: (1) oxidative cleavage of inter-units linkages (primarily those present in α-O-4 and β-O-4 linkages), (2) oxidative modification of lignin side-chains, mainly involving the conversion of primary and secondary OH groups in the lignin polymer (Cα-OH and Cγ-OH groups found in lignin β-O-4 linkages are primary targets), and (3) the oxidation of aromatic rings and ring cleavage, which are typically associated with one-electron mechanisms.

**1.5.1 Oxidative cleavage of lignin inter-unit linkages**

In most plant lignin, phenylpropanoid units are connected by C-O (ether) and C-C linkages, however, the C-O linkages are predominant, corresponding to α-O-4 and β-O-4 linkages.[22, 31] Oxidative cleavage of these linkages provides oxygenated functional groups (aldehyde, ketones etc.) in the products. Boosting the number of oxygenated functional groups on the lignin macromolecule enhances the distance between π-π stacked rings, therefore weakening the inter-unit forces holding lignin together and facilitating dissociation of the lignin macromolecule.[43]

Because of the high abundance of β-O-4 inter-unit linkage in many types of lignin, significant effort has been targeted at developing an efficient method to cleave the β-O-4 linkages. However, the C-O linkages are more labile than C-C bonds. Therefore, cleavage of a significant portion of C-O linkages occurs during biomass pretreatments and lignin isolation processes.[48] On the other hand, selectively cleaving C-C linkages has always been a challenge. Therefore, high temperatures and high loadings of expensive noble-metal catalysts (e.g., ruthenium, palladium, platinum) are frequently essential to the cleavage of C-C linkages and these severe conditions help to promote the condensation of lignin fragments.[31]

Oxidative reagents ($O_2$, $H_2O_2$ and $O_3$) cleave mainly C-O linkages as well as a small portion of the C-C linkages with different mechanisms during lignin treatment.[11, 49, 50] However, the reactivity of the oxidant can be enhanced by adding transition metal ions to this process (e.g., $Ce^{4+}$, $Fe^{3+}$, $Mn^{3+}$, $Co^{2+}$, and $Zr^{4+}$), consequently facilitating the cleavage of β-O-4 linkages and pinacol-type C–C linkages.[51, 52] Recently, the use of metal oxides was investigated for lignin oxidation. Hedges et al. produced monomeric phenolics from lignin isolated from Amazon wood by treatment with alkaline cupric oxide (CuO).[53] Kurek et al. treated lignin with a $MnO_2$/oxalate system to oxidize it based on the mechanism of lignin degradation by wood rot fungi which secretes oxalate that can weaken the cell wall.

However, the system showed very limited reactivity toward cleaving lignin inter-unit linkages because the $MnO_2$/oxalate system is unable to directly support oxidation of nonphenolic structures; therefore, only the free phenolic hydroxyl groups in the spruce wood lignin could be modified.[47, 54]

Based on the high reduction potential of photocatalysts ($TiO_2$ and ZnO), photocatalysts were utilized to degrade lignin into organic compounds (phenolic aldehydes, ketones, and acids) at a fast rate using $O_2$ as a primary oxidant.[55, 56] The pH of the photocatalytic reaction medium also has a significant effect on product yield. Ma et al. reported that a large amount of OH radicals were produced when the photocatalytic process was operated under acidic conditions. However, the reaction rate decays over time as a result of side reactions and accumulation of negative species on the catalyst surface. According to their study, the addition of Pt to the $TiO_2$ support (Pt/$TiO_2$) avoids the accumulation of the negative species, consequently resulting in better photocatalytic activity.[57]

Vanadium group (V, Nb, Ta) catalysts for oxidative lignin depolymerization have been examined by both Hanson and Toste.[58, 59] Hanson et al. conducted oxidative depolymerization of lignin and reported the use of vanadium-based organometallic complexes to catalyze cleavage of C-O and C-C bonds in lignin model compounds that contain pinacol structures.[60] In pinacol structures, the C-H bond next to the alcohol group can break and oxidize to produce the corresponding alcohol and aldehyde. The vanadium catalyzed oxidative lignin depolymerization reactions are typically conducted at relatively mild temperatures (~373 K) under ambient pressure. Both reaction rates and the product slate are strongly dependent on the type of solvent used in the catalytic system.[43] Catalysts based on niobium (Nb) also have a unique catalytic property for oxidative lignin depolymerization. Ma et al. has recently discovered that $Nb_2O_5$, in conjunction with peracetic acid, can rapidly solubilize and depolymerize lignin. Also, the catalyst was shown to be effective at breaking both C-O and C-C linkages.[43]

## 1.5.2 Oxidative modification of lignin side-chains

Most of the phenylpropane units in lignin are connected through the side chain. One of the main challenges of using metal and metal oxide catalysts for oxidative lignin depolymerization is the inability to completely cleave all inter-unit linkages. One approach is to use a catalyst to modify the electron density of the lignin side-chains. This modification may interrupt the integrity of the lignin macromolecule, consequently enhancing the lignin depolymerization efficiency. By introducing new oxygen-containing groups into the lignin side-chains, $\pi$-$\pi$ interactions among phenylpropane units are weakened.

Ketones are the main products of the oxidative modification of the lignin side-chains. These products are generated during lignin degradation by organocatalysts, which is a large family of organic compounds typically containing nitrogen, sulfur, or phosphorus as active sites to enhance chemical reactions. For instance, 2,2,6,6-tetramethylpiperidine-1-oxyl (TEMPO) is used as a catalyst for the oxidation of primary and secondary alcohols in lignin into aldehydes and ketones, respectively.[61] Stahl et al. verified alcohol conversion in the lignin structure using the dimeric model compound 3-(3,4-dimethoxyphenyl)-2-(2-methoxyphenoxy)-2-propenol.[62] The oxidized lignin model compounds can be further cleaved following other treatments, such as alkaline treatment to remove ether linkages.

Metal-organic frameworks (MOFs) is another group of catalysts that can oxidize lignin. Kustov and co-workers reported the oxidation of vanillyl alcohol to vanillin by 5% Pt on $[Zn_4O(BDC)_3]$ MOF.[43] Similar reactions were also studied by Sun et al. using gold supported on MIL-101 MOF.[63] They observed the conversion of primary and secondary benzylic alcohols to aldehydes and ketones, respectively, with high yield and selectivity. The reactivity and pore structure of the MOF can be tuned by changing the organic linker component. These modifications are beneficial for performing specific catalytic functions because the highly porous structure can provide a large accessible catalytic surface.

Zakzeski et al. studied the oxidation of veratryl alcohol and vanillyl alcohol to their respective aldehydes in toluene at 150 °C under 0.5 MPa $O_2$ after 4 hours by using a cobalt-based MOF.[64] The reaction stopped upon formation of the carbonyl group without the formation of further degradation products. The unique catalytic activity of cobalt-based MOF to oxidize olefinic structures to epoxides was demonstrated by using cinnamyl alcohol as a model compound.

## 1.6    Objectives and Dissertation Outlines

Lignin, the second most abundant terrestrial polymer after cellulose, represents a substantial portion of lignocellulosic materials, accounting for approximately 15-30% of their dry weight. However, it is currently considered a waste material due to the complexity and heterogeneity of lignin, which makes its controlled depolymerization a challenging task. This dissertation aims to address this issue by pursuing four primary research objectives, ultimately enhancing our understanding of lignin depolymerization through oxidative processes over heterogeneous catalysts. The central objective of this research is to develop an efficient bimetallic heterogeneous catalyst for the oxidative depolymerization of lignin into low molecular weight aromatic compounds. To attain this main goal, the dissertation is organized around the following four specific objectives: (1) Preparation of heterogeneous catalysts using the sol-immobilization method to support AuPd bimetallic nanoparticles on Li-Al layered double hydroxide (LDH) with varying molar ratios; (2) Application of the synthesized catalysts in the oxidation of 1-phenyl ethanol to identify the most effective catalysts for oxidizing simple benzylic alcohols and β-O-4 lignin linkage model dimers; (3) Assessment of the capacity of the most effective catalysts identified in objective (2) to depolymerize lignin by applying them to the oxidative depolymerization of γ-valerolactone extracted maple lignin, with a focus on generating low molecular weight aromatic compounds and (4) Investigation of potential

pathways and transformations in oxidative lignin depolymerization processes by employing the most effective catalysts identified in objective 2 to oxidize β-O-4, β-1, and β-β model compounds.

To fulfill these research objectives, this dissertation is structured into six chapters.

Chapter 1: This chapter offers an introduction to the motivation behind lignin utilization, elucidates the structure of lignin, explores common methods of lignin isolation, and highlights the advantages of oxidative lignin depolymerization over reductive techniques. It also introduces the primary objectives of the dissertation.

Chapter 2: This chapter provides an extensive overview of the applications of bimetallic catalysts based on Au. It encompasses catalyst preparation, characterization, and their application in oxidation reactions.

Chapter 3: In this section, catalysts employing layered double hydroxide (LDH)-supported AuPd bimetallic nanoparticles with varying Au:Pd molar ratios are investigated. It includes catalyst characterization and an examination of catalyst performance with simple benzylic alcohols and β-O-4 linked lignin model compounds under mild conditions.

Chapter 4: Building upon the findings of Chapter 3, this chapter explores the oxidative depolymerization of lignin extracted from γ-valerolactone, particularly focusing on maple lignin.

Chapter 5: This chapter delves into the specific products obtained from the oxidation of β-O-4, β-1, and β-β lignin model compounds, shedding light on the pathways and transformations involved in oxidative lignin depolymerization.

Chapter 6: The concluding chapter offers a summary of the dissertation's findings and presents a general conclusion. It also outlines potential directions for future research in this field.

# CHAPTER 2.    GOLD-BASED BIMETALLIC CATALYSTS AND THEIR APPLICATIONS

## 2.1    Introduction

Heterogeneous catalysts play a vital role in the modern world, and are involved in the manufacture of over 80% of the world's chemical products, according to the most recent data available.[65, 66] In 2019, the global catalyst market surged to a value of USD 33.9 billion and was predicted to maintain consistent growth, with an expected annual growth rate of 4.4% from 2020 to 2027.[65] Catalysts play a pivotal role in enhancing the efficiency and selectivity of various chemical transformations, impacting fields ranging from energy production and environmental remediation to pharmaceutical synthesis and materials science.

Over the past decades, there has been a growing fascination with metal nanoparticles (NPs) owing to their distinctive properties, which make them of interest for a wide array of applications in the field of catalysis.[67] Generally, metal nanoparticles are inherently unstable and show low catalytic activity due to aggregation, agglomeration, and even precipitation out of solution. Therefore, metal nanoparticles must usually be supported on solid surfaces.[68-70] During a catalytic reaction, supports can play either direct or indirect roles, such as providing specific defect sites and stabilizing metastable particles.[69] Supports can provide additional functionalities to the supported metal catalyst such as acidity or basicity and may transfer electrons between the metal particles and support.[71, 72] All these factors have a significant impact on the catalytic properties of supported metal catalysts.[72]

In late 1970s, supported gold (Au) was demonstrated as the catalyst of choice for producing vinyl chloride monomer via the acetylene hydrochlorination reaction.[69, 73] Later, oxide-supported Au nanoparticles were introduced as an effective catalyst for low-temperature oxidations of $H_2$ and CO.[74] Since then, Au catalysis has become the subject of

attention from both the academic and industrial research communities. Over the past decade, supported Au nanoparticles have gained recognition as effective and discriminating catalysts in the oxidation and hydrogenation of a wide range of organic compounds, notably hydrocarbons with diverse structures and organic compounds containing oxygen, such as alcohols and carbohydrates.[75]

Bimetallic catalysts, which consist of two different metal components, are widely used in catalysis to enhance catalytic activity, selectivity, and stability compared to single-metal catalysts due to the synergistic effect of the two metals.[76] Among them, Au-based bimetallic catalysts are of particular interest due to the unique properties of Au, such as its high catalytic activity for various reactions and its ability to stabilize other metal nanoparticles such as Pd, Pt, Ag, Cu etc.[77, 78] It was observed that several factors significantly influence the activity, selectivity, and stability of Au bimetallic catalysts. These factors include the choice of the second metal, the ratio of gold to the second metal, the structural configuration of the bimetallic catalysts, as well as the size and shape of the nanoparticles. The synthesis method of these bimetallic catalysts plays a crucial role in determining the nanoparticles' size and shape, which subsequently impacts their performance.[79, 80]

The objective of this review is to make a substantial and critical contribution to the field by shedding light on the advancements related to supported Au-based bimetallic catalysts. This review will encompass several key aspects, including the structural characteristics of these catalysts, the various methods employed in their preparation, characterization techniques and their most notable and impactful applications.

## 2.2    Types of Nanoalloys

According to Ferrando et al.[81] various factors play a role in determining the type of mixing that takes place between two metals. These factors include the relative strength of

the bond between the two different metals, the surface energy of the metals, the relative sizes of their atoms, and the presence of stabilizers.[81, 82] In certain cases, the strength of the bond between two different metals in an alloy can be stronger than that of the individual pure metals. When this occurs, it tends to promote a thorough mixing of the metals within the alloy. Conversely, if the bond strength is weaker, it can lead to the segregation of the two metals. Additionally, when considering the surface properties of the two metals, the metal with the lower surface energy tends to migrate to the alloy's surface, forming an outer layer or shell. Conversely, smaller atoms have a preference for occupying the inner core of the alloy. Furthermore, the phenomenon of charge transfer plays a role. Electron transfer from less electronegative elements to more electronegative ones encourages the mixing of elements within the alloy.[81] Based on these factors, nanoalloys can be categorized into four main types based on the way metal atoms mix together. These categories are core-shell nanoalloys, subcluster nanoalloys, mixed nanoalloys, and multi-shell nanoalloys, as illustrated in Figure 2.1.[82]
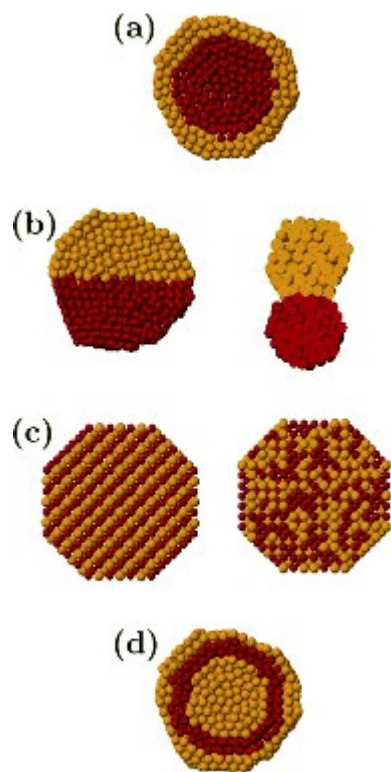
Figure 2.1 Representative mixing patterns of core–shell (a), subcluster segregated (b), mixed (c), multi-shell nanoalloys (d). Reprinted with permission of chemical society reviews: Sankar, M.; Dimitratos, N.; Miedziak, P. J.; Wells, P. P.; Kiely, C. J.; Hutchings, G. J., Designing bimetallic catalysts for a green and sustainable future. *Chemical Society Reviews* **2012,** *41* (24), 8099-8139.[82]

In the case of core-shell alloys, one metal forms a shell around the core made of another metal. Zhang et al.[83] introduced a novel method for synthesizing FeAu core-shell nanoparticles. This method involves using wet chemistry to create an Fe core, followed using 532 nm laser irradiation on the Fe nanoparticles and Au powder in a liquid medium to deposit an Au shell. Finally, the nanoparticles are purified through sequential magnetic extraction and acid washing.

Mixed nanoalloys can have either a random atomic structure or an ordered atomic structure at the interface. Random atomic structures are more common than ordered ones,

especially in Au-based bimetallic nanoalloys like PdAu and MnAu.[84, 85] Subcluster-segregated nanoalloys are composed of two distinct types of atoms organized into subclusters. These subclusters can either interact at a mixed interface, or they may be connected by only a limited number of bonds within a bimetallic catalyst. In theory, such a mixing pattern is feasible, but there are no reported instances of this specific pattern in the existing literature.[81] Lastly, multi-shell nanoalloys can occur when there are multiple concentric shells covering the core metal, resulting in an "onion-like" structure. Some recent reports in the literature have described bimetallic and trimetallic alloys with this type of structure.[86, 87]

## 2.3    Synthesis of Au-Based Bimetallic Catalyst Systems

Bimetallic nanoalloys can be synthesized using various techniques, such as gas-phase synthesis, solution-based methods, or deposition onto a solid support matrix.[82, 88] Some of these approaches for making bimetallic nanoalloys resemble those used for producing monometallic nanoparticles.[89] However, due to the inclusion of a second metal component, the complexity in fabricating these materials increases significantly. The choice of preparation method depends on the specific catalytic application, desired composition, and structure of the bimetallic catalyst. It is essential to consider factors such as catalytic activity, stability, and cost when selecting a method for synthesizing bimetallic catalysts.[90] Additionally, characterizing the catalyst's structure and composition is crucial to understanding its catalytic performance. Hence, it is imperative to carefully select the synthesis method to achieve the desired structure and properties for the bimetallic material in question.[82] In this section we will summarize the most used synthesis methods to preparation of supported gold based bimetallic catalysts.

### 2.3.1 Sol-immobilization method (SIM)

The Sol-Immobilization Method (SIM) represents a widely adopted technique for fabricating bimetallic catalysts, including those incorporating gold (Au) and another metal.[91] This method requires the synthesis of bimetallic nanoparticles within a solution, followed by their subsequent immobilization or deposition onto a solid support material. SIM offers precise control over key catalyst attributes, such as composition, size, and structure.[82, 92] To implement this approach, the first step is to dissolve metal precursors of both metals in an appropriate solvent. It is essential to ensure that the ratios of the two metal precursors align with the desired bimetallic composition, a decision guided by the specific catalytic application and the targeted properties. Next, to prevent the aggregation of nanoparticles and ensure their stability, a suitable stabilizing agent, such as surfactants or polymers, is introduced into the solution.[92, 93] Subsequently, a reducing agent, such as $NaBH_4$, is gradually added to the mixed metal precursor solution. This step initiates the reduction process, ultimately leading to the formation of bimetallic nanoparticles within the solution. Following the generation of the nanoparticle-containing sol, the colloid is immobilized by addition of an appropriate support material under vigorous stirring. Careful washing of the immobilized nanoparticles, using an appropriate solvent, is crucial to remove any excess or unbound nanoparticles and stabilizers. Finally, the solid support with the immobilized bimetallic nanoparticles is dried under controlled conditions to obtain the final supported bimetallic catalyst.

The design and utilization of Au–Pd catalysts have been thoroughly investigated by the Hutchings group.[71] They synthesized Mg–Al mixed metal oxide supported Au–Pd catalysts using the sol-immobilization method. The resulting materials exhibited excellent catalytic activity for alcohol oxidation. Notably, when using this Mg–Al mixed metal

support, alloying Pd with Au resulted in an increase in both activity and selectivity for benzyl alcohol oxidation to benzaldehyde, and, moreover, an improved resistance to catalyst deactivation compared with the monometallic Pd and Au catalysts.

Bianchi et al.[94] conducted the synthesis of carbon-supported bimetallic catalysts featuring gold (Au) as the primary metal and either palladium (Pd) or platinum (Pt) as the second metal. This was achieved using the sol-immobilization method, with a specified Au to other metal (Pt or Pd) ratio of 1:1. However, they introduced variations into the sol-immobilization method through three different approaches. In the first method, the procedure started with the dissolution of the Au precursor in deionized water (DI $H_2O$). Subsequently, a stabilizer (polyvinyl alcohol, PVA) and reducing agent ($NaBH_4$) were added to generate Au(0) nanoparticles. Following this, a stock aqueous solution of the other metal (either Pd or Pt) and a $NaBH_4$ solution were introduced into the solution containing the Au nanoparticles. In the second method, the catalyst preparation process was reversed compared to the first method. Initially, Pd or Pt nanoparticles were prepared, and then the Au precursor and reducing agent were added. The third approach involved adding a stock aqueous solution (Pd or Pt) and PVA solution to a solution of Au in DI $H_2O$. Subsequently, the metals were reduced using a $NaBH_4$ solution. Ultimately, these three distinct bimetallic nanoparticles were individually deposited onto the carbon (C) support.

In the context of catalyst characterization techniques, the researchers employed X-ray Photoelectron Spectroscopy (XPS) to analyze the surface atomic composition of the bimetallic catalyst samples. The XPS findings revealed variations in the Au/Pd ratios among the catalysts prepared through different methods. Notably, the (Au–Pd)/C catalyst prepared using the first method exhibited the lowest Au/Pd ratio, while the one prepared via the second method showed the highest ratio. Qualitatively, it was observed that the (Au–Pd)/C catalyst prepared with the third method approached a surface metallic composition of Au/Pd that closely matched the bulk formulation. These catalyst samples were then applied to the oxidation of glycerol. The results of the oxidation experiments

indicated that the (Au–Pd)/C catalyst prepared using the third method exhibited superior glycerol conversion and displayed a higher selectivity toward glyceric acid. In contrast, a comparative analysis of various preparation methods suggested that the first and second methods, whether involving Pd or Pt catalysts, yielded similar catalytic activity.

## 2.3.2 Deposition-precipitation (DP) method

Deposition-precipitation methods are a common choice for the synthesis of Au-based bimetallic catalysts, offering precise control over the dispersion of metal nanoparticles on a support material.[69] In this approach, metal precursors are initially deposited onto the support's surface from a solution, often forming metal ions adsorbed onto the support. Subsequently, a precipitation step is introduced, where these adsorbed metal ions are converted into solid metal nanoparticles. This transformation is frequently facilitated by the addition of a reducing agent, such as sodium borohydride ($NaBH_4$) or another suitable chemical species, which induces the reduction of metal ions into the metallic form. The result is a well-dispersed and stable bimetallic catalyst comprising Au and the second metal. One of the key advantages of deposition-precipitation methods is their ability to achieve a high degree of control over the size, composition, and distribution of metal nanoparticles on the support. Researchers can fine-tune these parameters by adjusting factors such as the concentration of metal precursors, the nature of the support material, the pH of the solution, and the choice of reducing agent.[95] This control is pivotal in tailoring the catalytic properties of Au-based bimetallic catalysts for specific reactions. Additionally, deposition-precipitation methods are applicable to various support materials, including oxides, carbon-based materials, and more, enabling the design of catalysts with diverse applications.[96-98]

This method can take the form of co-deposition-precipitation (co-DP) or successive deposition-precipitation.[89] It is important to note, however, that this method is not suitable

for the deposition-precipitation of Au when the supports are oxide materials with a low point of zero charge (PZC <5), examples of which include silica (PZC ~2), silica-alumina (PZC ~1) , or activated carbons.[89, 99, 100] In this process, the Au precursor or the secondary metal is dissolved in an appropriate solvent. Subsequently, this solution is introduced into a solvent containing the suspended support material, with continuous stirring. It is crucial to maintain the gold precursor's concentration at a level that achieves the desired loading of gold on the support. The adjustment of pH in the mixture is then necessary to induce the precipitation of Au or the secondary metal onto the support. It is worth noting that pH plays a pivotal role in influencing the deposition process.[101, 102] The ideal pH for the deposition of metal particles onto a support can vary depending on the specific metal and support material under investigation. This choice is significant because it can impact several factors, including the stability of metal ions in the solution, the electrochemical characteristics of the metal, and the interaction between the metal and the support material.

Subsequently, the addition of a reducing agent, such as $NaBH_4$, to the mixture occurs incrementally. This reducing agent serves to convert any remaining Au ions into Au(0) nanoparticles on the support. It is essential to regulate the rate of addition to prevent rapid precipitation. Subsequently, the same process is repeated for depositing the second metal onto the support, following the same methodology employed for the initial gold deposition. The precursor solution of the second metal is introduced into the mixture containing the previously deposited Au. If necessary, the pH is adjusted again to align with the optimal pH conditions for the second metal's deposition. Upon the completion of the deposition-precipitation process, the catalyst material undergoes thorough washing to eliminate any residual reactants or byproducts. This typically involves a series of centrifugation or filtration steps employing an appropriate solvent. The catalyst is subsequently dried to prepare it for further use.

Zanella et al.[103] conducted an investigation on bimetallic Au–Ag catalysts supported on $TiO_2$ for CO oxidation, while systematically varying the Au/Ag atomic ratio.

They employed a sequential deposition–precipitation method to synthesize the bimetallic catalyst, utilizing NaOH for metal deposition onto the support. In this synthesis process, Ag was initially deposited onto the $TiO_2$ substrate, followed by drying at 80°C for 2 hours. Subsequently, Au was deposited using the DP method. Notably, urea served as the reducing agent in this catalyst preparation, and the pH of the medium was meticulously controlled within the range of 2 to 3. Furthermore, following the addition of the $TiO_2$ support to this solution, the suspension's temperature was maintained at 80°C and held constant for a duration of 16 hours under continuous stirring.

Based on the results obtained from the ICP-OES analysis, they observed that in the case of bimetallic samples, the actual Au loadings closely approximated the theoretical value of 4 wt%. However, for Ag, the actual loading consistently fell below the nominal loading. They concluded that there may have been a leaching of silver during the gold deposition process, possibly because the silver was initially deposited on the $TiO_2$ support. Additionally, through TEM analysis, the particle size distribution of each catalyst sample was determined. Regardless of the Au/Ag ratio in the bimetallic catalyst samples, they found that the average particle size remained fairly consistent at approximately 3.7–3.9 nm. Notably, these particle sizes were significantly smaller compared to the Ag particles in the $Ag/TiO_2$ catalyst (9 nm) and similar in size to the Au particles in the $Au/TiO_2$ catalyst (4.1 nm).

Mimura et al.[104] investigated glycerol oxidation using a bimetallic $Au–Pd/TiO_2$ catalyst system prepared via the Deposition–Precipitation (DP) method with certain modifications. Their modified DP approach deviated from the standard DP procedure as follows. Initially, they dissolved the Pd precursor ($PdCl_2$) in deionized water (DI $H_2O$). Given that palladium chloride exhibits limited solubility in water, a small quantity of hydrochloric acid (HCl) was introduced as a solvent to facilitate preparation of the $PdCl_2$ solution. Subsequently, the Au precursor was added, forming an Au–Pd mixed solution.

The pH of this mixed aqueous solution was adjusted to fall within the range of 6.3–7.0 through the addition of a sodium hydroxide solution. Following this pH adjustment, titanium dioxide powder was introduced into the solution, and the mixture was stirred for a duration of 3 hours at a temperature of 343 K. Subsequently, the solid fraction was isolated, and a thorough washing with distilled water was carried out to eliminate sodium cations and chloride anions. The washed catalyst precursor underwent a calcination process at 673 K for a period of 4 hours in an air environment.

Based on the results of catalyst characterization, they observed that the actual atomic ratios of metals in the bimetallic catalysts were consistently lower than the theoretical atomic ratios anticipated from the solution employed during their preparation. Additionally, the STEM analysis revealed that the average diameter of the Au-Pd particles was 7.1 nm, notably larger than the particle size of monometallic Au particles, which measured approximately 3.4 nm. Moreover, the presence of hemisphere-shaped particles was observed in both bimetallic and monometallic catalyst samples, firmly adhering to the TiO$_2$ support surface. High-resolution EDS images revealed a distinctive metal distribution within the Au-Pd nanoparticles, resembling a core-shell-like rather than a homogeneously mixed alloy.

### 2.3.3 Chemical reduction method

Chemical reduction methods are widely employed in the synthesis of Au-based bimetallic catalysts due to their simplicity, versatility, and effectiveness.[105, 106] These methods involve the reduction of metal precursors to form nanoparticles on a support material. In the case of Au-based bimetallic catalysts, this approach allows for the controlled incorporation of another metal, creating unique catalytic materials with enhanced properties. Typically, metal salts or complexes of both Au and the second metal are dissolved in a suitable solvent, and a reducing agent is introduced to facilitate the

reduction process. Common reducing agents include sodium borohydride ($NaBH_4$), hydrazine ($H_2N_2$), and $H_2$.[82] The primary challenge encountered in this catalyst preparation is the absence of uniformity in terms of particle size and shape, as well as the difficulty in achieving a precise match between the theoretical and experimental Pd/Au metallic ratio.[107] By adjusting parameters such as the concentration of metal precursors, the type and amount of reducing agent, and reaction conditions such as temperature and pH, researchers can tailor the catalyst's properties to meet specific requirements.[89] This fine-tuned control over composition and morphology is crucial for optimizing catalytic performance.[89] Additionally, these methods are compatible with a wide range of support materials, allowing for the synthesis of Au-based bimetallic catalysts on diverse substrates, including oxides, carbon-based materials, and more.[82]

Liu et al.[105] developed a method to create bimetallic catalysts composed of Au-Cu and Au-Ag on silica supports, specifically SBA-15, which had been previously functionalized with APTES (3-aminopropyl triethoxysilane). Their approach employed a chemical reduction method for catalyst designed to catalyze CO oxidation. Initially, a solution of $HAuCl_4$ was introduced to the support, followed by reduction using $NaBH_4$. Subsequently, the resulting solid was subjected to a thorough washing process. It was then immersed in an aqueous solution containing either copper or silver nitrate, with subsequent reduction accomplished through the addition of $NaBH_4$. Following another round of washing and drying, the solid underwent a two-step heat treatment: initial calcination at 500°C, followed by reduction at 550°C in the presence of hydrogen gas ($H_2$). The authors emphasized that this thermal treatment involving $H_2$ reduction was critical for the formation of the Au-Cu or Au-Ag alloy in the catalyst structure.

Through TEM analysis, the examination of the particle size distribution in the Au-Cu alloy was carried out, revealing a uniform dispersion of all nanoparticles within the

channels of SBA-15. Notably, the Au particles within the Au/SBA-15 exhibited an average particle size of approximately 5.6 nm, whereas the copper particles in the Cu/SBA-15 ranged from 2 to 3 nm in size. An intriguing observation emerged when alloying Au with Cu, resulting in significantly smaller particle sizes compared to pure Au, measuring 2.9 nm for Au:Cu in a 3:1 ratio and 3.0 nm for Au:Cu in a 1:1 ratio. Evidently, these particle size distribution findings align well with the XRD results.

## 2.4    Characterization of Au-Based Bimetallic Catalysts

The synergy between Au and another metal in bimetallic catalysts can lead to enhanced catalytic performance, making them valuable tools in catalysis research.[108] The introduction of additional metals into gold alloys has substantially expanded our ability to fine-tune the structural features of these catalysts, albeit with increased structural complexity.[109] Beyond considerations of particle size and morphology, factors such as composition, distribution, and surface ordering emerge as crucial determinants of catalyst activity, selectivity, and stability. To establish meaningful connections between specific sites within bimetallic systems and their catalytic behaviors, it becomes imperative to conduct structural characterization of these catalysts at nanometric and even atomic scales.[110] A range of characterization techniques for identification and characterization of the Au based bimetallic catalysts. This section offers an in brief exploration of the characterization techniques employed for the analysis of Au-based bimetallic catalysts, with a particular focus on their structural, chemical, and catalytic attributes.

X-ray Diffraction (XRD) is an essential tool for structural characterization. It provides information about the crystallographic structure of the catalyst, helping identify the crystalline phases present in the catalyst.[111] In the case of Au-based bimetallic catalysts, XRD can reveal the presence of alloy phases formed between Au and the second metal.[112, 113] The diffraction patterns obtained can be matched with known crystallographic databases

to identify the specific phases and their relative proportions. This technique also provides information about the lattice parameters and can confirm the existence of an alloy structure in bimetallic catalysts.[114] XRD is also commonly employed for assessing particle size based on the width of the diffraction peaks.[115] However, its effectiveness diminishes for particles smaller than 3 nm.

Transmission Electron Microscopy (TEM) is a powerful technique used to investigate the morphology and particle size distribution of catalyst nanoparticles.[116] Au-based bimetallic catalysts often consist of metal nanoparticles supported on various substrates. TEM allows researchers to visualize the shape and dispersion of these nanoparticles, providing valuable insights into the catalyst's structure. Furthermore, Energy-Dispersive X-ray Spectroscopy (EDS) can be coupled with TEM to determine the elemental composition of individual nanoparticles.[116] This aids in confirming the presence and distribution of the second metal within the bimetallic catalyst. This comprehensive characterization approach offers insights into the structure-function relationships of Au-based bimetallic catalysts, essential for optimizing their performance in catalytic applications.

X-ray Photoelectron Spectroscopy (XPS) is a powerful surface analytical technique employed for the characterization of Au-based bimetallic catalysts, providing valuable insights into their chemical composition and surface properties.[90, 117] It is also  is used to identify oxidation states, and provide information about the chemical environment of the elements present.[90, 113, 117] In the case of Au-based bimetallic catalysts, XPS can be particularly useful in elucidating the distribution and interaction of the constituent metals (e.g., Au and another metal like Pt or Pd) on the catalyst surface, which is crucial for understanding the catalyst's catalytic activity and selectivity. Furthermore, XPS can provide detailed information about the surface chemistry of Au-based bimetallic catalysts, revealing the presence of surface oxides, functional groups, and adsorbed species.[118] This characterization technique is essential for optimizing catalyst synthesis and modification

processes, as it helps researchers fine-tune the catalyst's surface properties to enhance its catalytic performance.

Characterization of Au-based bimetallic catalysts using Diffuse Reflectance Infrared Fourier-Transform Spectroscopy (DRIFTS) is an invaluable analytical technique that provides insights into the surface chemistry and catalytic activity of these materials.[119, 120] DRIFTS allows for the examination of the catalyst's surface adsorption properties and the identification of active sites by probing molecular vibrations at the catalyst's surface.[119, 120] By adsorbing various probe molecules such as CO onto the catalyst's surface, researchers can monitor the changes in their vibrational spectra, thus revealing the interactions and binding strengths between the catalyst and these molecules. This information is critical for understanding the catalyst's catalytic mechanism and its potential applications in various chemical reactions. Furthermore, DRIFTS enables the in-situ monitoring of catalytic reactions, offering real-time data on reaction intermediates and products, which is essential for elucidating reaction mechanisms and optimizing catalytic processes.

## 2.5    Applications of Au-Based Bimetallic Catalysts

The utilization of Au in catalysis has garnered considerable attention in recent decades, primarily owing to its distinctive electronic and geometric attributes.[70, 121, 122] Gold nanoparticles exhibit exceptional stability and can facilitate reactions under mild conditions that often present challenges for other metallic elements.[75, 123] However, single-metal Au-based catalysts often encounter limitations, including constrained activity and selectivity, in a variety of catalytic processes. To overcome these constraints, researchers have turned to bimetallic catalysts, merging the unique qualities of Au with those of another metal, to achieve enhanced catalytic performance. Indeed, bimetallic systems featuring Au nanoparticles have attracted significant attention. Combining Au with a second metal

allows for the development of catalytic systems featuring unique physical and chemical properties not typically observed in individual monometallic catalysts.[124] This is largely due to the synergistic effect generated by the interaction between the two metals. It has been observed that various factors, such as the choice of the second metal, the Au to second metal ratio, the structural characteristics of bimetallic catalysts, as well as the size and shape of nanoparticles, which are, in turn, determined by the synthesis method of these bimetallic catalysts, exert a significant influence on their activity, selectivity, and stability.[124] These bimetallic catalysts have generated substantial interest due to their capacity to synergistically adjust catalytic behavior by modifying electronic, structural, and adsorption properties.[125] The applications of Au-based bimetallic catalysts span a wide spectrum of fields, encompassing environmental catalysis, energy conversion, chemical synthesis, biomedical applications, and sensing technologies. In this section, we will delve into the applications of Au-based bimetallic catalyst for oxidation reactions.

## 2.5.1 Benzyl alcohol oxidation

Benzyl alcohol is important as a versatile precursor in the synthesis of various fine chemicals, fragrances, and pharmaceuticals.[126-128] The oxidation of benzyl alcohol to benzaldehyde or benzoic acid represents a fundamental and industrially relevant chemical transformation.[127, 128] This process is not only crucial for the production of valuable intermediates but also serves as a model reaction to study catalytic mechanisms and explore the potential of novel catalysts.[129] Gold and its bimetallic counterparts have emerged as promising catalysts for the oxidation of benzyl alcohol.[130]

The study of benzyl alcohol oxidation with Au-based bimetallic catalysts is not only of academic interest but also holds practical significance in the synthesis of key intermediates for various industries.[130] This catalytic system exemplifies the potential of bimetallic catalysts in fine chemical synthesis and showcases the evolving landscape of

catalysis, where innovative materials and strategies are continuously explored to meet the demands of sustainable and efficient chemical processes. In this context, understanding the mechanisms and optimizing the performance of Au-based bimetallic catalysts in benzyl alcohol oxidation remains a compelling area of research with broad implications for both academic and industrial applications.[130, 131]

Depending on the specific reaction parameters, such as temperature, choice of solvent, and oxygen pressure applied in the oxidation of benzyl alcohol, many side-products including benzene, benzoic acid, benzyl benzoate, and toluene have been reported to be formed besides the main product, benzaldehyde (see scheme 2.1).[91, 110]
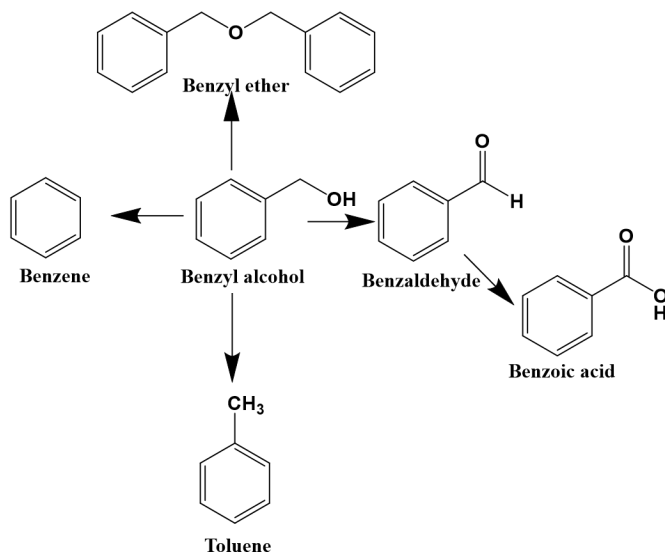


Scheme 2.1 Benzyl Alcohol Oxidation Reaction Network

Numerous research papers have explored the use of Au-based bimetallic systems for the oxidation of benzyl alcohol in the literature. However, conducting a comprehensive comparison among these studies is challenging due to the variations in reaction conditions and catalyst preparation methods.[91, 110] Additionally, researchers have investigated a diverse array of supports, including activated carbon, carbon nanotubes, $TiO_2$, $SiO_2$, and polymers, further complicating direct comparisons.[110] Table 2.1 present a selection of

instances where benzyl alcohol oxidation has been performed using Au-Pd based bimetallic catalyst systems.[110]

Table 2.1 Oxidation of benzyl alcohol over supported AuPd bimetallic catalyst. Reprinted with permission of the Royal Society of Chemistry: Villa, A.;  Wang, D.;  Su, D. S.; Prati, L., New challenges in gold catalysis: bimetallic systems. *Catalysis Science & Technology* **2015,** *5* (1), 55-68.[110]

| | | Reaction Conditions | | | | | Selectivity | | | |
| | Catalyst | Solvent | T(K) | pO$_2$ (bar) | Metal/sub ratio | TOF | Benzaldehyde | Toluene | Benzyl benzoate | Benzoic acid |
|---|---|---|---|---|---|---|---|---|---|---|
| 1 | 1% Pd/AC | Toluene | 333 | 1.5 | 1/500 | 38 | >99 | - | - | |
| 2 | 1% Pd40@(Au60/AC) | Toluene | 333 | 1.5 | 1/500 | 54 | 94 | - | - | - |
| 3 | 1% Pd10@(Au90/AC) | Water | 333 | 1.5 | 1/500 | 780 | >99 | - | - | - |
| 4 | 1%Pd20@(Au80/AC) | Water | 333 | 1.5 | 1/500 | 1021 | >99 | - | | - |
| 5 | 1%Pd40@(Au60/AC) | Water | 333 | 1.5 | 1/500 | 985 | >99 | - | | - |
| 6 | 1%Pd80@(Au20/AC) | Water | 333 | 1.5 | 1/500 | 716 | >99 | - | - | - |
| 7 | 1%Pd10@(Au90/AC)a | Water | 333 | 1.5 | 1/500 | 1140 | 28 | - | 2 | 40 |
| 8 | 1%Pd20@(Au80/AC)a | Water | 333 | 1.5 | 1/500 | 1189 | 46 | - | 22 | 32 |
| 9 | 1%Pd40@IJAu60/AC)a | Water | 333 | 1.5 | 1/500 | 1071 | 45 | - | 24 | 31 |
| 10 | 1%Pd80@IJAu20/AC)a | Water | 333 | 1.5 | 1/500 | 776 | 50 | - | 24 | 26 |
| 11 | 5%Au50–Pd50/TiO$_2$ | None | 383 | 1 | Nd | 14270 | Nd | Nd | Nd | Nd |
| 12 | 5%Au50–Pd50/TiO$_2$ | None | 393 | 1 | Nd | 26400 | Nd | Nd | Nd | Nd |
| 13 | 5%Au50–Pd50/TiO$_2$ | None | 433 | 1 | 1/55000 | 86500 | Nd | Nd | Nd | Nd |
| 14 | 1% Au + Pd/ACSI | None | 393 | 10 | 1/55000 | 1800 | 79 | 2 | - | 4 |
| 15 | 1% Au + Pd/ACI | None | 393 | 10 | 1/55000 | 500 | 69 | 10 | - | 3 |
| 16 | 1% Au + Pd/TiO$_2$ | None | 393 | 10 | 1/55000 | 15360 | 69 | 27 | 2 | 2 |
| 17 | 1% Pd50@Au50/TiO$_2$ | None | 393 | 10 | 1/55000 | 19250 | 77 | 18 | 3 | 2 |

| 18 | 1% Au50@Pd50/TiO$_2$ | None | 393 | 10 | 1/55000 | 17360 | 72 | 23 | 3 | 2 |
|----|----------------------|------|-----|-----|---------|-------|----|----|---|---|
| 19 | 1% Au50 + Pd50/AC | None | 393 | 10 | 1/55000 | 35400 | 55 | 41 | 2 | 1 |
| 20 | 1% Pd50@Au50/AC | None | 393 | 10 | 1/55000 | 41930 | 63 | 35 | 0 | 2 |
| 21 | 1% Au50@Pd50/AC | None | 393 | 10 | 1/55000 | 24310 | 65 | 29 | 3 | 3 |
| 22 | 1% Au + Pd/TiO$_2$ calc. 673 K | None | 393 | 10 | 1/55000 | 3940 | 70 | 22 | 6 | 2 |
| 23 | 1% Pd50@Au50/TiO$_2$ calc. 673 K | None | 393 | 10 | 1/55000 | 8650 | 72 | 21 | 5 | 2 |
| 24 | 1% Au50@Pd50/TiO$_2$ calc. 673 K | None | 393 | 10 | 1/55000 | 8780 | 69 | 25 | 4 | 1 |
| 25 | 1% Au50 + Pd50/AC calc. 673 K | None | 393 | 10 | 1/55000 | 2490 | 79 | 2 | 10 | 4 |
| 26 | 1% Pd50@Au50/AC calc. 673 K | None | 393 | 10 | 1/55000 | 2430 | 75 | 3 | 13 | 4 |
| 27 | 1% Au50@Pd50/AC calc. 673 K | None | 393 | 10 | 1/55000 | 3410 | 79 | 5 | 11 | 4 |
| 28 | 1% Pd40@IJAu60/CNFs) | None | 393 | 1.5 | 1/35000 | 6076 | 74 | 18 | 3 | 1 |
| 29 | 1% Pd40@IJAu60/N-CNFs) | None | 393 | 1.5 | 1/35000 | 52638 | 76 | 11 | 7 | 5 |
| 30 | 2% Au70 + Pd10/PANIa | Toluene | 373 | 1 | 1/150 | 16 | 71 | Nd | Nd | Nd |
| 31 | 2% Au50 + Pd50/PANIa | Toluene | 373 | 1 | 1/150 | 16 | 82 | Nd | Nd | Nd |
| 32 | 2% Au10 + Pd90/PANIa | Toluene | 373 | 1 | 1/150 | 14 | 98 | Nd | Nd | Nd |
| 33 | 3Au–1Pd/APS-S16 | None | 413 | 1 | Nd | 4052 | 89 | 11 | Nd | 0 |
| 34 | 1Au–1Pd/APS-S16 | None | 413 | 1 | Nd | 4715 | 94 | 6 | Nd | 0 |
| 35 | 1Au–2Pd/APS-S16 | None | 413 | 1 | Nd | 6575 | 94 | 5 | Nd | 1 |
| 36 | 1Au–3Pd/APS-S16 | None | 413 | 1 | Nd | 7864 | 91 | 8 | Nd | 1 |
| 37 | 1Au–5Pd/APS-S16 | None | 413 | 1 | Nd | 8667 | 94 | 5 | Nd | 1 |
| 38 | 1% Au–0.5% Pd/γ-Al$_2$O$_3$ | Toluene | 333 | 1 | 1/500 | 5.5 | 81 | - | 19 | - |
| 39 | 1% Au + 0.5% Pd/γ-Al$_2$O$_3$ | Toluene | 333 | 1 | 1/500 | 26.4 | 84 | - | 14 | - |

| 40 | 1% Pd40@IJAu60/AC) | Cyclohexane | 353 | 2 | 1/5000 | 2261 | 89 | 8 | 2 | 1 |
| 41 | 1% Au50 + Pd50/TiO$_2$ | None | 393 | 10 | 1/100000 | 63800 | 67 | 3 | 7 | 23 |
| 42 | 1%Au45 + Pd45+ Pt10/TiO$_2$ | None | 393 | 10 | 1/100000 | 31900 | 80 | - | 6 | 13 |

Hutchings' group was among the first researchers to demonstrate the efficiency of the sol immobilization method for creating uniform AuPd alloys supported on Mg–Al mixed metal oxides (MgAl-MMO) and to test this catalyst for the solvent-free oxidation of benzyl alcohol in the presence of $O_2$.[71] In their study, a range of catalysts was synthesized by varying the Au to Pd molar ratio, including monometallic Au and Pd catalysts supported on Mg–Al mixed metal oxides. The impact of the Au: Pd ratio on the benzyl alcohol oxidation reaction was explored. The results indicated that Au:Pd with a 1 : 1 weight ratio exhibited the highest catalytic activity, with a turnover number of 13,000 achieved after 240 minutes, while maintaining a benzaldehyde selectivity of 93%. Additionally, they assessed catalyst stability by subjecting the used catalyst to repeated oxidation reactions under the same conditions and performed a leaching study using ICP analysis. The reusability test revealed a significant decline in catalytic activity for the monometallic Au and Pd catalysts during these recycling tests. However, ICP analysis confirmed only 6.5% Au leaching, with negligible Pd leaching observed. The researchers attributed the deactivation to potential agglomeration and poisoning of Au and Pd nanoparticles. In contrast, the bimetallic Au–Pd catalyst exhibited complete reusability with high catalytic activity and showed no metal leaching. In summary, the bimetallic Au–Pd catalyst displayed superior activity, benzaldehyde selectivity, and stability during the solvent-free oxidation of benzyl alcohol.

The same researchers also investigated the role of the support in benzyl alcohol oxidation using the AuPd bimetallic catalyst system. To do this, they immobilized Au–Pd nanoparticles on commercial MgO for comparison with the Au–Pd/MgAl-MMO catalyst. The results indicated that the Au–Pd/MgAl-MMO and Au–Pd/MgO catalysts exhibited similar selectivity to benzaldehyde but showed significantly lower benzyl alcohol conversion in the case of the Au–Pd/MgO catalysts. Their conclusion highlights the significance of the support material in relation to the catalyst's performance in the oxidation of benzyl alcohol. They found that MgAl-MMO, having both acidic and basic sites,

enhances both the activity and selectivity in this process, whereas the MgO support, characterized by basic sites only, primarily enhances the selectivity of the reaction.

Based on their experimental findings and prior research, the Hutchings et al.[71] proposed a plausible mechanism involving Au–Pd nanoparticles as active sites (Figure 2.2). This mechanism illustrates that the oxidation of benzyl alcohol proceeds through a collaboration between bimetallic Au–Pd nanoparticles and the base–acid sites on the surface of the MgAl-LDH support. In the first step, benzyl alcohol interacts with a basic Mg–OH$^{\delta-}$ site on the MgAl-LDH to form an alkoxide intermediate. In the second step, the intermediate undergoes coordination to form a metal-H bond with the coordinately unsaturated active center, generating unstable metal-alcoholate-LDH species. This species then undergoes β-hydride elimination to produce metal-hydride species at the catalyst interface, along with the corresponding carbonyl compound. The third step involves the rapid oxidation of the metal hydride by oxygen, facilitated by the acid sites of the support, while the initial metallic site is regenerated, completing the catalytic cycle.
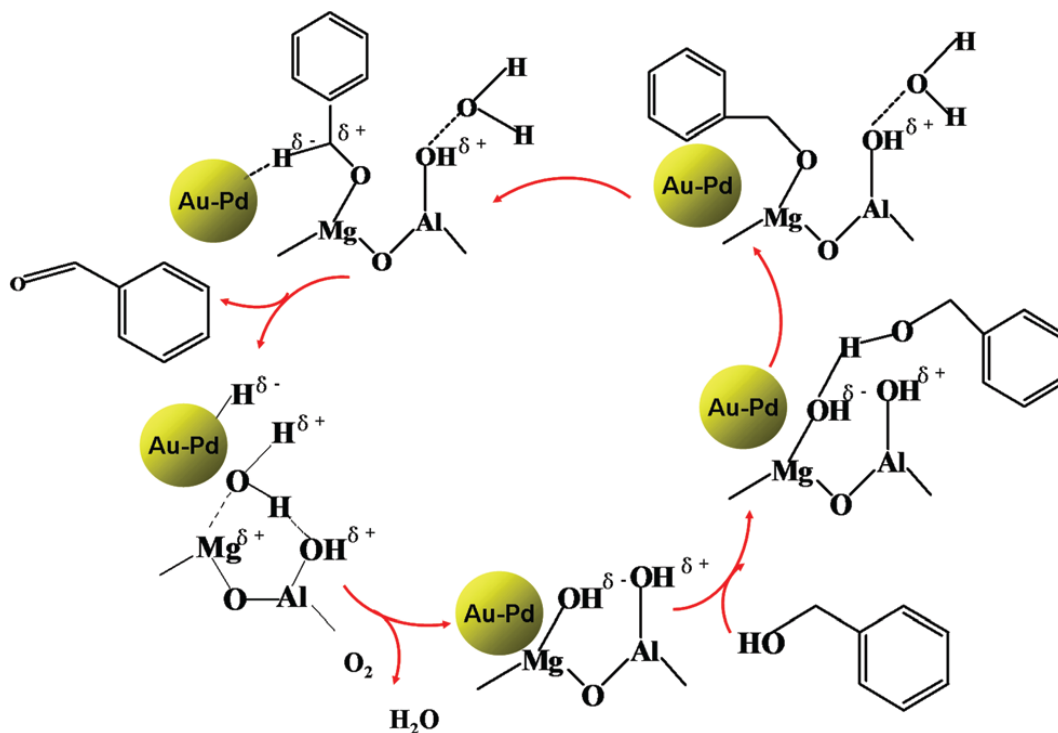
Figure 2.2 The possible reaction pathway of the solvent free oxidation for benzyl alcohol over Au–Pd/MgAl-MMO catalyst. Reprinted with permission of the Royal Society of Chemistry: Feng, J.; Ma, C.; Miedziak, P. J.; Edwards, J. K.; Brett, G. L.; Li, D.; Du, Y.; Morgan, D. J.; Hutchings, G. J., Au–Pd nanoalloys supported on Mg–Al mixed metal oxides as a multifunctional catalyst for solvent-free oxidation of benzyl alcohol. *Dalton Transactions* **2013,** *42* (40), 14498-14508.[71]

Prati's research group was among the early pioneers in showcasing the effectiveness of the sol immobilization technique for creating homogeneous AuPd and AuPt alloys supported on activated carbon (AC).[132] They conducted experiments comparing monometallic (Au, Pd, Pt) and bimetallic (Au−Pd and Au−Pt) nanoparticles supported on activated carbon, evaluating their performance in the conversion of benzyl alcohol under mild conditions (T = 60 °C, $pO_2$ = 1.5 atm) and in two different solvents: toluene and water. Based on their findings, in both solvents, monometallic Au/AC catalysts displayed low activity, while Pt/AC exhibited higher activity than Pd/AC. Interestingly, the introduction of Au alongside Pd had a promotional effect on activity, which was not observed with bimetallic Au−Pt catalysts. Their analysis led to the conclusion that this difference might arise from distinct interactions involving geometric and electronic effects in Au−Pd and Au−Pt catalysts. They suggested that in the former catalyst, these effects synergistically enhance activity, whereas in the case of AuPt catalysts, they may have a counteractive impact.

Additionally, this research highlighted that all of the catalysts exhibited greater activity in water compared to toluene. The synergistic effect of adding Au was particularly evident in water: it positively influenced Pd (resulting in an increase in TOF from 30 to 160 $h^{-1}$) but negatively affected Pt (resulting in a decrease in TOF from 98 to 55 $h^{-1}$). Notably, the results clearly demonstrated that the catalyst's superior performance was only

observed when Pd was combined with Au. These trends were also observed in cinnamyl alcohol oxidation experiments.

Ebitani et al.[133] conducted a comprehensive investigation into the impact of negatively charged gold (Au) states on the aerobic oxidation of alcohols using PVP protected hydrotalcite-supported AuPd nanoclusters (designated as $Au_xPd_y$-PVP/HT). Their study revealed a notable influence of palladium (Pd) content on the catalytic activity of these catalysts during the aerobic oxidation of 1-phenylethanol to acetophenone. Various $Au_xPd_y$-PVP/HT catalysts, differing in Pd content, were employed for these aerobic oxidation reactions, and the corresponding results are presented in Table 2.2. Among these catalysts, $Au_{100}$-PVP/HT exhibited no catalytic activity, whereas the bimetallic $Au_xPd_y$-PVP/HT catalysts displayed varying levels of activity. Particularly noteworthy was the outstanding performance of $Au_{60}Pd_{40}$-PVP/HT, which achieved the highest acetophenone yields.

Table 2.2 Aerobic oxidation of 1-phenylethanol using AuxPdy-PVP/HT catalysts with various Pd content.[133]

| | Catalyst | Conv (%) | Yield (%) | Particle size (nm) | Metal amount (mmol g$^{-1}$) | |
| --- | --- | --- | --- | --- | --- | --- |
| | | | | | Au | Pd |
| 1 | $Au_{100}$-PVP/HT | 2 | 0 | Agglomerate | 0.075 | 0 |
| 2 | $Au_{80}Pd_{20}$-PVP/HT | 100 | 99 | 3.1 | 0.115 | 0.034 |
| 3 | $Au_{60}Pd_{40}$-PVP/HT | 100 | >99 | 2.6 | 0.054 | 0.042 |
| 4 | $Au_{40}Pd_{60}$-PVP/HT | 58 | 57 | 2.6 | 0.052 | 0.098 |
| 5 | $Au_{20}Pd_{80}$-PVP/HT | 19 | 19 | 2.6 | 0.023 | 0.135 |

The investigation further explored the correlation between charge transfer between Au and Pd and the catalytic activity of the $Au_xPd_y$-PVP/HT catalysts using advanced characterization techniques, including X-ray photoelectron spectroscopy (XPS) and X-ray absorption near-edge structure (XANES) analysis. The XPS results revealed a distinctive

shift in the Au 4f peaks towards lower energy values as the Pd content increased, indicative of electron transfer from Pd to Au atoms in accordance with Pauling's electronegativity principle.

Moreover, the authors proposed a comprehensive catalytic cycle for alcohol oxidation over the $Au_xPd_y$-PVP/HT catalysts, as illustrated in Figure 2.3. This catalytic cycle proceeds through a series of steps involving alkoxide intermediates and radical-like peroxo-species. Initially, molecular oxygen ($O_2$) attaches to the negatively charged Au site on the $Au_xPd_y$ nanoclusters, followed by the dissociation of the adsorbed $O_2$ molecule due to electron donation from Au 5d orbitals to the antibonding $2\pi^*$ orbital of $O_2$, leading to the formation of $AuO^{2-}$ peroxo- and/or $AuO_2^{2-}$ superoxospecies. Subsequently, alcohol molecules are adsorbed onto Au and/or Pd sites, forming metal-alkoxide complexes. Importantly, the basic nature of the hydrotalcite (HT) support facilitates this step by abstracting protons from alcohol molecules, resulting in the formation of $[H–HT]^+$ species. In the next stage, hydrogen atoms on the α-carbon of the adsorbed alkoxide undergo transformation into Au-peroxo- (and/or superoxo-) species through β-hydrogen elimination. This transformation leads to the formation of the corresponding carbonyl compounds and Au-hydroperoxide species. Finally, another $O_2$ molecule interacts with the Au surface, leading to the removal of the hydroperoxide species and the generation of $H_2O$, thereby completing the catalytic cycle.
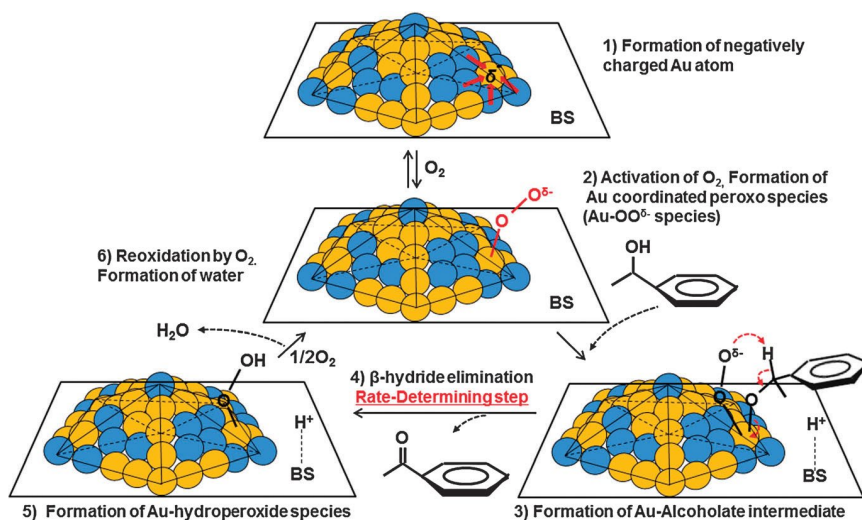
Figure 2.3 The possible reaction pathway of the solvent free oxidation for 1-penyl ethanol over AuxPdy-PVP/HT catalyst. Reprinted with permission of the Royal Society of Chemistry: Nishimura, S.; Yakita, Y.; Katayama, M.; Higashimine, K.; Ebitani, K., The role of negatively charged Au states in aerobic oxidation of alcohols over hydrotalcite supported AuPd nanoclusters. *Catalysis Science & Technology* **2013,** *3* (2), 351-359.[133]

Nagy et al.[134] conducted a comprehensive investigation into the selective oxidation of benzyl alcohol to benzaldehyde using molecular $O_2$ as the oxidizing agent. Their study focused on catalysts comprising sol-derived alumina supports with bimetallic combinations of Au-Ru and Au-Ir, each with a nominal atomic ratio of 1:1. These catalysts were compared to monometallic counterparts consisting of Au, Ru, and Ir, both in calcined and subsequently reduced states, in the presence and absence of equimolar $K_2CO_3$, all of which were tested in toluene at 80 °C. The oxidation results, summarized in Table 2.3, revealed that the monometallic $Au/Al_2O_3$ catalyst exhibited the highest activity across all catalytic tests. In contrast, $Ru/Al_2O_3$ and $Ir/Al_2O_3$ monometallic catalysts displayed minimal activity, while the bimetallic catalysts fell in between these extremes.

In reactions conducted without a base such as $K_2CO_3$, Nagy et al. observed catalyst deactivation at low conversions and lower initial reaction rates compared to those measured

in the presence of $K_2CO_3$. This deactivation was attributed to the poisoning effect of trace amounts of benzoic acid. When a base was introduced into the reaction system, the initial reaction rates for both calcined and reduced Au-Ru and reduced Au-Ir catalysts approached those of $Au/Al_2O_3$.

Table 2.3 Comparison of the initial reaction rates in the benzyl alcohol oxidation and the relative amount of CO adsorbed on gold.[134]

| Catalysts | Initial reaction rate mmol/h/gcat | | | | Relative IR band intensity of CO adsorbed on Au | | Initial reaction rate mol/h/mol$_{metal}$ | | | |
|---|---|---|---|---|---|---|---|---|---|---|
| | without $K_2CO_3$ | | with $K_2CO_3$ | | | | without $K_2CO_3$ | | with $K_2CO_3$ | |
| | Calc | Red | Calc | Red | Calc | Red | Calc | Red | Calc | Red |
| $Au/Al_2O_3$ | 34 | 26 | 102 | 87 | 1.00 | 0.87 | 373 | 284 | 1122 | 956 |
| $Ru/Al_2O_3$ | 2 | 1 | 1 | 1 | - | - | 33 | 16 | 24 | 29 |
| $AuRu/Al_2O_3$ | 9 | 11 | 73 | 79 | 0.07 | 0.07 | 113 | 130 | 885 | 965 |
| $Ir/Al_2O_3$ | 1 | 2 | 1 | 11 | - | - | 8 | 11 | 3 | 58 |

Furthermore, the authors noted that since the activity of the alumina-supported monometallic Ru and Ir catalysts was negligible in comparison to that of Au, it was reasonable to assess the effect of the second metal by comparing the initial reaction rates relative to the accessible Au sites. They observed that the incorporation of Ru or Ir with Au led to an increase in the particle size of the bimetallic catalysts, with mean diameters of ≥3.7 nm for Au-Ru and ≥5.0 nm for Au-Ir, while $Au/Al_2O_3$ had a mean diameter of approximately 2.0 nm, i.e., the particle sizes in the monometallic $Au/Al_2O_3$ catalyst were at least twice as small as those in the bimetallic catalysts. Additionally, the researchers investigated the enrichment of Au on the catalyst surface using X-ray photoelectron spectroscopy (XPS). The results suggested that the presence of Ir and Ru on the surface of the bimetallic particles further reduced the concentration of surface Au atoms. This result

indicated that the amount of surface Au atoms in the bimetallic particles is much lower than the Au/Al$_2$O$_3$ catalyst. Since the activity of the three catalysts in the presence of K$_2$CO$_3$ is similar, this implies that the surface Au atoms in the bimetallic catalysts must be much more active than in the monometallic Au catalyst. Hence, this is a synergistic effect of Au with Ru and Ir.

## 2.5.2 CO oxidation reaction

CO oxidation using heterogeneous catalysis is a significant area of research with profound implications for both environmental and industrial applications.[135] The catalytic oxidation of carbon monoxide (CO) is of utmost importance in the context of air purification, particularly in exhaust gases from vehicles and industrial processes.[135] Heterogeneous catalysis, in this context, involves the use of a solid catalyst to facilitate the conversion of CO into carbon dioxide (CO$_2$) at relatively mild temperatures.[136] The mechanism of CO oxidation typically involves a Langmuir-Hinshelwood mechanism, where CO molecules adsorb onto the catalyst surface, resulting in re-ordering of the catalyst surface sites for reaction.[137] Oxygen molecules also adsorb on the catalyst, and the reaction proceeds through the interaction of adsorbed CO with adsorbed oxygen.[136, 137] This reaction is exothermic, releasing energy in the form of heat, which further promotes the oxidation process. The choice of support material and the nature of the metal catalyst play a crucial role in determining the catalytic activity.[138] The size and dispersion of metal nanoparticles, as well as the support's oxygen storage capacity, can also significantly impact the catalyst's performance.[138] One of the most widely studied type of catalyst for CO oxidation is supported metal catalysts, with noble metals such as gold (Au), platinum (Pt), silver (Ag) and palladium (Pd) being particularly effective due to their high catalytic activity and resistance to poisoning.[70, 139]

Furthermore, researchers have explored various strategies to enhance the catalytic performance of CO oxidation catalysts, including the addition of promoters, alloying with other metals, and optimizing the catalyst's structure.[140-142] The catalytic activity is also influenced by the reaction conditions, such as temperature, pressure, and the presence of co-reactants.[143, 144 145] Understanding these factors is crucial for tailoring catalysts to specific applications. Additionally, researchers continue to investigate the fundamental aspects of CO oxidation using heterogeneous catalysis to develop more efficient and environmentally friendly catalysts.[135] These studies are not only vital for improving air quality but also for enabling more sustainable energy production and industrial processes by mitigating the harmful effects of CO emissions.

The oxidation of CO has garnered substantial attention in the context of catalysis by Au, especially in light of the pioneering work by Haruta et al.[74] This research revealed that Au nanocrystals can display remarkable catalytic efficiency for CO oxidation even at temperatures below 0°C.[74, 146] It is widely acknowledged that the method of preparation, the choice of support material, and the control of particle size play pivotal roles in determining the catalytic performance of Au catalysts.[145, 146] Numerous reviews within the field of CO oxidation by supported Au particles have provided comprehensive insights into various crucial aspects of this chemistry.[146-149] These reviews have shed light on key factors such as the influence of the support material on reactivity, Au's active oxidation state, the significance of water in the oxidation reaction, as well the effects of particle size and morphology, all contributing to a deeper understanding of Au-based catalysts for CO oxidation.[146]

Furthermore, bimetallic catalysts, particularly those based on Au, have received significant attention in the field of catalysis, particularly for the crucial CO oxidation reaction.[103, 150-152] Au possesses remarkable catalytic properties, such as high catalytic activity and excellent stability, making it an ideal candidate for various catalytic reactions. However, its catalytic prowess in CO oxidation can be further enhanced by alloying it with

another metal. Commonly used co-catalysts include silver (Ag), palladium (Pd), and platinum (Pt), among others. The incorporation of these metals in controlled compositions and structures can tune the catalyst's activity, selectivity, and thermal stability, making bimetallic Au-based catalysts highly versatile for CO oxidation applications.

In the specific context of CO oxidation, Venezia et al.[153] conducted a study on bimetallic Au–Pd catalysts supported on silica, exploring the impact of different Au:Pd ratios. They created these bimetallic Au-Pd catalysts on a silica support by simultaneously reducing Pd and Au precursors using ethanol in the presence of the polymer polyvinylpyrrolidone (PVP).[153] The results of CO oxidation tests indicated that monometallic Pd catalysts exhibited significantly higher activity compared to monometallic Au catalysts. Interestingly, bimetallic catalysts with a high proportion of Pd behaved similarly to pure Pd catalysts. Venezia et al.[153] observed a reduction in the intrinsic activity of Pd when alloyed with Au, which was attributed in part to alterations in Pd's redox properties, potentially reducing its ability to activate $O_2$. Notably, they did not observe a substantial synergistic effect between the two metals on the silica support, and the authors attributed the lower catalytic activity of $Au/SiO_2$ catalysts to the larger particle size of gold. Additionally, they concluded that silica did not play a significant role in the CO oxidation process, and there was no discernible interaction between the support and the metal in this particular case.

Guczi's research group introduced titanium dioxide ($TiO_2$)-supported bimetallic AuPd catalysts. These catalysts were prepared by using Au(III) and Pd(II) precursor ions in an aqueous medium, and they were reduced by a mixture of sodium citrate and tannin.[93] This process produced stable metal sols with a narrow size distribution. In the context of CO oxidation, conducted at 60°C with a gas mixture of 5.6 mbar CO and 91.8 mbar $O_2$, their experiments revealed that the activity of the AuPd bimetallic system was only slightly higher than that of a physical mixture of Au and Pd. This suggests that there was only a minimal synergistic effect. They did find a slight synergistic effect between Au and Pd

when supported on titania for CO oxidation. Their conclusion was that this slight synergy between the support and bimetallic particles can be attributed to the support's ability to facilitate the production of activated oxygen.

Chung and colleagues conducted an investigation into the application of Au–Ag alloy nanoparticles supported on mesoporous aluminosilicate as catalysts for low-temperature CO oxidation reactions.[154] They prepared monometallic Au and Ag catalysts, as well as AuAg bimetallic catalysts, by varying the Au to Ag molar ratio while controlling the total metal loading to 8 wt%. This synthesis was carried out in a single step, where the formation of nanoparticles was coupled in an aqueous solution with the construction of a mesoporous structure. Initially, they prepared the alloy Au–Ag nanoparticles in an aqueous solution, employing a quaternary ammonium surfactant, and subsequently reduced the nanoparticles by slowly adding a NaBH$_4$ solution. The resulting Au–Ag alloy nanoparticle solution was then directly introduced into a sodium aluminosilicate solution with a pH adjusted to approximately 9.0. Finally, the gel solution underwent a hydrothermal reaction at 100 °C for 6 hours. The particle size of the catalyst was determined through both XRD and TEM characterizations, revealing that the alloy particles were significantly larger than the monometallic gold particles, with an increase in size corresponding to higher amounts of Ag.

In the study of CO oxidation at room temperature, it was observed that pure Au had low activity, while Ag exhibited no catalytic activity. In contrast, Au–Ag alloy catalysts displayed substantially higher activity than their monometallic counterparts at low temperatures. Moreover, the activity of the alloy catalysts exhibited significant variations with changes in the Au/Ag ratios. The catalyst with a Au/Ag ratio of 3:1 exhibited the highest activity, achieving complete CO conversion at room temperature. However, as the Au/Ag ratio was increased (e.g., 5:1 and 8:1) or decreased (e.g., 1:1) from this optimal ratio, the activity decreased.

These researchers also investigated the effect of temperature on CO oxidation for this catalyst system. Interestingly, the temperature-dependent activity of the alloy catalysts differed from that of the monometallic catalysts. While pure metallic catalysts, including both Au and Ag, exhibited a monotonic increase in activity with rising reaction temperature, the Au–Ag alloy catalysts displayed a more complex behavior. Their activity initially increased at low temperatures (up to 80 °C), then decreased in the range of 80–160 °C. Subsequently, with further increases in reaction temperature (160–300 °C), the activity rose again, similar to the monometallic catalysts. This temperature-dependent activity profile suggests a difference in the underlying reaction mechanisms between monometallic and bimetallic catalysts.

Chung and colleagues also proposed a potential mechanism for the Au–Ag alloy system in CO oxidation. Their XPS results indicated that Au–Ag alloy catalysts exhibited a greater propensity to lose electrons compared to their monometallic counterparts. Given that oxygen adsorption and activation are pivotal steps in CO oxidation, the exceptional high-temperature activity of Au–Ag alloy catalysts suggests that oxygen can be adsorbed and activated on the alloy catalyst surface even at low temperatures. Furthermore, the binding energy shifted when Au was incorporated with Ag, with Au's binding energy shifting to higher values and Ag's to lower values. Consequently, the authors concluded that oxygen adsorption and activation primarily occurred on Ag, while the presence of Au facilitated the molecular adsorption of oxygen and the formation of $O^{2-}$ species on the Ag surface. Simultaneously, CO adsorption occurred on Au, culminating in the reaction between $O^{2-}$ and adsorbed CO, leading to the removal of $CO_2$ from the system.

The same research team conducted an investigation into the use of Au–Cu alloy nanoparticles supported on silica gel as a catalyst for CO oxidation and studied how the ratio of Au to Cu affects the reaction.[155] They prepared a series of well-dispersed bimetallic catalysts with Au/Cu ratios ranging from 3/1 to 20/1, along with monometallic Au and Cu catalysts. This synthesis involved a two-step process, initially depositing Au onto a silica

gel support, followed by depositing Cu onto the Au nanoparticles supported on silica gel. The particle size of the catalyst was analyzed using TEM, revealing that the average particle sizes increased only slightly from 3.0 to 3.6 nm as the Au/Cu ratio was increased from 3/1 to 20/1. In comparison to the $Au/SiO_2$ catalyst, which had an average particle size of 5.7 nm, all the Au–Cu bimetallic catalysts displayed significantly reduced particle sizes.

During CO oxidation, the $SiO_2$-supported Au catalyst exhibited good activity at low temperatures. CO conversion reached approximately 50% even at temperatures below 0 °C. However, for $Au/SiO_2$, the conversion level remained relatively constant as the reaction temperature increased up to 150 °C. The silica-supported Au catalyst achieved complete CO conversion only at 200 °C. In contrast, the $Cu/SiO_2$ sample displayed rather poor catalytic activity, with an onset temperature higher than 100 °C. Notably, the Au–Cu bimetallic catalysts exhibited a synergistic catalytic effect between Au and Cu, distinct from both $Au/SiO_2$ and $Cu/SiO_2$. Irrespective of the Au/Cu ratios, all the Au–Cu bimetallic catalysts achieved similar CO conversions below 0 °C and complete CO conversion at 30 °C.

Additionally, these authors investigated the Preferential Oxidation of CO (PROX), an important reaction for reducing CO concentration in excess hydrogen to an acceptable level for fuel cell operation. In this context, both CO conversion and $CO_2$ selectivity decreased as the reaction temperature increased due to the competitive oxidation of $H_2$.

### 2.5.3 $H_2O_2$ Synthesis

The synthesis of hydrogen peroxide ($H_2O_2$) holds paramount importance in both industrial and scientific contexts due to its range of applications. As a powerful and eco-friendly oxidant, $H_2O_2$ is instrumental in numerous industries, including paper and pulp, wastewater treatment, textile, electronics, and pharmaceuticals, where it serves as a bleaching agent, disinfectant, and reactant in various chemical processes.[156, 157] Currently,

over 95% of the world's $H_2O_2$ is manufactured through the sequential hydrogenation and oxidation of alkyl anthraquinone (known as the AO process), a method that has remained largely unchanged since the 1940s.[156] This dated technology involves multiple unit operations, generates substantial waste, and demands a significant energy input, consequently undermining its sustainability and elevating production costs.[158] Considering both environmental and economic perspectives, the direct synthesis of $H_2O_2$ from $H_2$ and $O_2$ in the liquid phase, particularly under mild conditions (e.g., at or below room temperature and atmospheric pressure), represents an appealing alternative to the current AO process.[158, 159] In the direct process, the development of an efficient catalytic system is critical to simultaneously enhance yield and selectivity, and notable advancements have been realized through the utilization of Pd.[159-161] Moreover, the application of supported Au-based bimetallic catalysts in $H_2O_2$ synthesis has attracted much attention.[162-164] These catalysts, where Au nanoparticles are combined with another metal, have demonstrated remarkable catalytic performance in the environmentally friendly and sustainable production of $H_2O_2$. By enhancing the catalytic activity, these bimetallic catalysts offer the potential to transform the traditional, energy-intensive, and byproduct-laden methods of $H_2O_2$ production. Their ability to improve selectivity, increase efficiency, and resist deactivation processes, such as metal particle sintering or poisoning, makes them a promising avenue for achieving more sustainable $H_2O_2$ synthesis.

Hutchings et al.[165] investigated the direct synthesis of $H_2O_2$ from $H_2$ and $O_2$ using a AuPd bimetallic catalyst system supported on $TiO_2$. In this study, two distinct methods, namely impregnation and deposition-precipitation, were employed to create the catalysts. These catalysts included monometallic Au and Pd, as well as various combinations of Au and Pd supported on $TiO_2$, all maintaining a 5% total metal loading. Subsequently, the catalysts underwent calcination at 400 °C. Catalyst testing was conducted using a stainless-steel autoclave at a temperature of 2 °C. The autoclave was filled with a mixture of 5% $H_2/CO_2$ and 25% $O_2/CO_2$ to establish a hydrogen-to-oxygen ratio of 1:2 at a total pressure

of 3.7 MPa. Notably, the results from the $H_2O_2$ production reaction favored the catalyst prepared via the impregnation method over the one prepared using the deposition-precipitation method. Among the catalysts calcined at 400 °C and prepared through impregnation, the bimetallic AuPd catalysts exhibited a superior yield of $H_2O_2$ compared to pure Au and Pd catalysts. The introduction of Pd to Au substantially improved the catalytic performance for $H_2O_2$ synthesis, with an optimal Pd-Au composition yielding a significantly higher rate of $H_2O_2$ production than that observed for the pure Pd catalyst, which itself was notably more active than pure Au. The most favorable outcomes were observed for the 2.5 wt% Au/2.5 wt% Pd/$TiO_2$ catalyst.

Han et al.[157] conducted an investigation into the promotional effects of Au on the direct synthesis of $H_2O_2$ from $H_2$ and $O_2$ using silica-supported Pd-Au alloy catalysts. They prepared these catalysts using the incipient wetness method, involving the use of an aqueous solution containing $PdCl_4^{2-}$ and $AuCl_4^{-}$ ions, followed by a reduction with $H_2$. The loading of Pd was consistently maintained at 3.3 wt %, while the content of Au was varied, ranging from 0.37 wt % to 19.2 wt %, the support being fumed $SiO_2$. The results of the $H_2O_2$ synthesis study revealed that the pure Pd catalyst exhibited greater reactivity than pure Au, implying that $H_2O_2$ formation predominantly occurs on the Pd surface. In contrast, the AuPd bimetallic systems exhibited significantly enhanced activity and selectivity. Interestingly, the rate based on the mass of Pd metal exhibited a substantial increase with increasing Au concentration until the Au content reached Pd:Au 1:1.6 molar ratio ($Pd_1Au_{1.6}$), after which it declined by approximately 50% as the Au content continued to rise to Pd:Au 1:3.4 molar ratio ($Pd_1Au_{3.4}$). Excessive Au content, such as $Pd_1Au_{3.4}$, seemed to negatively impact catalytic reactivity, possibly due to the high coverage of Au on the Pd surface, hindering $O_2$ adsorption. The optimal Au:Pd molar ratio for synthesis was determined to be 1:1.6.

Geun et al.[166] conducted an investigation into the preparation of catalysts containing a bimetallic shell composed of AuPt on the surface of Pd nanocubes (AuPt@Pd), which

were subsequently employed as catalysts for the direct synthesis of $H_2O_2$. The preparation of these AuPt@Pd core-shell nanoparticles involved a direct seed-mediated growth method, utilizing PVP and l-ascorbic acid as stabilizers and protective agents. In the process, an aqueous solution of $Na_2PdCl_4$ was dissolved in an aqueous KBr solution and heated at 80°C for 3 hours. Subsequently, an aqueous solution of l-ascorbic acid, $HAuCl_4$, and $K_2PtCl_4$ were simultaneously introduced into the mixture. After 5 hours of heating and cooling to ambient temperature, the resulting products were collected by centrifugation and washed with a DI water and acetone mixture. A series of catalyst samples was prepared, in which the mol% of Au and Pt (e.g., 2:1, 5:2.5, and 25:5) was varied. To enhance the reusability and recoverability of the AuPt@Pd core-shell nanoparticles, they were supported on $SiO_2$. Low magnification EDS mapping was employed to confirm the presence of the AuPt bimetallic shell on the Pd core surface.

The highest $H_2O_2$ selectivity, reaching 85%, was observed with a Pt/Au mol% ratio of 3.75:3.75. However, further increases in the ratio led to a gradual decline in $H_2O_2$ selectivity (70%, 50%, and 40% on AuPt@Pd 2.5:5.0, 1.9:5.6, and 1.5:6.0, respectively). In terms of the $H_2O_2$ production rate, the maximum rate (914.8 mmol $H_2O_2$ $g_{metal-1}$ $h^{-1}$) was achieved with a AuPt@Pd mol% ratio of 2.5:5.0, which improved both $H_2O_2$ selectivity and $H_2$ conversion. The findings suggested that higher proportions of Au enhance $H_2O_2$ selectivity, while increased Pt content reinforces $H_2$ dissociation, collectively enhancing catalytic activity.

## 2.6    Conclusion

Bimetallic catalysts, which are composed of two different metal components, play a pivotal role in catalysis by significantly improving catalytic activity, selectivity, and stability compared to their single-metal counterparts. This enhancement arises from the synergistic interplay between the two metals. Among bimetallic catalysts, those centered

around Au hold particular fascination due to the distinctive qualities of Au. Gold exhibits remarkable catalytic activity across a range of reactions and serves as an effective stabilizer for other metal nanoparticles such as Pd, Pt, Ag, Cu and more. The performance of Au-based bimetallic catalysts hinges on several critical factors, including the choice of the second metal, the Au-to-second-metal ratio, the structural arrangement of the bimetallic catalyst, and the size and shape of the nanoparticles involved. The applications of Au-based bimetallic catalysts span a diverse array of fields, encompassing environmental catalysis, energy conversion processes, chemical synthesis, biomedical applications, and advanced sensing technologies. These catalysts represent a pivotal facet of modern materials science and play a essential role in enabling groundbreaking advancements in a multitude of industries.

# CHAPTER 3. CATALYTIC OXIDATION OF SIMPLE BENZYLIC ALCOHOLS AND LIGNIN MODEL COMPOUND OVER Li-Al LAYERD DOUBLE HYDROXIDE SUPPORTED Au:Pd BIMETALLIC NANOPARTICLES

## 3.1    Introduction

### 3.1.1 Supported gold nanoparticles

In late 1970s, supported gold was demonstrated as the catalyst of choice for producing vinyl chloride monomer via the acetylene hydrochlorination reaction.[69, 73]Later, oxide-supported gold nanoparticles were introduced as an effective catalyst for low-temperature oxidations of $H_2$ and CO.[74] Since then, gold catalysis has become the subject of attention from both the academic and industrial research communities.[69] Generally, metal nanoparticles are unstable catalysts and show low catalytic activity due to aggregation, agglomeration, and even precipitation out of solution. Therefore, metal nanoparticles must usually be supported on solid surfaces.[68-70] During a catalytic reaction, supports can play either direct or indirect roles, such as providing specific defect sites and stabilizing metastable particles. The supports provide additional functionalities such as acidity or basicity to the overall supported metal catalyst and may transfer electrons between metal particles and support. All these factors have a significant impact on the catalytic properties of supported metal catalysts, and this is especially true for supported Au-based nanoparticle catalysts.[69]

In gold-catalyzed alcohol oxidation studies, an inorganic base such as NaOH or $Na_2CO_3$ is required to facilitate the formation of an alkoxide intermediate. Therefore, use of a basic support can avoid the need for adding these external bases. Song et al. studied three different materials, namely, LiAl-LDH, MgAl-LDH, and NiAl-LDH (LDH = layered double hydroxide) as supports for gold nanoparticles to demonstrate the effect of the support on the catalytic activity of Au. Depending on the surface sites on these supports, such as acidic and basic sites, their ability to promote reactant conversion can be tuned. In this work, Au-LiAl-LDH showed excellent selectivity and activity for the oxidation of benzylic alcohols with >99% conversion of 1-phenyl

ethanol. Moreover, this LiAl-LDH supported Au catalyst was applied to oxidize primary, secondary alcohols, and ß-O-4 lignin model dimers, exhibiting remarkable activity and selectivity to provide the corresponding carbonyl compounds with high yield. Furthermore, this catalyst was used for oxidation of ɣ-valerolactone (GVL) extracted lignin and kraft lignin and was able to produce a range of aromatic monomers in high yield. It was reported that hydrolysis of Au/LiAl-LDH oxidized lignin increased the degree of lignin depolymerization, with monomer yields achieving 40% for GVL extracted lignin.[167] Therefore, in the present work, gold functionalized LiAl-LDH was used for lignin depolymerization with modification of the catalyst, involving the alloying of Au with Pd. In this manner, an effort was made to reduce the loading of Au required and to increase the activity of the catalyst by selection of the optimal Au:Pd ratio.

### 3.1.2 Layered double hydroxide (LDH) supports

Over the past 20 years, various LDHs (Ni-Al LDH, Cu-Al LDH etc.), as well as Au nanoparticles supported on metal oxides ($TiO_2$, $CeO_2$, $Fe_2O_3$, $Co_3O_4$), have been shown to selectively catalyze aerobic oxidations of alcohols to the corresponding carbonyl compounds.[168] Hydrotalcite (HT) compounds, also known as LDHs, are composed of mixed hydroxides with interlayer spaces containing exchangeable anions. LDHs contain tunable surface basic sites, attaining high catalytic performance in reactions that require proton abstraction. Because of these qualities, LDH materials are used to catalyze various reactions such as deoxygenation, chemo-selective reduction, and oxidation.[169]

In general, LDHs can be prepared using simple co-precipitation methods. Other than hydrothermal synthesis, homogeneous precipitation and anion exchange methods are typically used to synthesize LDHs. The generalized formula to describe the chemical composition of such compounds is $[M^{II}_{1-x}M^{III}_x(OH)_2]A^{n-}_{x/n} \cdot mH_2O$. Structurally, LDHs resemble the mineral brucite, $Mg(OH)_2$, in which each $Mg^{2+}$ ion is octahedrally surrounded by six $OH^-$ ions (Figure 3.1).[71, 169]

A three-dimensional structure is formed by infinite sheets, which are formed as a result of the different octahedra sharing edges. These infinite sheets with hydroxide layers are stacked together by van der Waals forces and hydrogen bonding. The LDH structure differs to that of brucite in that $Mg^{2+}$ ions are partially replaced by cations with higher charge but similar radius (e.g., $Cr^{3+}$, $Al^{3+}$) causing the brucite-type sheets to become positively charged. This charge is balanced by anions such as carbonate, hydroxide, etc., which are located in the interlayer region.[169] The most well-known example is the mineral hydrotalcite, which has the chemical formula $[Mg_{0.75}Al_{0.25}(OH)_2].(CO_3)_{0.125}.0.5H_2O$. A variety of LDHs can be designed by changing the type of cations and relative proportions of the di-and tri-valent cations. Moreover, in some cases the monovalent lithium ion can be incorporated in the LDH structure, exemplified by $[LiAl_2(OH)_6]^+[An^-]_{1/n} \cdot mH_2O$.[167]
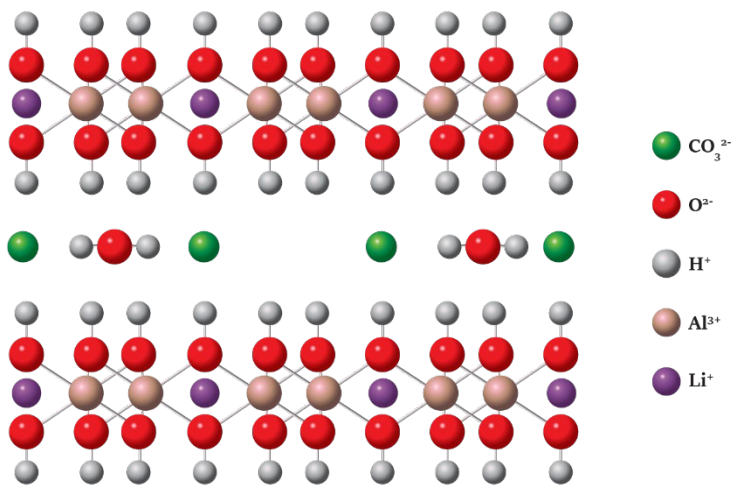


Figure 3.1· Representation of LDH structure[170]

### 3.1.3 Au-Pd bimetallic nanoparticles

Bimetallic nanoparticles can enhance the activity and selectivity of gold-based catalysts towards desired products due to synergetic electronic interactions between the two different metal atoms

in the individual nanoparticles.[71] Indeed, catalytic properties such as activity and selectivity can frequently be tuned by changing the composition of bimetallic nanoparticle catalysts. For instance, in the selective oxidation of primary alcohols to aldehydes, bimetallic Au–Pd catalysts showed superior activity and selectivity compared to catalysts based on either pure Au or pure Pd.[71, 171] Other than the selective oxidation of alcohols, the use of bimetallic Au–Pd catalysts has been expanded to other catalytic reactions such as the synthesis of vinyl acetate, CO oxidation, direct synthesis of hydrogen peroxide, and $N_2O$ decomposition.[171]

The design and utilization of Au–Pd catalysts has been thoroughly investigated by the groups of Hutchings and Kiely.[172] They synthesized supported Au–Pd catalysts using an impregnation method. The resulting materials exhibited excellent catalytic activity for a diverse range of reactions such as the direct synthesis of hydrogen peroxide and alcohol and polyol oxidation. In the case of hydrogen peroxide synthesis, the best catalytic performance was obtained using an Au–Pd/$TiO_2$ catalyst that was prepared by an impregnation method and calcination at 400 °C. The catalytic activity of the Au–Pd/$TiO_2$ was higher by a factor of 2–9 with respect to the monometallic catalysts. In addition, the bimetallic Au–Pd catalysts exhibited an enhancement in stability and re-usability relative to their monometallic counterparts. In alcohol oxidation, Hutchings and co-workers reported that high catalytic efficiency could be achieved with Au–Pd/$TiO_2$ catalysts prepared by simple impregnation. From a study of the effect of the Au: Pd weight ratio, it was empirically determined that a 1:1 ratio produced the highest catalytic activity, whereas Au-rich catalysts showed the highest selectivity in the oxidation of benzyl alcohol.[82]

Venezia et al. have studied silica-supported bimetallic Au–Pd catalysts with different ratios for CO oxidation.[153, 171] The authors stated that a synergistic effect between the two metals was not observed on silica because of the low catalytic activity of Au/$SiO_2$ resulting from the large Au particle size. They also reported that the monometallic Pd catalyst was much more active than the monometallic Au catalyst, while Pd-rich catalysts behaved quite similarly to Pd. Prati and Ma et al. also studied homogeneously dispersed Au–Pd bimetallic catalysts supported on carbon and found an enhancement of the reaction rate compared to monometallic Au and Pd catalysts.[71, 173,]

[174] Furthermore, they observed that the alloying of Pd and Au prevented the leaching of Pd from the catalyst support.[71]

Surface scientists have also studied Au–Pd interactions and CO oxidation under well-defined conditions. Goodman and co-workers found that addition of Pd to Au improved its capacity to activate dioxygen, forming an active catalyst for CO oxidation. They also observed that the surface composition of AuPd (100) planes changed significantly under reaction conditions; for example, high reaction temperatures cause Au to segregate at the surface. Meanwhile, the low binding energies of CO on the Au–Pd alloys resulted in decreased CO residence times on the surface at high temperatures.[175] Peter et al. studied $TiO_2$-supported 1 wt% bimetallic Au–Pd catalysts prepared by a sol-immobilization method for cinnamyl alcohol oxidation at 120 °C under oxygen. They found that conversion and selectivity varied depending on the Au-Pd metal ratio, the most active catalyst being Au: Pd = 3:1 by weight.[176]

Herein, we introduce heterogeneous catalysts utilizing Li-Al LDH supported AuPd bimetallic nanoparticles in different molar ratios for simple benzylic alcohols and β-O-4 linked lignin model dimer oxidation. These bimetallic catalysts are prepared using a sol-immobilization method. First, the catalytic system is used to oxidize a series of simple benzylic alcohols into their ketones under mild conditions. The most effective catalysts identified are then applied to GVL-extracted maple lignin with the aim of assessing their ability to depolymerize the lignin.

## 3.2    Experimental Information

### 3.2.1 Materials and methods

Commercially available reagents were used as received. $Al(NO_3)_3 \cdot 9H_2O$ (99 wt.%), 1-phenylethanol (98 wt.%), acetophenone (99 wt.%), benzyl alcohol (99.8 wt.%), vanillic acid (97 wt.%), sinapic acid (98 wt.%), pyridine-d5 (99.5 wt.%), polyvinylpyrrolidone (PVP) and $HAuCl_4 \cdot 3H_2O$ (99.9 wt.% trace metal basis) were purchased from Sigma Aldrich. Syringaldehyde (98 wt.%), 4-hydroxy-3-methoxycinnamic acid, $Pd(NO_3)_2 \cdot xH_2O$ (metal basis 47.5 wt.% Pd),

benzaldehyde (99 wt.%), n-dodecane (99 wt.%), $KBH_4$ (98 wt.%), N,O-bis(trimethylsilyl)trifluoroacetamide (BSTFA) (99.9 wt.%), and $LiOH·H_2O$ (99 wt.%) were purchased from Alfa Aesar. $K_2CO_3$ (99.0 wt.%) and $Na_2CO_3$ (99.5 wt.%) were purchased from Fisher Scientific. 4-Methyoxyphenyl methyl carbinol was purchased from Oakwood Chemical. 4'-Methoxyacetophenone, vanillin (99 wt.%), dimethyl sulfoxide-d6 (99.9 wt.%), $NaBH_4$ (99 wt.%) and gamma-valerolactone (98 wt.%) were purchased from Acros Organics. Dimethylformamide (DMF), tetrahydrofuran (THF) and hydrochloric acid (36.5-38.0 wt.%) were purchased from BDH VWR Chemicals. p-Anisic acid was purchased from TCI America.

## 3.3    Catalyst Preparation

### 3.3.1  Synthesis of Li-Al LDH support

Li-Al (1:2) LDH was prepared according to a literature protocol.[177] An aqueous solution of $Al(NO_3)_3·9H_2O$ (250 ml, 0.4 M) was added dropwise to 600 ml of a mixture of $LiOH·H_2O$ (1.5 M) and $Na_2CO_3$ (0.08 M) in deionized water at room temperature. Vigorous stirring was maintained throughout the 60 min addition period. The mixture was left to age under continuous stirring at 75°C overnight. A series of centrifuging/ decanting/ washing steps with deionized water were applied to the resulting slurry until the washings attained a pH of 7. The solid was then dried at 60 °C in a vacuum oven for 24 h.

### 3.3.2  Synthesis of LDH supported AuPd bimetallic nanoparticles

LDH-supported AuPd bimetallic nanoparticle catalysts with different Au:Pd ratios, namely, 7:3, 1:1, and 3:7, as well as monometallic Au and Pd nanoparticle catalysts, were prepared according to a literature protocol.[71] The detailed preparation procedure for the bimetallic catalyst with Au:Pd molar ratio of 1:1 is described below.

Two solutions of HAuCl$_4$ (0.0389 g, 0.10 mmol) and Pd(NO$_3$)$_2$·xH$_2$O (0.0221 g, 0.10 mmol) were prepared separately in 50 mL of deionized water. Subsequently, the two solutions were mixed and stirred together for a duration of 2 min. Next, an aqueous polyvinyl alcohol (PVP) solution (5 ml, 1 wt%, PVP/(Au + Pd) (wt/wt) = 1.2) was added. A freshly prepared aqueous solution of NaBH$_4$ (10 mL, 0.0374 g,1.0 mmol) was then added, resulting in a dark-brown solution. After 30 min of sol generation, the colloid was immobilized by adding 3 g of Li-Al LDH support under vigorous stirring. After 1 h the slurry was filtered, the solid was washed thoroughly with hot distilled water and was dried at 50 °C in a vacuum oven for 24 h. This sample is denoted as Au$_1$Pd$_1$/Li-Al LDH.

The required amount of support material was calculated to achieve a total final metal loading of 1% wt. Other bimetallic catalysts with different Au/Pd molar ratios were prepared as stated above, keeping the total metal loading of 1% wt. Monometallic catalysts containing only Au or Pd were prepared using a similar methodology, and these are denoted as 1% Au/Li-Al LDH and 1% Pd/Li-Al LDH, respectively.

## 3.4    Catalyst Characterization

Surface area and pore volume measurements of samples were performed according to the Brunauer−Emmett−Teller (BET) method by nitrogen adsorption at -196 °C using a Micromeritics Tri-Star system. Samples were outgassed overnight at 160 °C under vacuum prior to the measurements. Elemental analysis of samples was performed using inductively-coupled plasma mass spectrometry (ICP-MS). Powder X-ray diffraction (XRD) measurements were performed on a Phillips X'Pert diffractomer using Cu Kα radiation (λ=1.5406 A) and a step size of 0.02°. Transmission electron microscopy (TEM) studies were conducted using a Talos F200X microscope. Particle size analysis was conducted using ImageJ software, particle diameters of 200 metal particles being measured for each sample. XPS measurements were performed on a Thermo

Scientific K-alpha X-ray photoelectron spectrometer using a monochromatic Al Kα source. The C 1s line (284.8.0 eV) was employed as a binding energy standard.

## 3.5 Synthesis of β-O-4 Linkage Lignin Model Compounds
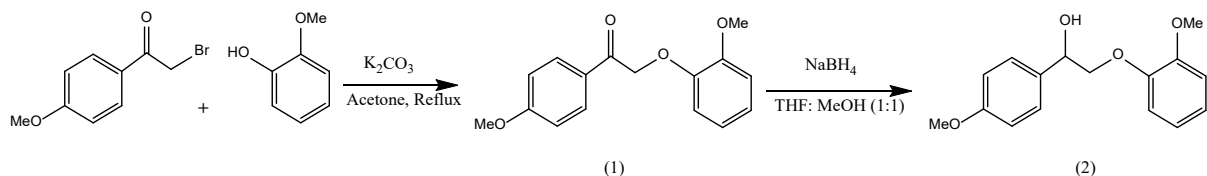


Scheme 3.1 Synthesis of β-O-4 linkage lignin model compounds

### 3.5.1 Synthesis of 2-(2-methoxyphenoxy)-1-(4-methoxyphenyl)-ethanone (1)

Compound (1) was prepared according to a literature procedure using guaiacol and 4'-methoxy-2-bromoacetophenone.[167] While stirring a solution of $K_2CO_3$ (20 g, 0.14 mol) and guaiacol (16 g, 0.13 mol) in acetone (100 ml), 2-bromo-4'-methoxyacetophenone (22 g, 0.11 mol) was added. After that, the reaction mixture was stirred at reflux temperature (80 °C) overnight. The reaction mixture was filtered, dried over anhydrous $MgSO_4$, and concentrated in vacuo. The crude product was recrystallized from ethanol. Yield: 23.40 g (78 %).

### 3.5.2 Synthesis of 4-methoxy-α-[(2-methoxyphenoxy)methyl]-benzenemethanol (2)

Compound (1) (5 g, 18 mmol) was dissolved in a mixture of THF: MeOH (50 ml, 2:1 v/v). Sodium borohydride (1.5 g, 39 mmol) was added in portions to the reaction mixture under stirring at 0 °C. The mixture was left to stir overnight at room temperature. The mixture was then concentrated in vacuo and diluted with deionized water (50 ml). After that, the mixture was extracted with dichloromethane (3 x 30 ml). The combined organic extracts were dried over anhydrous $MgSO_4$ and concentrated in vacuo. The crude product was recrystallized from ethanol to afford the pure alcohol (2). Yield: 3.8 g (76%).

### 3.6 Oxidation of Simple Benzylic Alcohols

Oxidation of benzylic alcohols was conducted in a 100 mL 3-neck round-bottom flask using a Radleys Starfish reactor to which the alcohol (1 mmol), catalyst (50 mg), dodecane (1 mmol, internal standard) and DMF (10 ml) were added. The alcohol was oxidized under flowing $O_2$ (10 mL/min) at 80 °C and 500 rpm stirring. An aliquot (150 μL) was taken periodically from the reaction mixture, to which 1 mL THF was added in a GC vial. The sample was then analyzed by gas chromatography-mass spectrometry (GC-MS).

### 3.7 General Procedure for Aerobic Oxidation of Lignin Model Compound

The oxidation of lignin model compound was conducted in a 100 mL 3-neck round-bottom flask using a Radleys Starfish reactor. The substrate (1 mmol), catalyst (100 mg), dodecane (1 mmol) and 10 mL of dimethylformamide (DMF) were added to the 3-neck round-bottom flask. The lignin model compound was oxidized under flowing $O_2$ (10 mL/min) at 120 °C and 500 rpm stirring. An aliquot (150 μL) was taken periodically from the reaction mixture, to which 1 mL THF was added in a GC vial. The sample was then analyzed by GC-MS.

### 3.8 Product Analysis

The conversion of the substrate, product yield and selectivity were monitored using GC-MS on an Agilent 7890 GC with a tandem Agilent 5975C MS detector. A DB-1701 column was used (60 m × 0.25 mm × 0.25 μm or 15 m × 0.25 mm × 0.25 μm as appropriate). Helium was used as carrier gas with the flow rate set to 1 mL/min for the 60 m column and 0.5 mL/min for the 15 m column. The inlet temperature for the 60 m column was maintained at 280 °C, with a method set to 45 °C for 3 min, ramp to 280 °C at 4 °C/min, and hold for 10 min. The inlet temperature for the 15 m column was maintained at 280 °C with a temperature ramp of 60 °C to 80 °C at 2 °C/min, then to 110 °C at 3 °C/min, followed by a 20 °C/min ramp to 190 °C, and finally a 2 °C/min ramp

to 280 °C. All analyses were quantified using a single point GC-MS internal standard method by obtaining internal response factors of all starting materials and products using n-dodecane as standard. All aliquots of monomers and their oxidation products, and respective calibration samples, were derivatized using BSTFA prior to GC-MS analysis.

## 3.9 Results and Discussion

### 3.9.1 Li-Al-LDH support characterization

The Li-Al LDH support was prepared according to a literature coprecipitation method requiring slow addition of an aqueous solution of $Al(NO_3)_3$ to an aqueous mixture of LiOH and $Na_2CO_3$.[1] Powder X-ray diffraction was used to determine the crystallinity and the domain size of the Li-Al LDH product. The X-ray diffractogram of the Li-Al LDH is presented in Figure 3.2, with the diffraction peaks being indexed according to the work of Sissoko et al.[178]



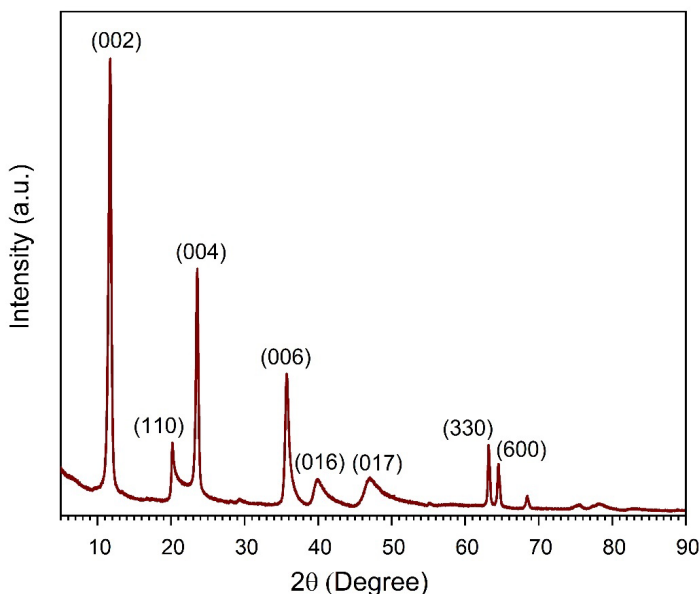Figure 3.2 Powder X-ray diffraction pattern of Li-Al LDH

These results are consistent with the presence of crystalline $[Al_2Li(OH)_6]_2CO_3.nH_2O$, as the observed d-spacings are in agreement with published values which are shown in Table 3.1.[178]

Applying the Scherr equation to the (002) peak, an average crystallite size of 18.49 nm in the 00*l* direction was calculated for the support.

Table 3.1 Indexing of powder pattern for $[Al_2Li(OH)_6]_2CO_3.nH_2O$

| hkl | d-spacing values (Å) | |
|-----|----------|-----------|
|     | Observed | Reference |
| 002 | 7.57     | 7.56      |
| 110 | 4.35     | 4.35      |
| 004 | 3.77     | 3.77      |
| 006 | 2.51     | 2.51      |
| 016 | 2.24     | 2.25      |
| 017 | 1.91     | 1.98      |
| 330 | 1.47     | 1.47      |
| 600 | 1.18     | 1.44      |

Inductively coupled plasma-mass spectrometry (ICP-MS) was used to determine the elemental composition of the LDH and $N_2$ adsorption and desorption isotherms were used to characterize the textural properties of the Li-Al LDH, the results being listed in Table 3.2. According to elemental analysis (also in Table 3.2), the Li:Al molar ratio in the support is reasonably close to the expected value of 1:2.

The surface area and structure of the support are important for its adsorption capacity. Indeed, previous studies have shown that several parameters, such as specific surface area, the chemical composition, and morphology of the support, can affect its adsorption performance.[179] According to the results in Table 3.2, the measured BET surface area of this LDH support is higher than that of typical values reported in the literature (which are typically in the range of 70 to 100 $m^2g^{-1}$).[177] A high  surface area support should be beneficial for stabilizing a high dispersion of metal nanoparticles and for the adsorption of reactants.

Table 3.2 Summary of ICP-MS and N₂ physisorption results for Li-Al LDH

| ICP-MS | | | BET surface area (m$^2$g$^{-1}$) | Average pore diameter (nm) | Average pore volume (cm$^3$g$^{-1}$) |
|---|---|---|---|---|---|
| Al (wt%) | Li (wt%) | Li:Al molar ratio | | | |
| 27.01 | 3.23 | 1:2.15 | 170 | 5.0 | 0.11 |

## 3.9.2 Catalyst characterization

Catalysts with different mole ratios of Au:Pd were synthesized by sol-immobilization methods. Polymer-stabilized Au-Pd bimetallic catalysts have been reported for the oxidation of benzyl alcohol.[71, 171] Hence, the same sol-immobilization method was used to prepared Au-Pd/Li-Al LDH catalysts to investigate their ability to catalyze oxidative depolymerization of lignin.

Prepared catalysts were analyzed using ICP-MS and N₂ physisorption to determine the loadings of Au and Pd present and to determine total surface area and pore volume, respectively. These results are summarized in Table 3.3. According to ICP-MS, for each catalyst the elemental composition was close to the expected value.

Table 3.3 Summary of ICP-MS and N₂ physisorption results for prepared catalysts

| Sample | ICP-MS (wt.%) | | Au: Pd Molar Ratio | BET Surface Area (m$^2$g$^{-1}$) | Average pore diameter (nm) | Average pore volume (cm$^3$g$^{-1}$) |
|---|---|---|---|---|---|---|
| | Au | Pd | | | | |
| Au/Li-Al LDH | 1.01 | - | - | 174 | 3.9 | 0.09 |
| Au₇Pd₃/Li-Al LDH | 0.86 | 0.19 | 7.33: 3:00 | 202 | 4.1 | 0.11 |
| Au₁Pd₁/Li-Al LDH | 0.62 | 0.33 | 1.01:1.00 | 179 | 4.3 | 0.12 |
| Au₃Pd₇/Li-Al LDH | 0.48 | 0.63 | 2.88: 7.00 | 187 | 4.9 | 0.13 |
| Pd/Li-Al LDH | - | 0.92 | - | 182 | 6.3 | 0.20 |

According to Fang et al., the particle size of Au NPs plays a vital role in catalytic reactions.[74] In that study, optimal catalyst activity was observed with metal particle sizes of < 4

nm. Valden et al. reported that the particle size of the Au NPs should be below 3.5 nm to obtain an optimal electronic transition between the metal and the support due to the quantum size effect of the Au NPs.[180] When the size of the Au NPs becomes smaller, the metal shows increased atomic properties as compared to bulk properties due to the existence of discrete energy levels for the Au NPs. Consequently, small Au NPs with higher dispersion provide more coordinatively unsaturated sites than larger, bulk-like particles and accept electron density from the basic Li-Al LDH support.[167] STEM images and particle size distributions (PSDs) of the prepared Li-Al LDH supported Pd, Au, and Au-Pd NPs are shown in Figure 3.3.
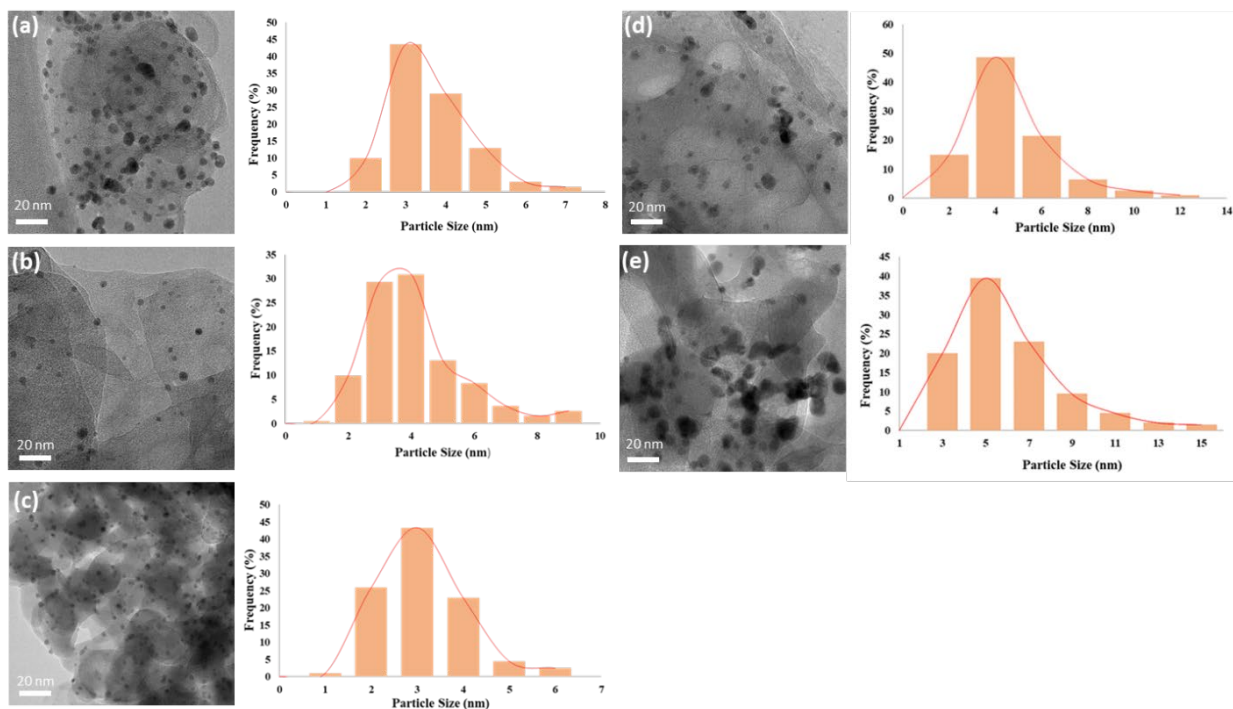


Figure 3.3 TEM images and particle size distribution for catalysts: (a) Au/Li-Al LDH, (b) $Au_7Pd_3$/Li-Al LDH, (c) $Au_1Pd_1$/Li-Al LDH, (d) $Au_3Pd_7$/Li-Al LDH and (e) Pd/Li-Al LDH

The average size of the particles in each sample was measured using TEM, the average size of Au and Pd NPs being found to be 3.1±0.4 nm and 5.0±0.5 nm, respectively, while the bimetallic Au-Pd NPs had average particle sizes of 2.6±0.1 nm (Au:Pd = 1:1), 3.6±0.6 nm (Au:Pd

= 7:3), and 3.7±0.9 nm (Au:Pd = 3:7). It was observed that Pd/Li-Al LDH contained aggregates of metal particles that are considerably larger than in the other samples, while the $Au_1Pd_1$/Li-Al LDH catalyst exhibited the best metal dispersion compared to the other samples.

Compositional analysis for Au and Pd was carried out using transmission electron microscopy-energy dispersive spectroscopy (TEM-EDS) for approximately 50 individual metal particles in the $Au_7Pd_3$/Li-Al LDH and $Au_1Pd_1$/LiAl LDH catalysts. The quantification of metal content in each particle is presented in Figure 3.4.
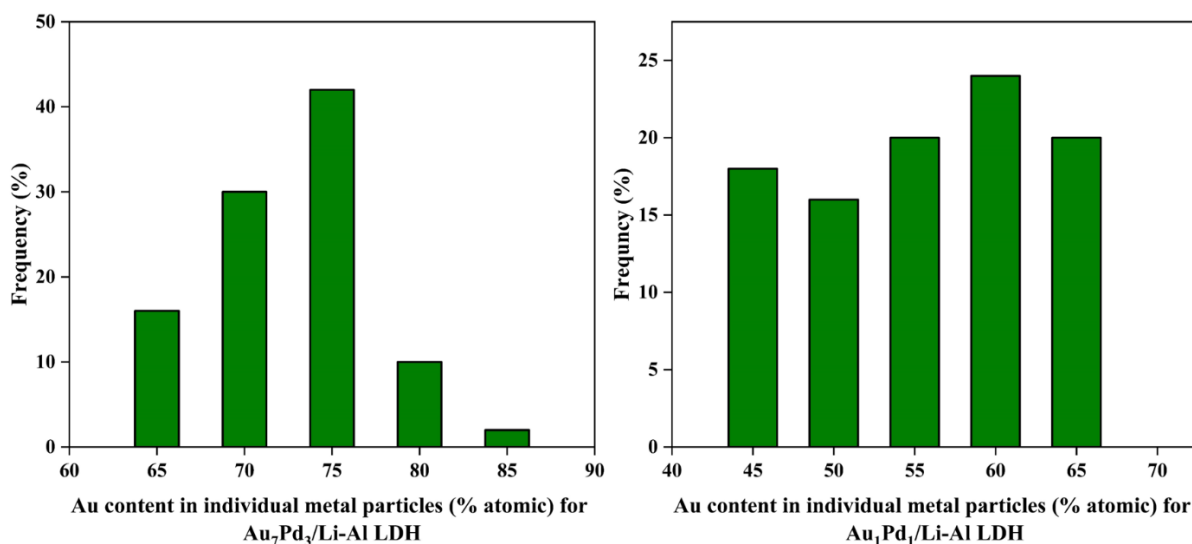


Figure 3.4 Metallic composition histograms for $Au_7Pd_3$/Li-Al LDH and $Au_1Pd_1$/Li-Al LDH

The results obtained from TEM-EDS indicate that the metal particles in the $Au_7Pd_3$/Li-Al LDH and $Au_1Pd_1$/LiAl LDH catalysts exhibit compositions closely resembling those of the bulk formulation. In the case of the $Au_7Pd_3$/Li-Al LDH catalyst, approximately 88% of the particles contain Au contents ranging from 65% to 75%, a range that closely matches the expected Au content in the bulk sample (70%). Conversely, within the $Au_1Pd_1$/LiAl LDH catalyst, 56% of the particles exhibit Au content ranging from 45% to 55%, which aligns with the expected Au content in the bulk sample (50%). Additionally, there is an observation of 44% of Au-rich particles containing around 55% to 65% Au.

The Au–Pd bimetallic NPs were characterized by XPS to explore possible electronic interactions between Au and Pd. The Au 4f and Pd 3d XPS spectra are shown in Figures 3.5 and 3.6, respectively. As shown in Figure 3.5, Au/Li-Al LDH, $Au_7Pd_3$/Li-Al LDH, $Au_1Pd_1$/Li-Al LDH and $Au_3Pd_7$/Li-Al LDH catalysts exhibit Au $4f_{7/2}$ binding energies (BE) at 82.9 eV, 82.9 eV, 83.0 eV and 83.1 eV, respectively. According to Wang et al.,[181] these values are all lower than the BE of 84.7 eV for bulk gold. The downshift of the Au $4f_{7/2}$ binding energy for these catalysts indicates that Au nanoparticles are negatively charged, which may be associated with electron transfer from the support to the Au nanoparticles.[167, 182] According to Pauling's scale of electronegativity, the Au 4f peaks should shift toward the low binding energy direction when the Pd content is increased.[133] However, in this study, there were no significant changes in the Au $4f_{7/2}$ binding energy with Pd content. According to Tsunoyama et al,[183] negatively charged Au nanoparticles are beneficial for the aerobic oxidation of alcohols because the negatively charged Au nanoparticles are effective for the activation of molecular oxygen. The resulting negatively charged superoxide facilitates β hydrogen elimination from the alcohol, which is the rate determining step in alcohol oxidation.[133]
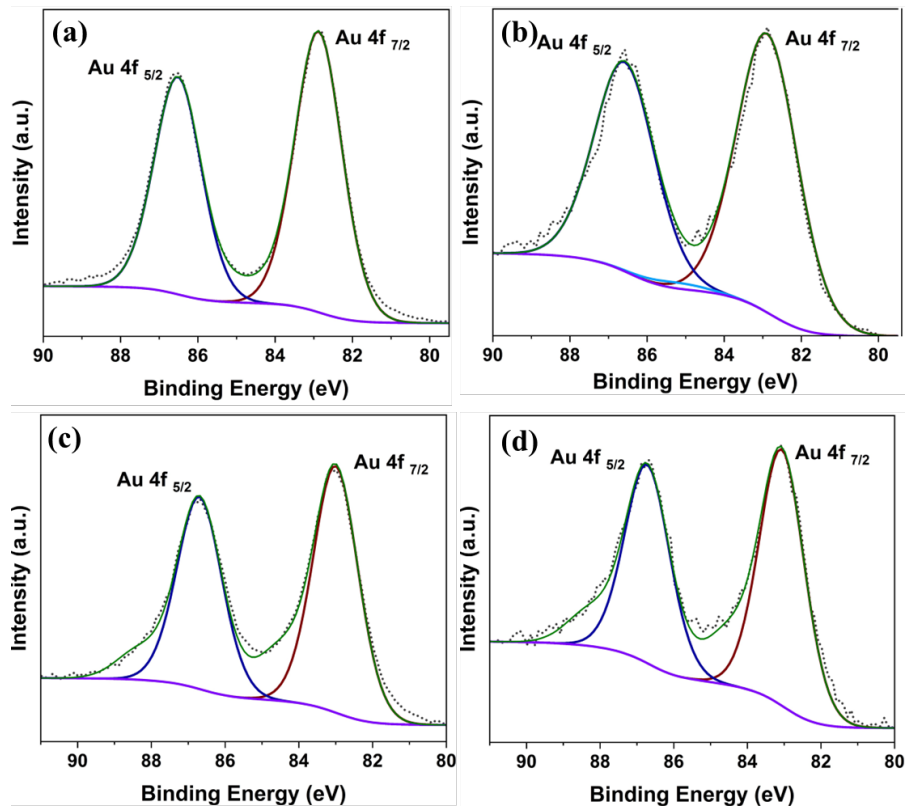
Figure 3.5 XPS Au 4f spectra of (a) Au/Li-Al LDH, (b) Au$_7$Pd$_3$/Li-Al LDH, (c) Au$_1$Pd$_1$/Li-Al LDH, and (d) Au$_3$Pd$_7$/Li-Al LDH

According to Figure 3.6, which depicts the Pd 3d XPS spectra, peak fitting for the monometallic Pd/Li-Al LDH catalyst yields Pd 3d$_{5/2}$ binding energies of 335.3 eV and 336.5 eV, which are close to the binding energies of the metallic Pd (335.5 eV)[184] and Pd$^{2+}$ (as PdO, 336.3 eV)[185] oxidation states. From this it can be concluded that both Pd oxidation states were present, as was the case for the bimetallic catalysts. In the latter case, XPS results suggest that the Pd is alloyed with Au, the Pd 3d$_{5/2}$ binding energies for metallic Pd and Pd$^{2+}$ tending to decrease relative to Pd/Li-Al LDH which may be indicative of two-way charge transfer between Au and Pd. Literature reports indicate that the electronic interaction between Au and Pd proceeds in both directions, with Au gaining *sp* type electrons and losing *d* electrons, while Pd loses *sp* electrons and gains *d* electrons.[186, 187] Fitting of the Pd 3d$_{5/2}$ signal for Au$_3$Pd$_7$/Li-Al LDH and Au$_1$Pd$_1$/Li-Al

LDH gave binding energies of 334.7 eV and 334.3 eV for the $Pd^0$ component, while the $Pd^{2+}$ component was observed at 336.2 eV, and 335.9 eV, respectively. The downshift of the Pd $3d_{5/2}$ BE for these catalyst samples is consistent with charge transfer from the Au to the Pd in the nanoparticles, albeit a shift in BE was not observed for the Au.[188, 189] For the $Au_7Pd_3$/Li-Al LDH catalyst such a shift in the Pd $3d_{5/2}$ BE was not observed, the Pd $3d_{5/2}$ XPS region displaying similar binding energies (335.3 eV and 336.7 eV) to the Pd/Li-Al LDH sample.
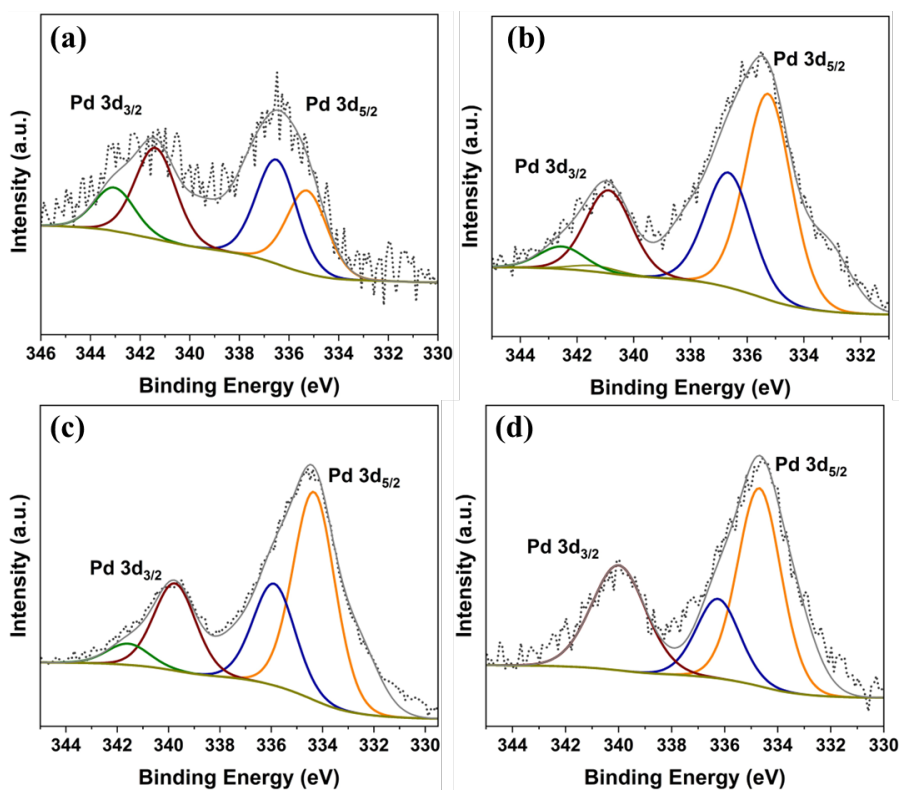


Figure 3.6 XPS Pd 3d spectra of (a) Pd/Li-Al LDH, (b) $Au_7Pd_3$/Li-Al LDH, (c) $Au_1Pd_1$/Li-Al LDH and (d) $Au_3Pd_7$/Li-Al LDH.

Table 3.4 summarizes the XPS results for the bimetallic catalysts. Based on the measured atomic concentrations, the Au:Pd ratio of the $Au_7Pd_3$/Li-Al LDH is slightly lower than the ratio calculated from ICP analysis. Since XPS is a surface-sensitive technique, these results suggest that Pd nanoparticles were enriched on the surface of the catalyst. On the other hand, the Au:Pd ratio

of the Au$_3$Pd$_7$/Li-Al LDH catalyst is higher than the bulk value, indicating that the metal nanoparticles were enriched in Au on the Au$_3$Pd$_7$/Li-Al LDH sample.

Table 3.4 Summary of XPS results for bimetallic catalysts with different Au:Pd molar ratios

| Catalyst | Binding energy (eV) | | | Au:Pd atomic ratio |
|---|---|---|---|---|
| | Au 4f$_{7/2}$ | Pd 3d$_{5/2}$ | | |
| | | Pd$^0$ | Pd$^{2+}$ | |
| Au/Li-Al LDH | 82.9 | - | - | - |
| Au$_7$Pd$_3$/Li-Al LDH | 82.9 | 335.3 (64%) | 336.7 (36%) | 7.0:4.1 |
| Au$_1$Pd$_1$/Li-Al LDH | 83.0 | 334.3 (67%) | 335.9 (33%) | 1.0:0.9 |
| Au$_3$Pd$_7$/Li-Al LDH | 83.1 | 334.7 (74%) | 336.2 (26%) | 3.0:3.6 |
| Pd/Li-Al LDH | - | 335.3 (46%) | 336.5 (54%) | - |

## 3.10    Oxidation of Benzylic Alcohols

The catalytic activity of the AuPd/Li-Al LDH bimetallic catalysts towards the oxidation of simple benzylic alcohols was measured at 80 °C under flowing oxygen (1 atm), the products of the reaction being determined using GC-MS at intervals of 1 h. Initial studies focused on the AuPd/Li-Al LDH bimetallic catalysts shown in Table 3.5 with the goal of comparing their ability to oxidize 1-phenylethanol.

Table 3.5 Oxidation of 1-phenylethanol to acetophenone using AuPd/Li-Al LDH catalysts

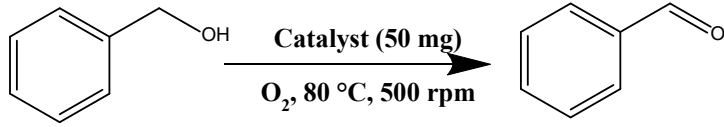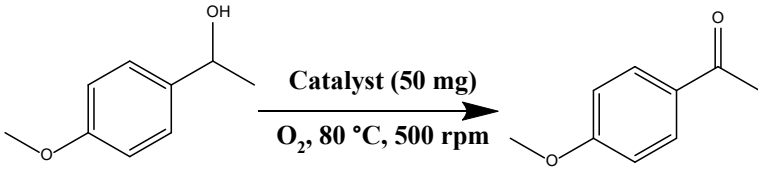| Entry no. | Catalyst | Acetophenone yield (%)[b] | | | | Selectivity (%)[b] | TOF (h$^{-1}$)[c] |
|---|---|---|---|---|---|---|---|
| | | 1 h | 2 h | 3 h | 4 h | | |
| 1 | Au/Li-Al LDH | 16 | 21 | 40 | 42 | >99 | 2360 |
| 2 | Au$_7$Pd$_3$/Li-Al LDH | 37 | 59 | 92 | >99 | >99 | 5385 |
| 3 | Au$_1$Pd$_1$/Li-Al LDH | 45 | 89 | 94 | >99 | >99 | 6558 |
| 4 | Au$_3$Pd$_7$/Li-Al LDH | 3 | 6 | 28 | 45 | >99 | 843 |
| 5 | Pd/Li-Al LDH | 1 | 1 | 1 | 3 | >99 | 85 |

[a]1-Phenylethanol (1 mmol), catalyst (0.100 mg), dimethylformamide (10 mL), 80 °C, p = 1 atm. O$_2$ (10 mL min$^{-1}$). [b] Conversion and selectivity were determined by GC-MS using dodecane as internal standard and the reported values are from the average of two runs. [c] TOF values are based on the number of surface metal (Au and Pd) atoms calculated for the mean particle size found via TEM analysis. Note: a control experiment conducted without catalyst showed no conversion.

Table 3.5 shows that the Pd to Au ratio exerts a significant effect on catalyst activity in the generation of acetophenone from 1-phenylethanol. The Au/Li-Al LDH catalyst displayed significantly higher oxidation activity than Pd/Li-Al LDH. However, when Pd was incorporated into the Au catalyst, the oxidation activity increased. This points towards a synergistic effect given that the bimetallic catalysts give higher conversions than the sum of the conversions given by the monometallic Au and Pd catalysts. According to entries 2 and 3 in the table, Au$_1$Pd$_1$/Li-Al LDH gave superior conversion to Au$_7$Pd$_3$/Li-Al LDH during the first 2 h of reaction. However, these two catalysts provided almost the same conversion from 3 h onwards. When the Pd content is further increased the oxidation activity of the catalyst decreases. This could be because of larger bimetallic particles and/or the smaller number of Au atoms present in the Au$_3$Pd$_7$/Li-Al LDH catalyst than the Au$_1$Pd$_1$/Li-Al LDH, Au$_7$Pd$_3$/Li-Al LDH and Au/Li-Al LDH catalyst samples.

In summary, Au$_7$Pd$_3$/Li-Al LDH, and Au$_1$Pd$_1$/Li-Al LDH showed the highest activity in the oxidation of 1-phenylethanol. Table 3.6 depicts the results of the oxidation of two other simple

benzylic alcohols using these catalysts under the same reaction conditions used for the oxidation of 1-phenylethanol. From these results it is evident that the reaction rate increases when the benzylic alcohol bears a methoxy functional group that is strongly electron donating in the electronically favorable *para*-position. It should also be noted that in the case of benzyl alcohol oxidation, benzaldehyde was the only oxidation product obtained.

Table 3.6 Oxidation of benzylic alcohols using AuPd/Li-Al LDH catalysts[a]

| Catalyst | Time (h) | Yield (%) [b] | Selectivity (%) [b] |
|---|---|---|---|
| |  | | |
| Au$_7$Pd$_3$/Li-Al LDH | 4 | 58 | >99 |
| Au$_1$Pd$_1$/Li-Al LDH | 4 | 67 | >99 |
| Au$_7$Pd$_3$/Li-Al LDH | 8 | >99 | >99 |
| Au$_1$Pd$_1$/Li-Al LDH | 8 | >99 | >99 |
| | | | |
| |  | | |
| Au$_7$Pd$_3$/Li-Al LDH | 1 | 80 | >99 |
| Au$_1$Pd$_1$/Li-Al LDH | 1 | >99 | >99 |

[a] Substrate (1 mmol), catalyst (0.50 mg), dimethylformamide (10 mL), 80 °C, p = 1 atm. O$_2$ (10 mL min$^{-1}$). [b] Yield of the products and selectivity were determined by GC-MS using dodecane as internal standard and the reported values are from the average of two runs.

Based on the foregoing results and previous findings,[133, 190, 191] we propose a possible mechanism in which the oxidation of benzylic alcohols proceeds through the involvement of

bimetallic Au–Pd nanoparticles and basic sites on the Li-Al LDH support (see Fig. 3.7). First, an $O_2$ molecule is activated through adsorption on the negatively charged Au and/or Pd sites on AuPd/Li-Al LDH with formation of a coordinated peroxo species. Experimental and theoretical studies in the literature suggests that neutral Au clusters can activate adsorbed $O_2$ molecules.[133, 192, 193] In the second step, an alcohol molecule attacks a basic Li–OH$^{\delta-}$ site on the Li-Al LDH; abstraction of the alcohol proton by the hydroxyl group on the support gives an alkoxide intermediate at the interface and forms a water molecule. A literature report indicates that alcohol molecules can be dissociatively adsorbed on Au and/or Pd forming metal-alkoxides, thereby providing another route to alkoxide formation.[133] In the case of the LDH support, the basicity of the LDH should promote this process through abstraction of a proton from the alcohol. Third, the β-H is eliminated via transfer to the Au and/or Pd nanoparticle to generate the corresponding carbonyl compound and a AuPd-hydroperoxide species. This is expected to be the rate-determining step, coordinatively unsaturated AuPd atoms being required for the cleavage of the C-H bond.[190] Finally, another $O_2$ attacks and removes the hydroperoxide species from the Au and/or Pd nanoparticle surface with the formation of $H_2O$, thereby completing the catalytic cycle.
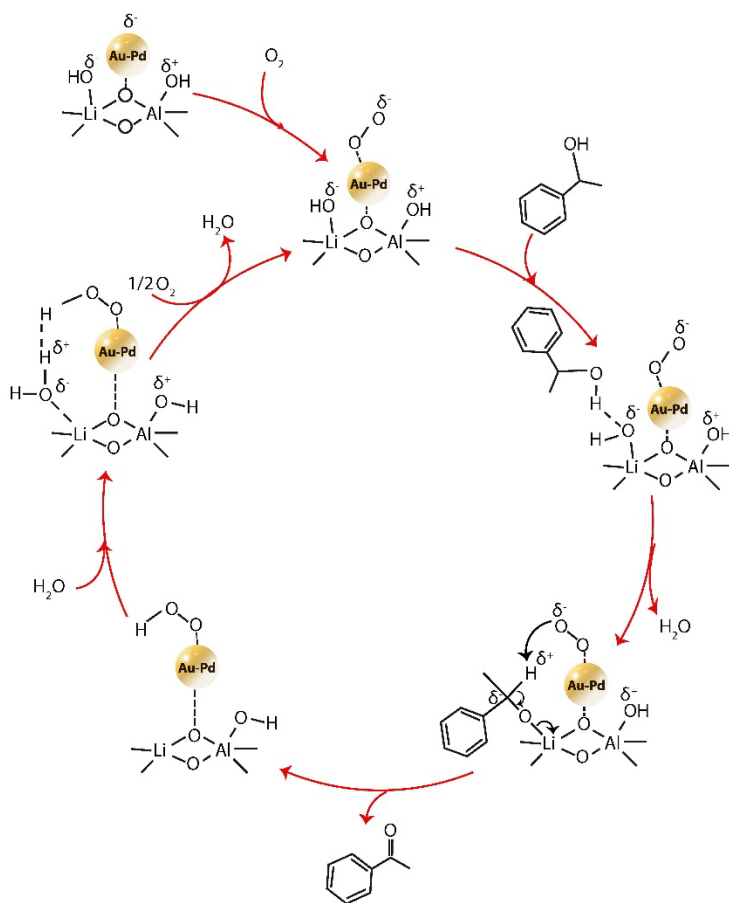
Figure 3.7 Possible reaction pathway for aerobic oxidation of 1-phenylethanol over Au–Pd/Li-Al LDH catalyst.

In the oxidation of lignin, the wide product distribution makes it difficult to follow the individual reactions taking place. For this reason, aerobic oxidation of a β–O–4 linked lignin model dimer was studied under the same reaction conditions used for the oxidation of 1-phenylethanol with the exception that the amount of catalyst used was doubled. As shown in Scheme 3.2, the β–O–4 model compound (2) was found to undergo two competing reactions. Compound (2a) is an enol ether, the product of dehydration and (2b) is the product of benzylic alcohol oxidation.[167] Product (2b) can undergo further oxidation to give guaiacol (2c) and p-anisic acid (2d). Oxidative cleavage of the β-O-4 linkage in (2b) has been attributed to the significantly weaker C–O bond

present as compared to the initial benzylic alcohol compound.[194] Finally, guaiacol (2c) and p-anisic acid (2d) can react to form product (2e) by esterification. Since the esterification is undesirable and reversible, (2e) can be cleaved by simple hydrolysis in a separate step.
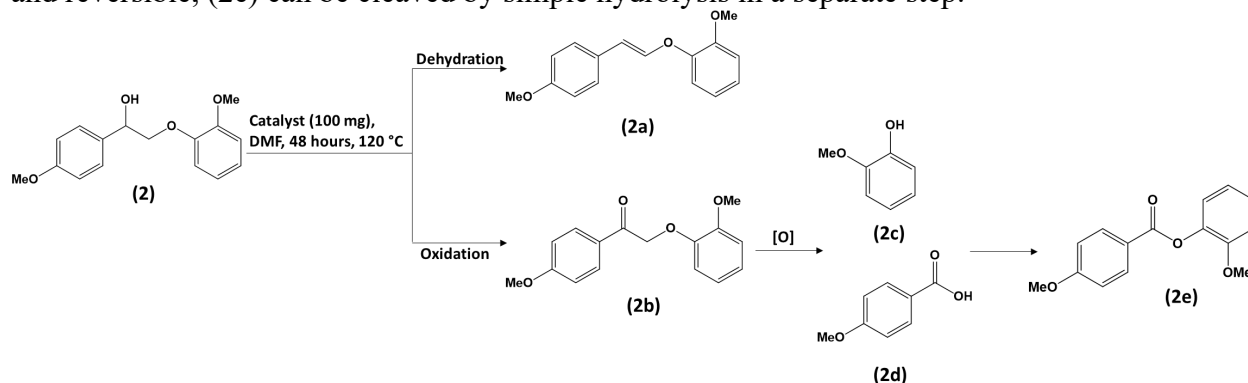


Scheme 3.2 Aerobic oxidation of β–O–4 lignin model compound (2)

Results for the aerobic oxidation of the β–O–4 linked lignin model dimer (2) are tabulated in Table 3.7. The $Au_1Pd_1$/Li-Al LDH catalyst afforded the best yield of the corresponding cleavage products and almost complete conversion (99%) of the benzylic alcohol group in the substrate after 48 h. The same oxidation reaction was studied by Song et al. for Au/Li-Al LDH (prepared by a deposition-precipitation method) under the same reaction conditions. It was reported that the conversion of the dimer was ~96% after 48 h.[167]

Table 3.7 Oxidation of β–O–4 lignin model compound (2) using AuPd/Li-Al LDH catalysts

| Catalyst | Conversion (%)[b] | Yield (%)[b] | | | | |
|---|---|---|---|---|---|---|
| | | (a) | (b) | (c) | (d) | (e) |
| Au/Li-Al LDH | 69 | 0 | 45 | 14 | 10 | 0 |
| $Au_7Pd_3$/Li-Al LDH | 77 | 3 | 44 | 15 | 11 | 4 |
| $Au_1Pd_1$/Li-Al LDH | >99 | 11 | 3 | 41 | 37 | 8 |

ᵃ Substrate (1 mmol), catalyst (100 mg), dimethylformamide (10 mL), 120 °C, p = 1 atm. $O_2$ (10 mLmin⁻¹). ᵇ Substrate conversion and product yields were determined by GC-MS using dodecane as internal standard.

Examining the recyclability of the $Au_1Pd_1$/Li-Al LDH catalyst sample is crucial. To assess this aspect, the $Au_1Pd_1$/Li-Al LDH catalyst was subjected to a β-O-4 linked lignin model compound (2) under oxidation conditions identical to those employed for the oxidation of the lignin model compound. After each reaction, the catalyst was carefully filtered and thoroughly rinsed with DI $H_2O$ before being dried at 50 °C in a vacuum oven for 24 hours prior to its use in the next cycle. The results concerning the recyclability of the $Au_1Pd_1$/Li-Al LDH catalyst in the context of β–O–4 linked lignin model dimer (2) oxidation have been compiled in Table 3.8. As per the findings, the $Au_1Pd_1$/Li-Al LDH catalyst demonstrated the high yield of the cleavage products and achieved nearly complete conversion (99%) of the benzylic alcohol group in the substrate during the initial two recycling reactions. In the third cycle, approximately 96% conversion was observed.

Table 3.8 Catalyst reusability study in the oxidation of β-O-4 model compound (2) with $Au_1Pd_1$/Li-Al LDH

| | Conversion of (2) (%) | Yield (%) | | | | |
|---|---|---|---|---|---|---|
| | | (a) | (b) | (c) | (d) | (e) |
| First Run | >99 | 10 | 8 | 41 | 33 | 8 |
| Second Run | >99 | 8 | 8 | 38 | 35 | 6 |
| Third Run | 96 | 11 | 10 | 35 | 32 | 4 |

## 3.11    Conclusion

In conclusion, a series of catalysts comprising Au, Pd, and bimetallic Au-Pd supported on Li-Al layered double hydroxide (LDH) was prepared using the sol-immobilization method. Our experiments involving the oxidation of simple benzylic alcohols revealed that the catalysts $Au_7Pd_3$/Li-Al LDH and $Au_1Pd_1$/Li-Al LDH exhibited significantly better catalytic activity when

compared to $Au_3Pd_7$/Li-Al LDH, as well as monometallic Au and Pd catalysts. Detailed examination through TEM imaging unveiled the presence of small Au-Pd nanoparticles on the Li-Al LDH support surface for $Au_7Pd_3$/Li-Al LDH and $Au_1Pd_1$/Li-Al LDH, which contributed to their outstanding performance in oxidation reactions. Furthermore, XPS data suggested that the transfer of charge from the basic Li-Al LDH support to the Au-Pd bimetallic nanoparticles played a significant role in enhancing the catalytic activity of these catalysts. Focusing on the oxidation of a β-O-4 linked lignin model dimer, we found that the $Au_1Pd_1$/Li-Al LDH catalyst effectively cleaved the linkage after selectively oxidizing benzylic alcohols into corresponding carbonyl. Encouraged by these promising outcomes, we evaluated the potential of the AuPd/Li-Al LDH system for the depolymerization of actual lignin, a valuable monomer production process.

# CHAPTER 4. DEVELOPMENT OF EFFECTIVE Au:Pd BIMETALLIC HETEROGENEOUS CATALYST FOR OXIDATIVE LIGNIN DEPOLYMERIZATION TO LOW MOLECULAR WEIGHT AROMATICS

## 4.1    Introduction

The environmental impact of fossil fuel usage, primarily due to greenhouse gas emissions, is well-documented.[195] As a result, there is a growing shift towards replacing fossil resources with sustainable alternatives. These alternatives must be renewable, carbon-neutral, readily available, and not compete with food production.[1] Among the available options, lignocellulosic biomass stands out as a resource that aligns with these critical criteria. Lignocellulosic biomass consists of three key biopolymers: cellulose, hemicellulose, and lignin, forming a composite material.[196, 197] Cellulose hydrolysis yields hexose sugars, such as glucose, primarily used in ethanol production, which can be blended with gasoline as a motor vehicle fuel.[4, 5] Hemicellulose finds applications as a plant gum for thickeners, adhesives, protective colloids, emulsifiers, and stabilizers. Additionally, it holds promise as a biodegradable oxygen barrier film.[4, 6, 7]. While cellulose and hemicellulose have well-established applications, lignin, the remaining component of biomass, is often considered a low-value by-product or a low-grade fuel.[198] Typically, lignin contains 40% of the energy stored within the biomass, possesses a high heating value, and encompasses various aromatic sub-units.[8, 9] Commercial applications of lignin are still limited,  primarily involving lignosulphonates in concrete admixtures, animal feed pellets, and road binders.[199, 200]

Significant endeavors have been dedicated to the advancement of techniques for breaking down lignin through chemical processes. Nonetheless, the deconstruction of lignin presents considerable challenges, primarily attributed to its rigid, irregular, and extensively cross-linked structure.[201] Even though lignin is an attractive renewable resource for the production of bio-based materials, fuels, and chemicals, its complicated structure poses a significant challenge when it comes to converting it into useful products. In this regard, reductive and oxidative depolymerization methods play an important role in the production of chemicals from lignin. The

reductive depolymerization pathway yields relatively lower-value aromatic products, including benzene, toluene, and xylene (BTX). [2, 39] Conversely, oxidative depolymerization can be harnessed to create oxygenated aromatic monomers from lignin, such as vanillin, vanillic acid, syringaldehyde, and various others.

These products have relatively high market value.[39] Against this background, numerous studies have determined that the sale of lignin as a co-product significantly enhances the economic feasibility of biofuels.[202] In fact, a U.S. National Renewable Energy Laboratory (NREL) report emphasized that lignin valorization was crucial to achieving the target cost of $3.00 per gallon of gasoline equivalent fuel derived from lignocellulosic biomass.[203] Likewise, Kautto et al.[204] developed a model for producing ethanol from hardwood, considering lignin, furfural, and acetic acid as co-products. Consistent with NREL's findings, the value of the lignin co-product played a pivotal role in determining the minimum ethanol selling price.

In early research, oxidative lignin depolymerization was conducted using oxidants alone or in combining with simple transition metal ions $Cu^{2+}$, $Mn^{3+}$, $Co^{2+}$, and $Zr^{4+}$.[43, 45, 205] Subsequently, the focus shifted to composite metal oxide and mixed metal oxide catalysts, containing elements like Co, Fe, Cu, and Mn (e.g., CuO, $MnO_2$), to improve lignin depolymerization.[43, 46] Additionally, supported metal nanoparticle catalysts were extensively explored for oxidatively breaking down lignin. Recently, Song et al. studied Au nanoparticles supported on Li-Al layered double hydroxide (LDH) for oxidation of both ɣ-valerolactone (GVL) extracted lignin and kraft lignin with $O_2$ and were able to produce a range of aromatic monomers in high yield. It was reported that hydrolysis of Au/LiAl-LDH oxidized lignin increased the degree of lignin depolymerization, with monomer yields of 40% for GVL extracted lignin.[167]

Bimetallic nanoparticles can enhance the activity and selectivity of gold-based catalysts towards desired products due to synergetic electronic interactions between the two different metal atoms in the individual nanoparticles.[71] Indeed, catalytic properties such as activity and selectivity can frequently be tuned by changing the composition of bimetallic nanoparticle catalysts. For instance, in the selective oxidation of primary alcohols to aldehydes, bimetallic Au–Pd catalysts

show superior activity and selectivity compared to catalysts based on either pure Au or pure Pd.[71,][171] In our previous study, detailed in Chapter 3, we conducted a comprehensive study to identify the most active AuPd bimetallic catalyst systems, for the oxidation of simple benzylic alcohols and a β-O-4 linked lignin model dimer compound. These catalysts displayed exceptional performance in those contexts. In the current research, we extend our findings by introducing the highly efficient catalysts identified in our previous work. We apply these catalysts to GVL-extracted maple lignin, a complex and renewable biomass source. Our primary objective is to evaluate their effectiveness in depolymerizing the lignin into smaller, low-molecular-weight aromatic compounds. This investigation aims to shed light on the potential of these catalysts in the context of lignin valorization and the production of valuable chemical building blocks from renewable resources.

## 4.2    Experimental Information

### 4.2.1 Lignin extraction using γ-valerolactone (GVL)

γ-valerolactone extraction was adapted from literature methods[206] using a stainless steel stirred batch microreactor (Parr reactor). 2.5 g of extractive-free maple biomass was dissolved in a mixture (22.5 g) of 80 wt% GVL, 19 wt% water, and 1 wt% sulfuric acid. The resulting biomass mixture was then treated at 120°C for 0.5 h in the Parr reactor (50 ml). The resulting solution was vacuum filtered and washed using 30 ml of a 1:9 mixture of GVL:water. Next, the lignin was slowly precipitated by adding the combined filtrate and washings to 500 mL of ice-cold water. The mixture was left in a refrigerator for 24 h to maximize the precipitation of lignin, which was then recovered by means of centrifugation (30 min, 1500 g). Finally, the precipitate was dried in a vacuum oven at 40 °C for 24 h.

### 4.2.2 General procedure for aerobic oxidation of lignin

The oxidation of lignin samples was conducted in a 100 mL 3-neck round-bottom flask using a Radleys Starfish reactor to which lignin (250 mg), catalyst (100 mg), and DMF (15 mL) were added. The lignin was oxidized under flowing $O_2$ (10 mL/min) at 120 °C and 500 rpm stirring for 24 h. The resulting mixture was filtered and washed with additional DMF (15 mL). The filtrate and washings were combined, and volatile matter removed on a rotary evaporator. The resulting solid was further dried in a vacuum oven at 50 °C for 46 h.

### 4.2.3 General procedure for hydrolysis of lignin

A mixture of oxidized lignin (50 mg) and aqueous NaOH (1 M, 5 ml) was stirred at room temperature for 30 min. The mixture was then acidified to pH 2 by the addition of 1 M HCl and stirred for an additional 30 min. Next, the mixture was extracted with EtOAc (3 x 15 ml). The combined organic extracts were washed with 50 ml each of saturated aqueous $NaHCO_3$, followed by brine, and dried over anhydrous $MgSO_4$. Solvent was then removed on a rotary evaporator to afford the products as a colorless oil.

### 4.2.4 Determination of average molecular weight distribution

Gel permeation chromatography (GPC) was carried out on an Agilent 1260 Infinity Quaternary LC system equipped with a G1311A Quaternary pump, G1329B Autosampler, G1364C Fraction Collector, G1316A Column Compartment, G1315C Diode-Array Detector (DAD), and a Corona CAD detector (ESA Magellan Biosciences). Samples were analyzed using SUPREMA analytical linear S 10μm (50 x 8 mm) and SUPREMA analytical linear S 10μm (300 x 8 mm) GPC columns (Polymer Standards Services) connected in series, and eluted using inhibitor free THF/DMSO (v/v=1:1, 0.4 mL/min) with a column oven temperature of 25 °C.

Approximately 2 mg of sample was acetylated in acetic anhydride/pyridine (2 ml, 1:1 v/v) at 40 °C for 4 h. Volatiles were removed in vacuo after addition of 2 ml each of ethanol followed

by toluene, and each addition/distillation procedure was repeated twice. Finally, the sample was dried overnight in a vacuum oven at 30 °C. For GPC analyses, the samples were dissolved in 1 mL THF/DMSO (2 ml, 1:1 v/v) and filtered through a 0.2 μm syringe filter prior to injection.

## 4.3    Results and Discussion

Oxidative lignin deconstruction was studied using gamma-valerolactone extracted lignin (GVL) from maple wood as substrate. Reaction conditions were similar to those used in the simple benzylic alcohol oxidations described in chapter 3 except that the reaction temperature was increased to 120 °C. Heteronuclear single quantum coherence NMR (2D HSQC) spectroscopic analysis allows for the evaluation of the reactivity of the various linkages in the lignin substrate when subjected to the different catalysts. Fig. 4.1 shows 2D HSQC NMR spectra comparing GVL before and after oxidation using Au/Li-Al LDH, $Au_7Pd_3$/Li-Al LDH, and $Au_1Pd_1$/Li-Al LDH as catalysts.
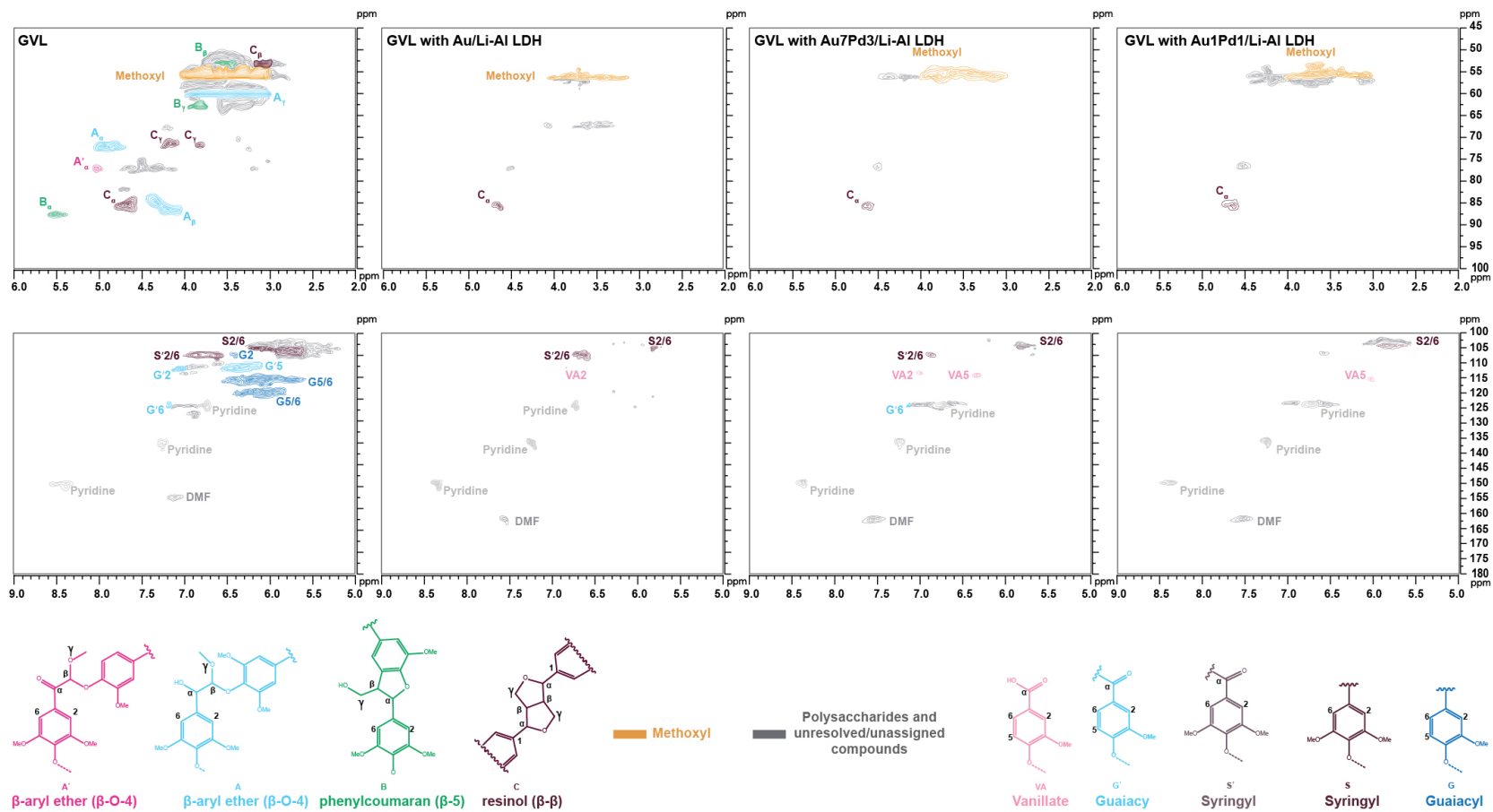
Figure 4.1 2D HSQC NMR spectra comparing GVL before and after oxidation with $O_2$ in the presence of Au/Li-Al LDH, $Au_7Pd_3$/Li-Al LDH, and $Au_1Pd_1$/Li-Al LDH

According to the 2D HSQC NMR results, the aliphatic region of GVL before oxidation showed signals corresponding to methoxy groups, β-aryl ether (A), β-5 phenylcoumaran (B) and β-β resinol (C) units. The main signals in the aromatic region of the GVL originated from syringyl (S), and guaiacyl (G) units. After the oxidation reaction, the aliphatic region of the GVL product in all cases showed the absence of signals corresponding to β-aryl ether (A) and β-5 phenylcoumaran (B) units, suggesting that the linkages of A and B are cleaved by the different catalysts. Based on the results obtained for oxidation of the β-O-4 lignin model compound, it is hypothesized the β-aryl ether units in lignin may have gone through a reaction pathway similar to that shown in Figure 4.1. Signals corresponding to β-5 linkages also disappeared in all oxidized lignin samples. Fang et al. investigated the effect of several oxidation methods, such as KMnO$_4$ under acidic conditions, DDQ (2,3-dichloro-5,6-dicyano-1,4-benzoquinone), and TEMPO-based (2,2,6,6-tetramethyl-piperidin-1-oxy) oxidation, on β-5 lignin linkages using β-5 model compounds. Benzofuran derivatives were mainly produced from oxidations of β-5 compounds with DDQ and TEMPO-based systems, although the dihydrofuran ring in a β-5 model was opened when treated with KMnO$_4$ at high temperature.[13] Hence, aromatization of the 5-membered ring, or possibly ring-opening, could explain the absence of HSQC NMR signals corresponding to β-5 linkages in the oxidized GVL.

For each of the oxidized GVL samples weak signals were observed corresponding to residual β-β resinol (C) units. The reason for the apparent weakening of these signals during the AuPd bimetallic/Li-Al LDH oxidation is unclear, although some degree of aromatization or ring-opening of the fused 5-membered rings in the β-β units may be indicated. Our previous study recorded similar observations for GVL oxidation with O$_2$ using Au nanoparticles supported on Li-Al LDH prepared using the deposition-precipitation method.[167] In addition, the HSQC spectrum of oxidized GVL displayed a significant decrease in syringyl (S) and guaiacyl (G) units, consistent with the release of aromatic monomers. Indeed, only small amounts of both units remained in the lignin

oxidized with $Au_1Pd_1$/Li-Al LDH, while only small amounts of syringyl (S) units were present in the other two samples. Furthermore, vanillate (VA) analogs were present in the HSQC spectrum of the oxidized GVL for each of the catalysts tested.

In order to cleave possible ester linkages created during the oxidation process (as shown in scheme 3.2), the oxidized lignin samples were hydrolyzed with NaOH (0.1 M), after which the mixture was neutralized with HCl (1.0 M). Soluble material was then extracted with ethyl acetate (EtOAc). The EtOAc soluble yield of the hydrolyzed samples for the Au/Li-Al LDH, $Au_7Pd_3$/Li-Al LDH, and $Au_1Pd_1$/Li-Al LDH catalysts was 48 wt%, 53 wt% and 60 wt%, respectively. Gel permeation chromatography (GPC) was carried out on the EtOAc soluble fraction in order to indicate the degree of depolymerization and the molecular weight distributions of the resulting product mixtures. Figure 4.2 shows the results of molecular weight distributions comparing GVL before and after the oxidation/hydrolysis treatment with Au/Li-Al LDH, $Au_7Pd_3$/Li-Al LDH, and $Au_1Pd_1$/Li-Al LDH.
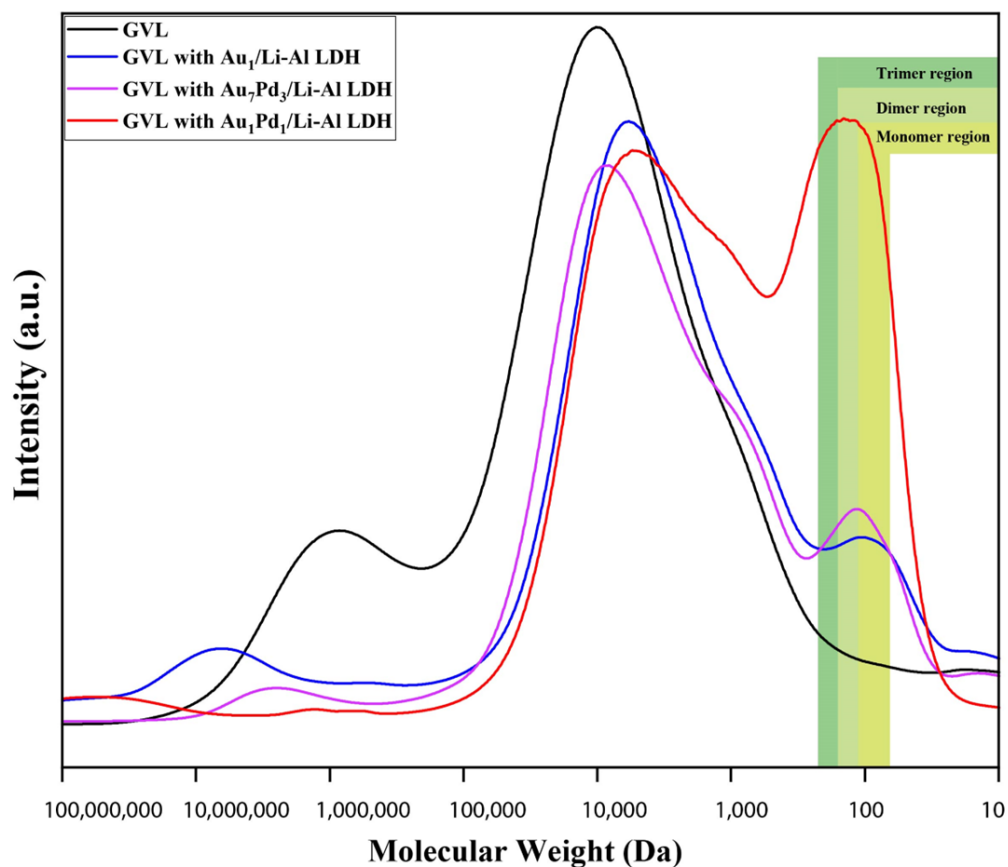
Figure 4.2 Molecular weight distributions measured using GPC comparing GVL before oxidation and the EtOAc soluble fraction after oxidation/hydrolysis with Au/Li-Al LDH, Au$_7$Pd$_3$/Li-Al LDH, and Au$_1$Pd$_1$/Li-Al LDH.

In all cases, the GPC chromatograms of the oxidized GVL after hydrolysis contain two peaks. The first peak in the chromatogram represents fractions containing high molecular weight lignin, and the second peak corresponds to low molecular weight components (mainly monomers, dimers and trimers). The high molecular weight region shows an approximately 5500 Da, 1400 Da and 6700 Da average decrease in molecular weight for oxidized post-hydrolysis maple lignin with Au/Li–Al LDH, Au$_7$Pd$_3$/Li-Al LDH, and Au$_1$Pd$_1$/Li-Al LDH, respectively. In the low molecular weight region, monomer production is apparent for GVL treated with the Au/Li-Al LDH and AuPd/Li-Al LDH catalysts. While use of the Au/Li-Al LDH and Au$_7$Pd$_3$/Li-Al LDH catalysts has a clear

effect on reducing the average lignin molecular weight, the best performance was obtained using $Au_1Pd_1$/Li-Al LDH, which gave the largest molecular weight shift for the main lignin peak and a significant amount of lower molecular weight components.

Product identification and quantification was performed using GC-MS. Figure 4.3 shows the yield of monomer products from the oxidized GVL with Au/Li-Al LDH, $Au_7Pd_3$/Li-Al LDH, and $Au_1Pd_1$/Li-Al LDH. The results revealed distinct product distributions from the oxidation of GVL lignin using the different catalyst systems. As shown in Fig. 4.3, S- and G-derived carboxylic acids and aldehydes were the most prominent products. Among the identified monomers, vanillin, vanillic acid, ferulic acid, syringaldehyde and syringic acid were present in all oxidized lignin samples. The catalyst system $Au_1Pd_1$/Li-Al LDH showed the highest monomer yields for all identified monomers compared to the other two catalysts, consistent with superior conversion of GVL lignin into valuable monomers. In terms of G-derived products, $Au_1Pd_1$/Li-Al LDH demonstrated remarkable catalytic activity, yielding significantly higher percentages of vanillin (2.1%) and vanillic acid (3.9%) compared to Au/Li-Al LDH (0.1% and 0.6%, respectively) and $Au_7Pd_3$/Li-Al LDH (1.0% and 3.1%, respectively), indicating its superior efficacy in G-unit degradation. Furthermore, in the case of S-derived products, $Au_1Pd_1$/Li-Al LDH outperformed the other catalysts, yielding higher amounts of syringaldehyde (10.7%) and syringic acid (3.6%). $Au_7Pd_3$/Li-Al LDH showed intermediate yields, while Au/Li-Al LDH exhibited the lowest values. Notably, $Au_1Pd_1$/Li-Al LDH catalysis resulted in the formation of sinapic acid, a significant finding highlighting its unique capability in S-unit depolymerization. Regarding the ferulic acid, $Au_1Pd_1$/Li-Al LDH exhibited higher yields of ferulic acid (3.9%) compared to Au/Li-Al LDH (0.9%) and $Au_7Pd_3$/Li-Al LDH (2.6%). Overall, the catalytic performance of $Au_1Pd_1$/Li-Al LDH was notably superior, displaying enhanced selectivity towards both G- and S-derived products, and producing higher amounts of valuable monomers such as vanillin, vanillic acid, syringaldehyde, and syringic

acid. These results underscore the potential of $Au_1Pd_1$/Li-Al LDH as an efficient catalyst for the valorization of GVL lignin into valuable chemicals.
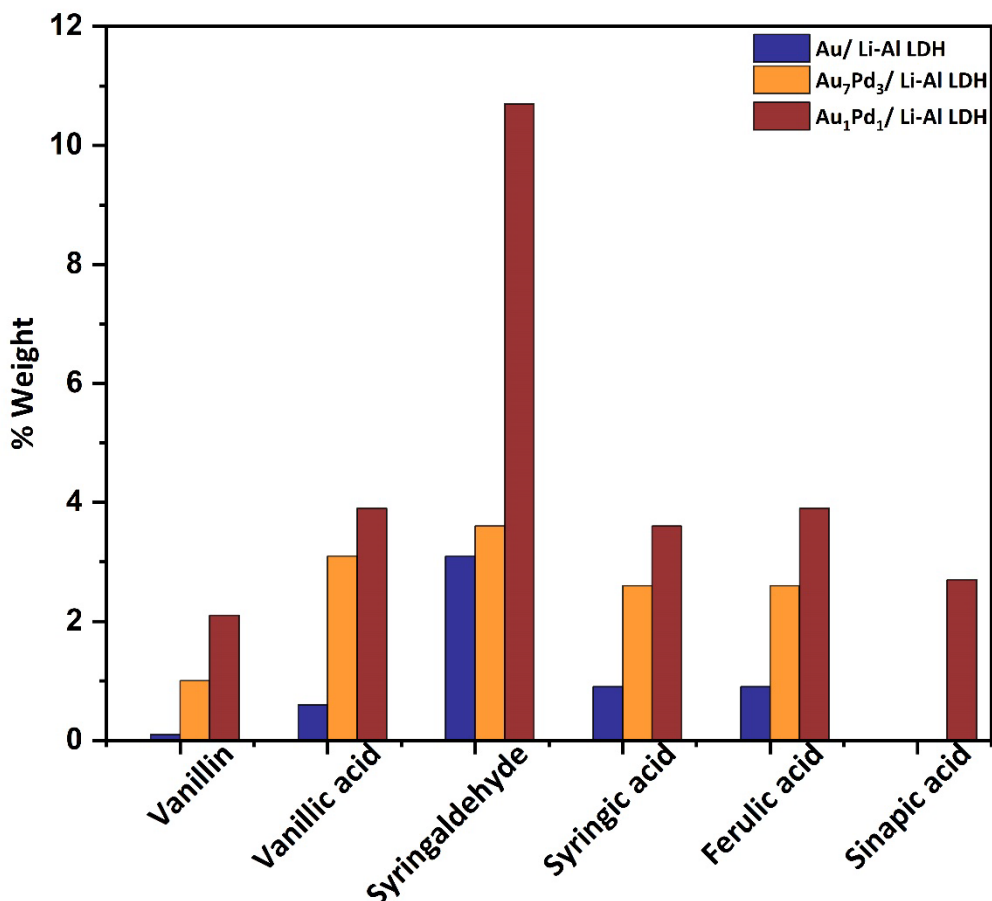


Figure 4.3 Yield of monomer products obtained from GVL in the presence of Au/Li-Al LDH, $Au_7Pd_3$/ Li-Al LDH, and $Au_1Pd_1$/ Li-Al LDH

The total yield of GC-MS identifiable monomers from oxidized GVL was measured at 6 wt.%, 13 wt.%, and 27 wt.% for Au/Li-Al LDH, $Au_7Pd_3$/Li-Al LDH, and $Au_1Pd_1$/Li-Al LDH, respectively. The significantly higher monomer yield observed with $Au_1Pd_1$/Li-Al LDH directly corresponds to its superior performance in reducing the average lignin molecular weight and generating a substantial amount of lower molecular weight components.

In the same oxidation reaction, Song et al.[167] investigated GVL lignin extracted from maple using Au/Li-Al LDH under identical reaction conditions, resulting in a notable 40 wt% yield of aromatic monomers. This monomer yield represents one of the highest reported for heterogeneously catalyzed oxidative lignin depolymerization, showcasing the potential of Au/Li-Al LDH as a promising catalyst system for lignin valorization into valuable low molecular weight aromatics. However, in our study, we obtained the lowest monomer yield of 6 wt.% when utilizing the Au/Li-Al LDH catalyst for GVL oxidation. The substantial difference in monomer yields between the two studies could potentially be attributed to variations in the particle size and catalyst preparation methods. Specially, we employed the sol-immobilization method for catalyst preparation, for the reason that this method provided smaller AuPd particles than the deposition-precipitation method and in turn afforded more active AuPd oxidation catalysts (results not shown). In contrast, Song et al. used the deposition-precipitation method for Au/Li-Al LDH catalyst preparation. These distinct catalyst preparation approaches influence the active site distribution, impacting the catalytic performance and subsequently affecting the monomer yield. Indeed, particle size is a crucial factor influencing catalytic activity. The catalyst prepared through the deposition precipitation method in the previous study exhibited a smaller mean Au particle size of 2.0±0.5 nm, whereas our catalyst, synthesized via the sol-immobilization method, displayed a larger mean Au particle size of 3.1±0.4 nm. This difference in particle size would be expected to significantly impact catalyst activity, leading to differences in the obtained monomer yield. In conclusion, our findings highlight the importance of catalyst preparation methods and particle size in determining the performance of Au/Li-Al LDH and AuPd/Li-Al LDH catalysts for lignin valorization. Optimizing these factors could potentially enhance the catalytic activity and improve monomer yields.

## 4.4    Conclusion

In Chapter 3, we presented the results of our study, focusing on the oxidation ability of Au-Pd bimetallic catalysts. Our findings highlight the effectiveness of $Au_1Pd_1$/Li-Al LDH and $Au_7Pd_3$/Li-Al LDH as catalysts for the oxidation of simple benzylic alcohols. Furthermore, our investigation into β-O-4 linked lignin model dimer oxidation revealed that the $Au_1Pd_1$/Li-Al LDH catalyst exhibited the ability to selectively oxidize benzylic alcohols, subsequently cleaving the linkage to produce the corresponding carbonyl products. Building upon these oxidation capabilities, we harnessed Au-Pd/Li-Al LDH bimetallic catalysts to facilitate the oxidative depolymerization of lignin into low molecular weight aromatics. The HSQC NMR data obtained from the oxidized GVL lignin confirmed the successful depolymerization by revealing the disappearance of major lignin linkages. Upon subjecting the oxidized lignin samples to hydrolysis, we observed encouraging results. The total yield of GC-MS identifiable monomers from oxidized GVL was found to be 6 wt.%, 13 wt.%, and 27 wt.% for Au/Li-Al LDH, $Au_7Pd_3$/Li-Al LDH, and $Au_1Pd_1$/Li-Al LDH, respectively. These results underscore the potential of $Au_1Pd_1$/Li-Al LDH as a promising catalyst system for lignin valorization, particularly in the production of value-added, low molecular weight aromatics.

# CHAPTER 5.  AEROBIC OXIDATION OF β-O-4, β-1 AND β-β LIGNIN MODEL COMPOUNDS WITH Au-Pd BIMETALLIC HETEROGENEOUS CATALYST

## 5.1  Introduction

The limited availability of fossil fuels for chemical production and the recognition that biomass represents a sustainable source of chemicals and materials have highlighted lignin as a prominent and promising renewable source of aromatic chemicals.[59, 207, 208] Lignin is a heterogeneous and highly oxygenated biopolymer, constituting approximately 15-30 % of biomass by weight.[13, 59] Typically, it possesses around 40% of the energy stored within the biomass, resulting from its high heating value, and contains a number of different aromatic sub-units.[8, 9, 209, 210] Globally, there is an estimated $3\times10^{11}$ metric tons of lignin, with an annual biosynthesis rate of approximately $2\times10^{10}$ metric tons.[211] Notably, industrial processes, particularly paper manufacturing and bio-ethanol production, generate roughly 50 million tons of lignin each year as a waste byproduct.[212-214] By the year 2030, it is projected that the annual production of lignin from cellulosic ethanol production will rise by 225 million tons per year. This significant increase is attributed to the implementation of the Renewable Fuel Standard (RFS) program, which mandates the annual production of 60 billion gallons of biofuel.[213]

Despite being the largest and only renewable source of aromatics, lignin remains the least utilized biopolymer due to its recalcitrant and irregular nature, unlike cellulose.[2, 31, 210, 214] In recent decades, there has been significant interest in using cost-effective, earth-abundant metal catalysts and air (or dioxygen) for the selective oxidation of lignin.[59, 210, 215] The aim is to convert lignin from non-food-based lignocellulosic biomass into value-added aromatic chemicals. However, the challenge of achieving selective lignin depolymerization and valorization is yet to be fully overcome, and it remains a prominent focus of scientific research. Numerous studies have explored lignin conversion and valorization through pathways involving alkaline oxidation, hydrotreating, and

pyrolysis.[210, 216] Although these processes can convert lignin into value-added products, they are hindered by their requirement for high temperatures and pressures, making them expensive and impractical. The majority of lignin produced by the paper industry continues to be burned as low-value fuel for electricity and heat generation; indeed, historically, the predominant use of lignin has been as a source of heat and power from its combustion. A mere fraction, accounting for less than 2% of the total lignin produced, has been commercially marketed. This limited amount of lignin has primarily found application in the formulation of dispersants, adhesives, and surfactants.[213] Overall, the efficient and selective utilization of lignin remains an ongoing scientific pursuit, with significant efforts aimed at overcoming the challenges associated with lignin depolymerization.

Lignin exhibits a diverse structure resulting from its enzymatic synthesis through radical condensation.[13, 59, 217] Lignin is composed of three p-hydroxycinnamyl alcohol monomers (monolignols), namely, p-coumaryl, coniferyl, and sinapyl alcohol units, that are connected by various types of inter-unit linkages, primarily involving C-O and C-C bonds.[218] Although the specific distribution of linkages varies across species, several key structures are common to all lignin. These structures include the aryl ether unit (β-O-4), phenylcoumaran unit (β-5), and the resinol unit (β-β), as well as 5-5', 4-O-5, and β-1 linkages (Figure 5.1).[219] During the lignification process, the predominant inter-unit linkage formed is the β-O-4 ether linkage. This structure typically represents around 50% of the linkages formed during lignin polymerization and possesses the lowest bond dissociation energy compared to other linkages.[210, 219] Consequently, many studies on lignin depolymerization target the β-O-4 linkage.[220] However, it is important to consider the presence of other linkages, such as β-1, β-5, and β-β, as they constitute significant portions of lignin biomass. The β-1 and β-β linkages represent between 2-9% and 9-12% of lignin inter-unit linkages, respectively, while the β-5 linkage accounts for 2-9% of all linkages, depending on the lignin source and processing methods employed.[22, 23]

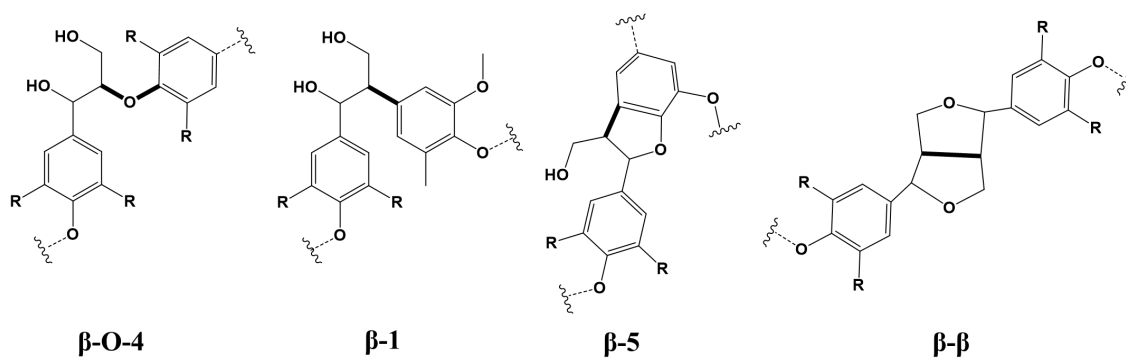Figure 5.1 Structures of β-O-4, β-1, β-5 and β-β linkages

To develop strategies for the selective cleavage of inter-unit linkages, it is common practice to utilize lignin model compounds. These models allow researchers to focus on specific linkages of interest and avoid the complexities associated with impurities and heterogeneous structures present in whole lignin samples. The bond dissociation energies of C-C linkages, compared to C-O linkages, are higher, resulting in greater stability and difficulty in breaking the linkages. However, for an efficient lignin depolymerization process, it is essential to cleave both types of linkages. While several catalytic routes have been reported for the cleavage of C-O bonds, particularly in the β-O-4 inter-unit linkage found in lignin model compounds, there is a scarcity of examples and limited knowledge regarding the breaking of β-1, β-5, and β-β linkages in the literature. These types of linkages require further exploration and investigation in the context of lignin depolymerization.

Fang et al. examined the impact of various oxidation methods on the cleavage of β-1 and β-5 lignin linkages using model compounds. The oxidation methods investigated included KMnO$_4$ under acidic conditions, DDQ (2,3-dichloro-5,6-dicyano-1,4-benzoquinone), and TEMPO-based (2,2,6,6-tetramethyl-piperidin-1-oxy) oxidation. In the case of β-1 model compounds, they observed the direct oxidative cleavage of C-C bonds using KMnO$_4$ under acidic conditions and TEMPO-based catalyst systems. As a result of this cleavage, predominantly ketones and carboxylic acids were formed (see scheme 5.1).

92

In the case of oxidations involving β-5 compounds, DDQ and TEMPO-based systems predominantly yielded benzofuran derivatives. Interestingly, when KMnO4 was employed at high temperatures, the dihydrofuran ring in the β-5 model compound underwent opening.[13]
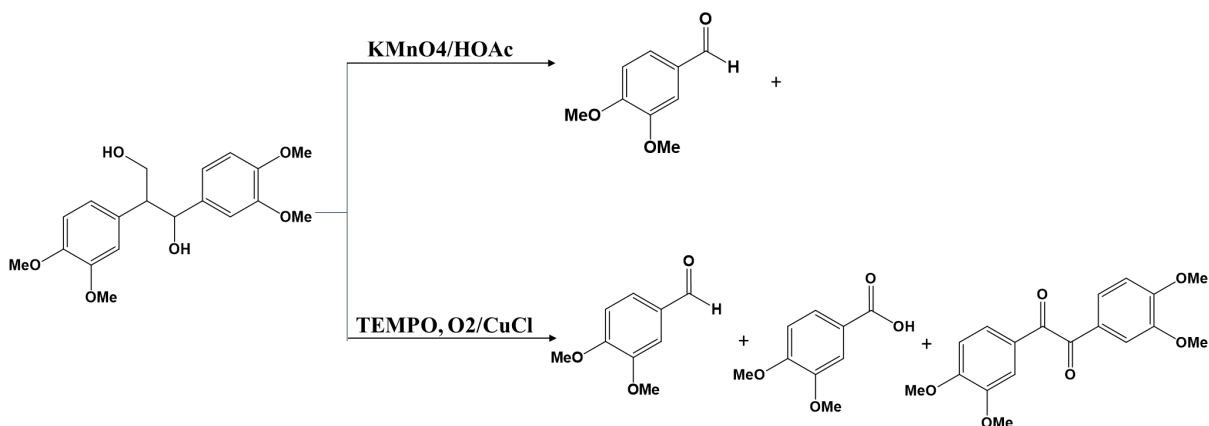


Scheme 5.1 Oxidations of β-1 models using KMnO4 and TEMPO based catalyst systems, reported by Fang.[59]

Sedai et al.[59] explored the reactivity of homogeneous oxovanadium and copper catalysts in the context of aerobic oxidation reactions involving phenolic and nonphenolic β-1 lignin model compounds. They found that the aerobic oxidation of diastereomeric, nonphenolic β-1 lignin models, employing the six-coordinate vanadium complex $(HQ)_2V^V(O)(O^iPr)$ (HQ = 8-oxyquinolinate) as the catalyst, resulted in the formation of ketone and dehydrated ketone products. These products were derived from the oxidation of secondary alcohols within the model compounds. In contrast, when the reaction was conducted using CuOTf/2,6-lutidine/TEMPO (OTf = trifluoromethanesulfonate) as the catalyst system, the major products observed were 3,5-dimethoxybenzaldehyde and 4-methoxybenzaldehyde (see scheme 5.2). These products were formed as a result of C-C bond cleavage.[59]

Cui et al. elucidated the oxidation reactions of three dimeric model compounds, containing β-O-4, β-1, and β-5 linkages, employing meso-tetra(2,6-dichloro-3-sulfonatophenyl)porphyrin iron chloride (TDCSPPFeCl) as the catalyst. The catalyst effectively cleaved the β-O-4 and β-1 model compounds, leading to the formation of the expected carbonyl compounds. On the other hand, the β-5 model compound underwent side chain oxidation and aromatic ring cleavage reactions upon exposure to the catalyst.[221]
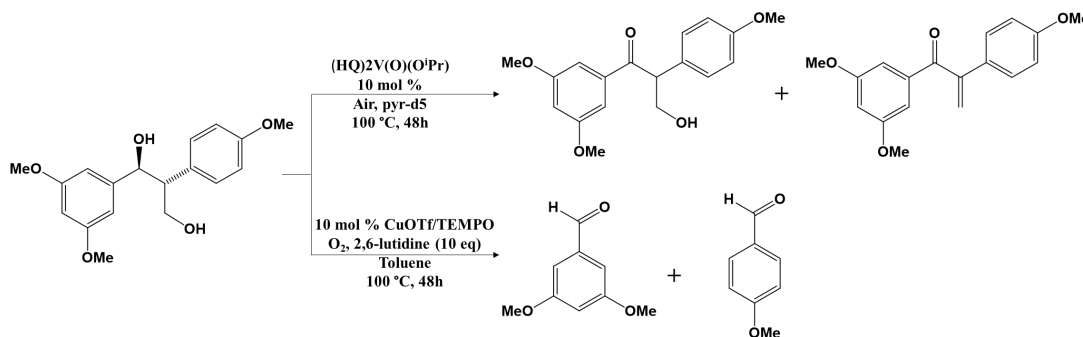


Scheme 5.2 Oxidations of β-1 models using vanadium complex based catalyst systems, reported by Sedai.[59]

In our previous investigation (see Chapter 4), we introduced heterogeneous catalysts comprising Li-Al layered double hydroxide (LDH) supported AuPd bimetallic nanoparticles in various molar ratios for the oxidative depolymerization of γ-valerolactone (GVL)-extracted maple lignin. These bimetallic catalysts were synthesized through a sol-immobilization method. The evaluation of oxidation outcomes revealed that the catalyst containing an Au:Pd molar ratio of 1:1, referred to as the $Au_1Pd_1$/Li-Al LDH catalyst, displayed remarkable catalytic activity, affording a monomer yield of 27% (based on the weight of lignin used). Subsequent analysis utilizing 2D HSQC NMR spectroscopic analysis revealed the disappearance of β-O-4, β-5, and β-β linkages in the oxidized lignin sample. The primary objective of this study is to offer insights into the specific products obtained from the oxidation of β-O-4, β-1, β-β, and β-5 model compounds using the

Au$_1$Pd$_1$/Li-Al LDH catalyst system, thereby elucidating the potential pathways and transformations that may occur during oxidative lignin depolymerization processes.

## 5.2    Experimental Information

### 5.2.1 Synthesis of β-O-4 linkage lignin model compounds
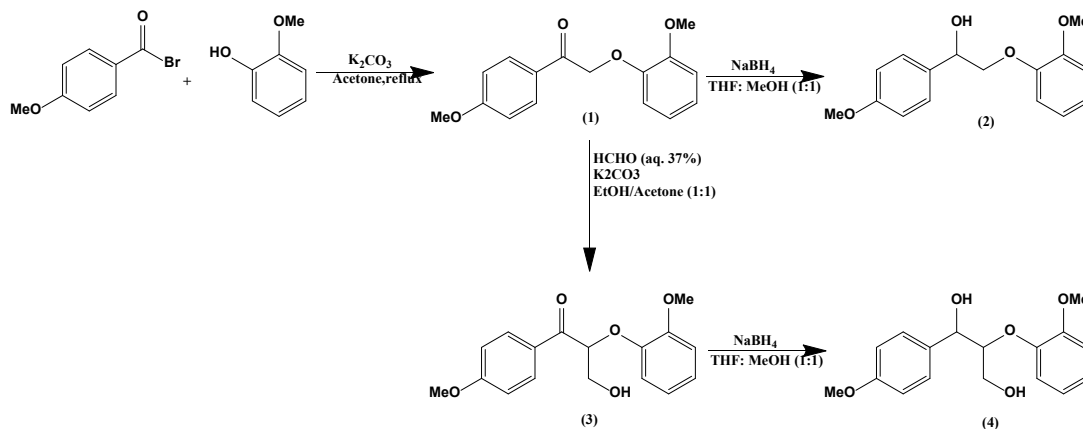


Scheme 5.3 Synthesis of β-O-4 linkage lignin model compounds

Compounds (1), (2), (3), and (4) were prepared according to a literature procedure.[170]

### 5.2.1.1 Synthesis of 2-(2-methoxyphenoxy)-1-(4-methoxyphenyl)-ethanone (1)

Compound (1) was prepared from guaiacol and 4'-methoxy-2-bromoacetophenone. While stirring a solution of K$_2$CO$_3$ (20 g, 0.14 mol) and guaiacol (16 g, 0.13 mol) in acetone (100 ml), 2-bromo-4'-methoxyacetophenone (22 g, 0.11 mol) was added. After that, the reaction mixture was stirred at reflux temperature (80 °C) overnight. The reaction mixture was filtered, dried over anhydrous MgSO$_4$, and concentrated in vacuo. The crude product was recrystallized from ethanol. Yield: 23.40 g (78 %).

### 5.2.1.2 Synthesis of 4-methoxy-α-[(2-methoxyphenoxy)methyl]-benzenemethanol (2)

Compound (1) (5 g, 18 mmol) was dissolved in a mixture of THF: MeOH (50 ml, 2:1v/v). Sodium borohydride (1.5 g, 39 mmol) was added in portions to the reaction mixture under stirring at 0 °C. The mixture was left to stir overnight at room temperature. The mixture was then concentrated in vacuo and diluted with deionized water (50 ml). After that, the mixture was extracted with dichloromethane (3 x 30 ml). The combined organic extracts were dried over anhydrous $MgSO_4$ and concentrated in vacuo. The crude product was recrystallized from ethanol to afford the pure alcohol (2). Yield: 3.8 g (76%).

### 5.2.1.3 Synthesis of 3-hydroxy-2-(2-methoxyphenoxy)-1-(4-methoxyphenyl)-1-propanone (3)

Compound (1) (5.0 g, 18 mmol) and $K_2CO_3$ (2.8 g, 20 mmol) were dissolved and stirred in a 1:1 mixture of ethanol and acetone (100 mL). Next, an aqueous solution of formaldehyde (37 wt.%) (0.82 mL, 11 mmol) was added to the stirred mixture. The mixture was left to stir overnight and then concentrated in vacuo, resulting in a yellow oil. The oil product was subjected to column chromatography on silica gel using a mixture of dichloromethane (DCM) and ethyl acetate (v/v = 6:1) as the eluent, yielding a yellow-colored oil. Then the oil was crystallized from ethanol, leading to the formation of a pale yellow solid. Yield: 4.9 g (88%).

### 5.2.1.4 Synthesis of 2-(2-methoxyphenoxy)-1-(4-methoxyphenyl)-1,3-propanediol (4)

Compound (3) (1.5 g, 5 mmol) was dissolved in a mixture of THF and MeOH (v/v=2:1, 30 mL). Sodium borohydride (0.4 g, 10 mmol) was added gradually to the reaction mixture while stirring at 0 °C. The resulting mixture was left to stir overnight at room temperature. Afterward, the reaction mixture was concentrated under vacuo and then

diluted with 50 mL of deionized water. The mixture was extracted with dichloromethane (3×20 mL). The combined organic extracts were dried using anhydrous MgSO4 and concentrated under vacuo, leading to a yellow oil. The crude product was further purified using column chromatography performed on silica gel using a mixture of dichloromethane and ethyl acetate (v/v=4:1) as the eluent, resulting in a yellow oil. Yield: 1.40 g (93%).

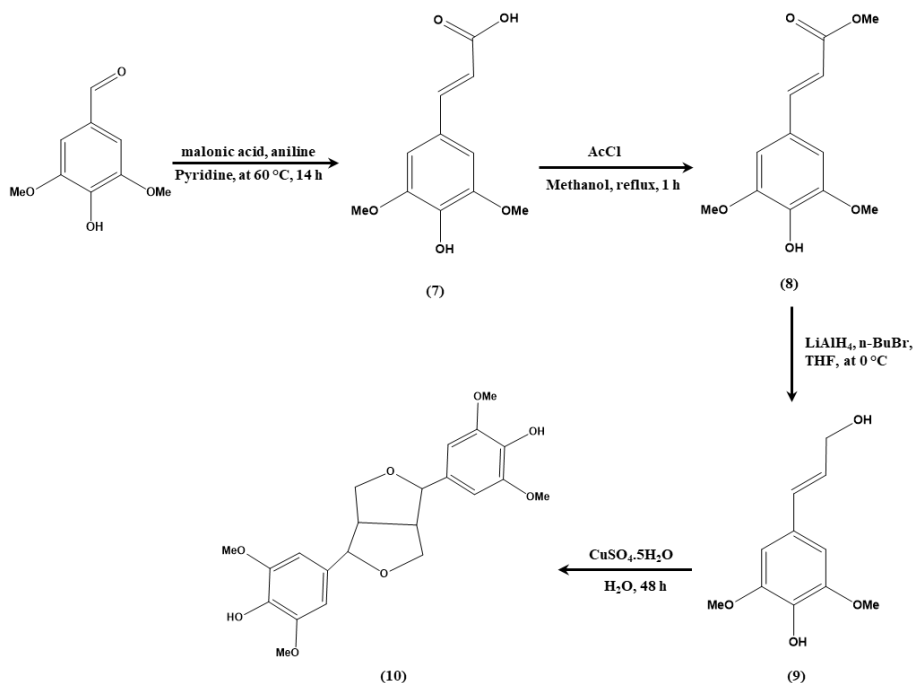### 5.2.2 Synthesis of β-1 linkage lignin model compound (6)
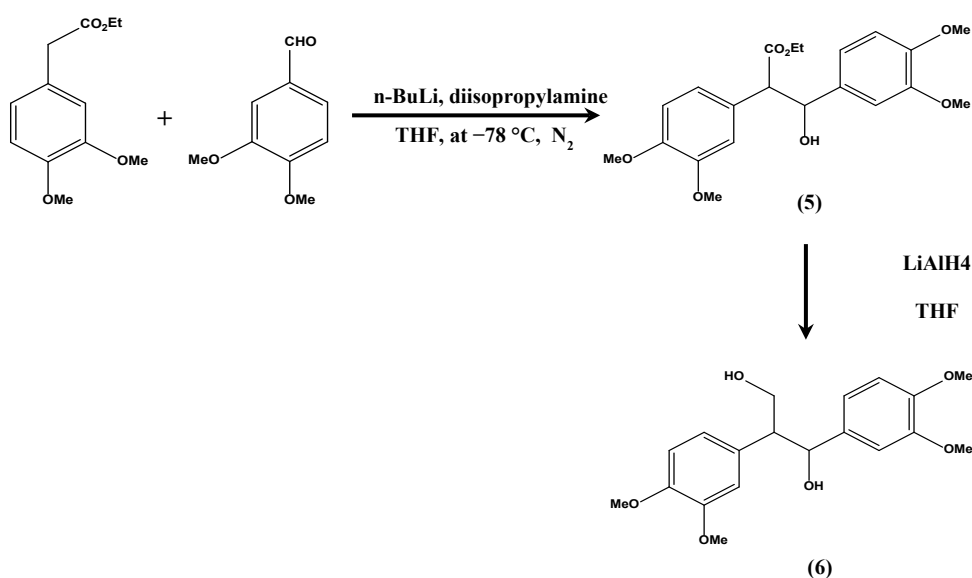


Scheme 5.4. Synthesis of β-1 linkage lignin model compound (6)

Compounds (5) and (6) were prepared according to a literature procedure.[13] A solution containing 6. 5 mL of 2.5 M n-BuLi (16.25 mmol) was added to a stirred solution of diisopropylamine (2.30 mL, 16.40 mmol) in 15 mL of dry THF at -78 °C under a nitrogen atmosphere. After 30 minutes, ethyl 3,4-dimethoxyphenyl acetate (3.70 g, 16.50 mmol) was added dropwise to the reaction mixture, which was then stirred for 1 hour. Subsequently, veratrylaldehyde (2.25 g, 13.54 mmol) was added, and the resulting solution was stirred for an additional 3 hours at the same temperature. After that, the reaction

mixture was diluted with 50 mL of water and then extracted three times with ethyl acetate (3 × 50 mL). The combined organic layers were dried using $Na_2SO_4$ and evaporated under vacuo. Purification was achieved through column chromatography on silica gel using a mixture of hexane and ethyl acetate (3:1) as the eluent, yielding (5) as a yellow oil. Yield: 2.22 g (5.69 mmol, 42 %)

A solution of 2.0 M $LiAlH_4$ (2.82 mL, 5.64 mmol) in THF was added to the ester (5) (1.10 g, 2.82 mmol) dissolved in 50 mL of THF within an ice bath. The resulting mixture was stirred for 30 minutes at 0 °C, followed by an additional 3 hours at room temperature. After this, the solution was diluted with 20 mL of water and acidified with 25 mL of 1 M HCl solution. The mixture was then extracted three times with ethyl acetate (3 × 50 mL). The combined organic layers were dried with $Na_2SO_4$ and evaporated under vacuo. To purify the crude product, column chromatography on silica gel was carried out using a hexane/ethyl acetate mixture (3 :1) as the eluent. This process yielded (6) as a yellow oil. Yield: 0.55 g (1.58 mmol, 56%)

### 5.2.3 Synthesis of β-β linkage lignin model compound (10)



Scheme 5.5. Synthesis of β-β linkage lignin model compound (10)

Compounds (7), (8), (9), and (10) were prepared according to a literature procedure.[222]

### 5.2.3.1 Synthesis of sinapic acid (7)

Malonic acid (12.6 g, 12.1 mmol) and aniline (658 μL, 7.21 mmol) were added to a solution of syringaldehyde (10.0 g, 54.9 mmol) in pyridine (27 mL). The resulting mixture was heated at 60 °C for 14 hours, followed by cooling and pouring onto a mixture of ice (55 g) and concentrated hydrochloric acid (37%, 33 mL). After stirring the mixture once, it was left to crystallize for 30 minutes. The product was collected by filtration, washed with a small volume of cold water, and then dried under reduced pressure over

CaCl$_2$ for 16 hours. This process yielded sinapic acid (7) as a pale yellow crystalline solid. Yield: 11.08 g (49.4 mmol, 90 %)

### 5.2.3.2 Synthesis of methyl sinapate (8)

Acetyl chloride (AcCl) (3.50 g, 44.6 mmol) was added dropwise to 100 mL of methanol at 0 °C, and the resulting mixture was stirred for 15 minutes. Subsequently, sinapic acid (7) (10.0 g, 44.6 mmol) was added, and the mixture was heated at reflux for 1 hour. After refluxing, the mixture was cooled, and the product began to crystallize. To remove most of the methanol, the mixture was carefully concentrated under vacuo. The resulting product was collected by filtration and washed with a small amount of cold methanol, resulting in methyl sinapate (8) as a crystalline pale yellow solid. Yield: 9.77 g (41.1 mmol, 92 %)

### 5.2.3.3 Synthesis of sinapyl alcohol (9)

LiAlH$_4$ (1.38 g, 36.4 mmol) was dissolved in THF (100 mL) at 0 °C. n-BuBr (4.98 g, 36.4 mmol) was then added dropwise to the solution, and the resulting mixture was stirred at room temperature for 3 hours. The mixture was subsequently cooled to -78 °C, and a solution of methyl sinapate (8) (4.0 g, 18.2 mmol) in 100 mL of THF was added using a cannula. The mixture was then allowed to warm to room temperature and stirred for 2 hours until TLC analysis indicated that the reaction was complete. Ethyl acetate (EtOAc, 20 mL) was then added slowly and the mixture was stirred for 30 minutes, followed by the gradual addition of water until gas evolution ceased. A saturated solution of NH$_4$Cl was then added until a semi-solid paste formed. The clear colorless organic layer was separated, and the remaining paste was re-extracted with EtOAc (5 x 250 mL). The organic extracts were combined, washed with brine (500 mL), dried using MgSO$_4$, and

concentrated in vacuo to obtain a light-yellow oil that was used immediately in the subsequent reaction. Yield: 3.35 g (15.9 mmol, 95 %)

### 5.2.3.4 Synthesis of syringaresinol (10)

Sinapyl alcohol (9) (3.20 g, 15.2 mmol) was dissolved in water (1000 mL), and $CuSO_4.5H_2O$ (3.79 g, 15.2 mmol) was then added to the solution. The reaction mixture was vigorously stirred in the presence of light and air for 48 hours, during which a gummy solid formed in the flask. Subsequently, the reaction mixture was extracted with ethyl acetate (EtOAc) (4 x 250 mL), and the combined organic extracts were washed with brine (1000 mL), dried with $Na_2SO_4$, and concentrated under vacuum. The resulting orange gum was dissolved in ethanol (approximately 20 mL) and left to crystallize in the refrigerator overnight. Afterward, the obtained white precipitate was collected by filtration and washed with cold ethanol, yielding syringaresinol (10) as a light yellow solid. Yield:1.91 g (4.57 mmol, 60 %)

### 5.2.4 General procedure for aerobic oxidation of β-O-4 linkage lignin model compound (4)

The oxidation of lignin model compound (4) was conducted in a 100 mL 3-neck round-bottom flask using a Radleys Starfish reactor. The substrate (1 mmol), catalyst (100 mg), dodecane (1 mmol) and 10 mL of dimethylformamide (DMF) were added to the 3-neck round-bottom flask. The lignin model compound was oxidized under flowing $O_2$ (10 mL/min) at 120 °C and 500 rpm stirring. An aliquot (150 μL) was taken periodically from the reaction mixture, to which 1 mL THF was added in a GC vial. The sample was then analyzed by GC-MS.

### 5.2.5 Product analysis

The conversion of the substrate, product yield and selectivity were monitored using GC-MS on an Agilent 7890 GC with a tandem Agilent 5975C MS detector. A DB-1701 column was used (60 m × 0.25 mm × 0.25 μm or 15 m × 0.25 mm × 0.25 μm as appropriate). Helium was used as carrier gas with the flow rate set to 1 mL/min for the 60 m column and 0.5 mL/min for the 15 m column. The inlet temperature for the 60 m column was maintained at 280 °C, with a method set to 45 °C for 3 min, ramp to 280 °C at 4 °C/min, and hold for 10 min. The inlet temperature for the 15 m column was maintained at 280 °C with a temperature ramp of 60 °C to 80 °C at 2 °C/min, then to 110 °C at 3 °C/min, followed by a 20 °C/min ramp to 190 °C, and finally a 2 °C/min ramp to 280 °C. All analyses were quantified using a single point GC-MS internal standard method by obtaining internal response factors of all starting materials and products using n-dodecane as standard. All aliquots of monomers and its oxidation products, and respective calibration samples, were derivatized using (N,O-bis(trimethylsilyl)trifluoroacetamide) (BSTFA) prior to GC-MS analysis.

### 5.2.6 General procedure for aerobic oxidation of β-1 linkage lignin model compound (6)

The oxidation of lignin model compound (6) was conducted in a 100 mL 3-neck round-bottom flask using a Radleys Starfish reactor. The substrate (0.5 mmol) and catalyst (50 mg) and 10 mL of dimethylformamide (DMF) were added to the 3-neck round-bottom flask. The lignin model compound was oxidized under flowing $O_2$ (10 mL/min) at 120 °C and 500 rpm stirring for 48 h. The mixture was then cooled, diluted with water (20 mL) and extracted with ethyl acetate (3 x 25 mL). The combined organic layers were then dried over $Na_2SO_4$ and concentrated under vacuo. The products were purified by column chromatography on silica gel (hexane/ethyl acetate = 6: 1). Then the products were analyzed by NMR.

### 5.2.7 General procedure for aerobic oxidation of β-β linkage lignin model compound (10)

The oxidation of lignin model compound (10) was conducted in a 100 mL 3-neck round-bottom flask using a Radleys Starfish reactor. The substrate (0.5 mmol) and catalyst (50 mg) and 10 mL of dimethylformamide (DMF) were added to the 3-neck round-bottom flask. The lignin model compound was oxidized under flowing $O_2$ (10 mL/min) at 120 °C and 500 rpm stirring for 48 h. The mixture was then cooled, diluted with water (20 mL) and extracted with ethyl acetate (3 x 25 mL). The combined organic layers were then dried over $Na_2SO_4$ and concentrated under vacuo. The products were analyzed by NMR spectroscopy.

### 5.2.8 NMR characterization of products obtained from the oxidation of β-1 and -β-β linkage lignin model compounds

$^1$H and $^{13}$C Nuclear Magnetic Resonance (NMR) spectra were obtained on a 400 MHz Bruker spectrometer. To prepare NMR samples, 10 mg of sample was directly added to the NMR tube. 600 µL $CDCl_3$ or DMSO was used as the solvent. Each spectrum was collected using 32 scans. The NMR spectra were processed using TopSpin software.

### 5.3 Results and Discussion

The performance of bimetallic catalysts based on $Au_1Pd_1$/Li-Al LDH was evaluated in the oxidation of lignin model compounds containing β-O-4, β-1 and β-β linkages. The oxidation reactions were conducted at a temperature of 120 °C while maintaining a continuous flow of oxygen (10 mL min$^{-1}$) at a pressure of 1 atm. In the initial phase of our experiments, we focused on oxidation of the β-O-4 linked lignin model compound labeled as (4). The resulting reaction products were analyzed using Gas Chromatography-Mass Spectrometry (GC-MS) at regular intervals over a span of 48 hours.

As illustrated in Figure 5.2, the $Au_1Pd_1$/Li-Al LDH catalyst exhibited remarkable selectivity in promoting the oxidation of the secondary benzylic alcohol within compound (4), yielding product (4a). It is noteworthy that compound (4a) undergoes two concurrent and competing reactions: the formation of compound (4b), an enol ether, through dehydration, and the generation of compound (4c), which represents a retro-aldol cleavage product resulting from the oxidation of the gamma-alcohol group in (4a). Notably, compound (4c) possesses the potential for further oxidation, leading to the formation of guaiacol (4d) and p-anisic acid (4e). The oxidative cleavage of the β-O-4 linkage within compound (4c) is attributed to the notably weaker C–O bond in (4c) compared to the initial benzylic alcohol compound.[167, 194, 223] Subsequently, the reaction between guaiacol (4d) and p-anisic acid (4e) gives rise to product (4f) via esterification. It is worth mentioning that due to the undesired and reversible nature of the esterification process, product (4f) can be readily cleaved via a straightforward hydrolysis reaction, which can be carried out as a separate step in the overall process.[194]
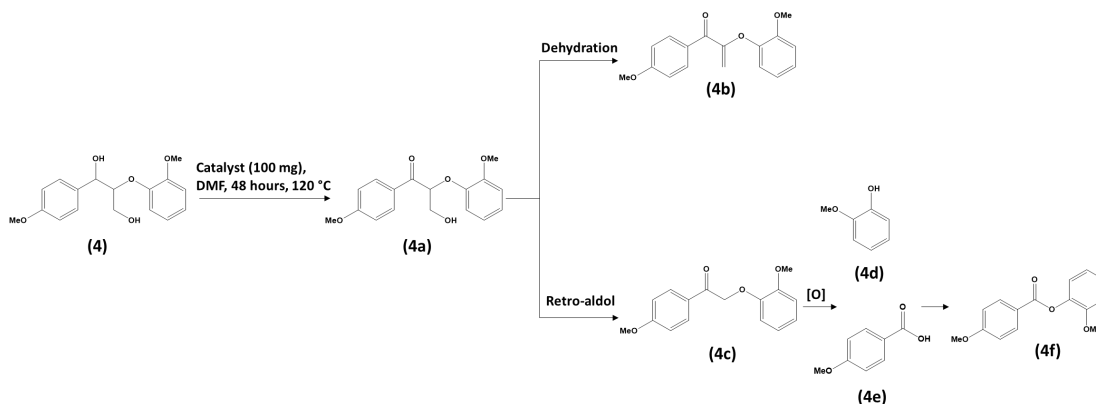


Figure 5.2 Oxidation of β–O–4 linked lignin model compound (4)

The evolution of the product yields with time provides valuable insights into the reaction kinetics and product selectivity. The yields of the various products resulting from oxidation of the β–O–4 linked lignin model dimer (4) are presented as a function of time in Figure 5.3. Under the given conditions, the catalyst system demonstrated a remarkable

ability to selectively oxidize the secondary benzylic alcohol in compound (4a), yielding a reaction rate of 1.1 mmol h$^{-1}$ gcat$^{-1}$.This resulted in a 60% yield of (4a) within an 8 hour timeframe, corresponding to 88% conversion of compound (4) (reaching nearly 98% conversion after 48 hours). Under these reaction conditions, compound (4a) underwent further transformations, leading to the formation of the dehydration product, (4b), at a rate of 0.12 mmol h$^{-1}$ gcat$^{-1}$,and the retro-aldol product, (4c), at a rate of 0.28 mmol h$^{-1}$ gcat$^{-1}$.The notably high reaction rate observed for the formation of the retro-aldol product (4c) can be attributed to the inherent basic properties of the Li-Al support, a phenomenon that has been previously documented in the literature.[167, 224] Although compound (4b) did not exhibit any further reactivity, compound (4c) reached a maximum yield of 33% after 24 hours, subsequently giving rise to guaiacol (4d) and p-anisic acid (4e) at a rate of 0.25 mmol h$^{-1}$ gcat$^{-1}$.The formation of products (4d) and (4e) through the cleavage of the β-O-4 bond in compound (4c) utilizing molecular oxygen has also been observed and documented across various literature sources.[167, 225] In a subsequent esterification reaction, compounds (4d) and (4e) formed compound (4f) with a rate of 0.05 mmol h$^{-1}$ gcat$^{-1}$.
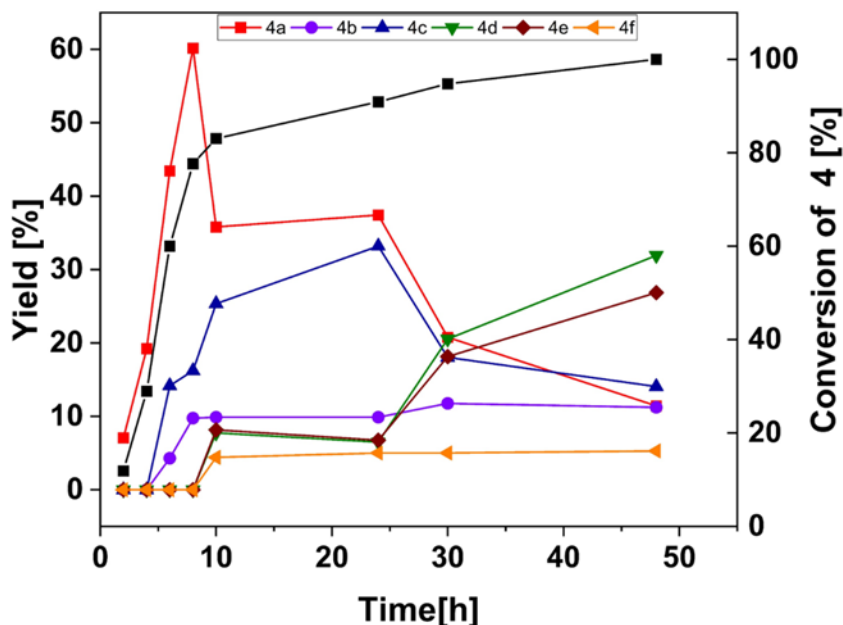
Figure 5.3 Aerobic oxidation of lignin model dimer (4) using $Au_1Pd_1$/Li–Al LDH. Conditions: Substrate (1 mmol), catalyst (100 mg), dimethylformamide (10 mL), 120 °C, p = 1 atm. $O_2$ (10 mL min$^{-1}$). Substrate conversion and product yields were determined by GC-MS using dodecane as internal standard

In a similar manner, Song et al. conducted an investigation of the oxidation of (4) using Au/Li-Al LDH (prepared through a deposition-precipitation method) as the catalyst, under identical reaction conditions. Their study revealed the occurrence of the same reaction pathways, and it was reported that the conversion of the dimer reached approximately 85% after 42 hours.[167] Furthermore, Yanjun et al.[194] explored the oxidation of compound (4) utilizing mesoporous $Fe_2O_3$-supported Au nanoparticles as the catalyst. Their findings demonstrated that the Au/meso-$Fe_2O_3$ catalyst displayed a remarkable selectivity for the oxidation of the gamma-alcohol, achieving an almost complete conversion of 96% within a 12-hour timeframe. Additionally, they observed the generation of corresponding carbonyl products resulting from the cleavage of β–O–4 linked lignin model dimers under sub-atmospheric pressure conditions.

Cui et al.[226] reported an electrochemical based oxidation of a β-O-4 lignin model compound as a representative substrate under mild conditions as presented in Scheme 5.4. They used atomically dispersed Pt–N$_3$C$_1$ sites deposited on nitrogen-doped carbon nanotubes (Pt$_1$/N-CNTs) as a catalyst. This approach yielded a mixture comprising benzaldehyde (with a yield of 52%) and guaiacol (31% yield), achieving an impressive overall conversion of 99%.
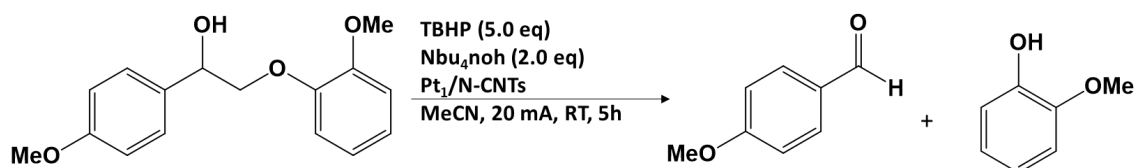


Scheme 5.4 Oxidation of (2) according to Cui et al.[6]

In lignin-first processes (utilizing reductive depolymerization), a substantial portion of the resulting lignin oil, exceeding 50%, remains unutilized.[227] This unutilized fraction comprises dimers and higher oligomers that are intricately bonded by robust C-C bonds with high bond dissociation energies (ranging from 80 to 120 kcal mol$^{-1}$).[228] Moreover, the dimeric and oligomeric fractions exhibit significant irregularities, making their effective utilization challenging. Recently, there has been growing interest in finding ways to make use of these dimers and oligomers.[229] In light of these considerations, we examined the oxidative cleavage of C-C bonds in β-1 and β-β model compounds by utilizing the Au$_1$Pd$_1$/Li-Al LDH catalyst.

To explore the potential of the Au$_1$Pd$_1$/Li-Al LDH catalytic system, we investigated its effectiveness in depolymerizing the β-1 model compound (6) under identical reaction conditions to those employed for the oxidation of the β-O-4 model compound (4). After the oxidation reaction, the mixture was extracted with ethyl acetate and the dissolved

products were purified by column chromatography on silica gel. Our experimental observations substantiate the effective oxidation and cleavage of the β-1 model compound, 42% conversion being achieved within a 48-hour timeframe. This process yields benzaldehyde (6a) and benzoic acid (6b) with yields of 44% and 41%, respectively, as exemplified in Figure 3. The identity of these products was validated through NMR analysis.
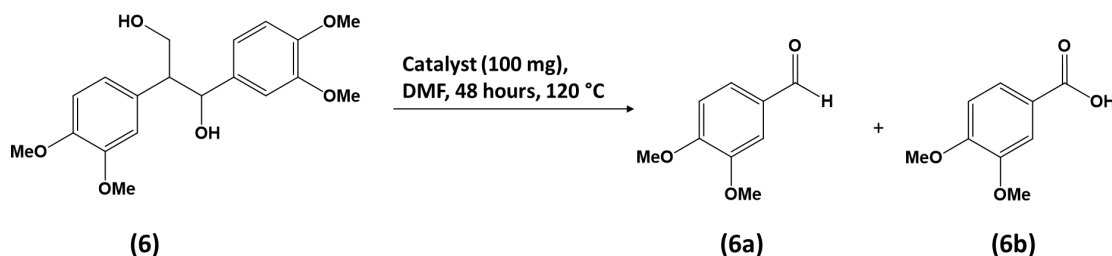


**(6)**              **(6a)**      **(6b)**

Figure 5.4 Oxidation of lignin model dimer (6) using $Au_1Pd_1$/Li–Al LDH. Conditions: Substrate (0.5 mmol), catalyst (100 mg), dimethylformamide (10 mL), 120 °C, p = 1 atm. O2 (10 mLmin-1). Substrate conversion and product yields were determined by gravimetric analysis

Fang et al.[13] conducted a detailed examination of various oxidation methods on the cleavage of β-1 lignin linkage using model compound (6). These methods encompassed KMnO4 under acidic conditions, DDQ (2,3-dichloro-5,6-dicyano-1,4-benzoquinone), and TEMPO-based (2,2,6,6-tetramethyl-piperidin-1-oxy) oxidation. In the case of the β-1 model compound treated with KMnO4 under acidic conditions, they observed the direct oxidative cleavage of C-C bonds, yielding same benzaldehyde and benzoic acid with efficiencies of 12% and 15%, respectively. When subjected to oxidation with DDQ, compound (6) afforded the corresponding ketone with a high yield of 93%, as illustrated in Scheme 5.6.
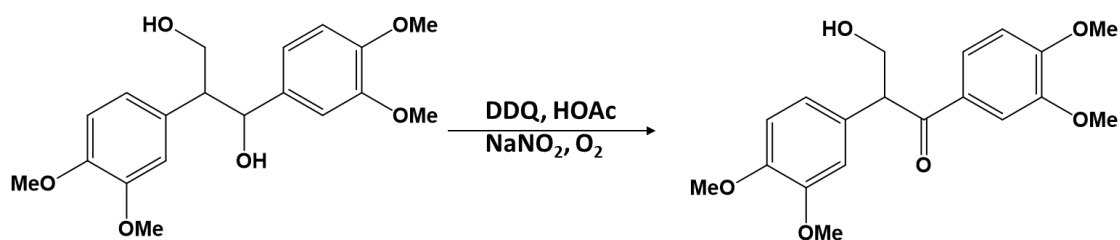
Scheme 5.5 Oxidation of (6) using DDQ[13]

In the case of TEMPO-based oxidation, a diverse array of oxidation systems, each employing TEMPO as a central component, has been developed. To facilitate a direct comparison among these distinct systems, a comprehensive analysis of oxidation product yields was carried out under standardized reaction conditions lasting 19 hours. When subjecting the β-1 model (6) to oxidation, the CuCl/TEMPO/$O_2$ system produced benzoic acid (27%), benzaldehyde (75%), and diketone (19%). Conversely, the Fe(NO$_3$)$_3$/TEMPO/$O_2$ system exclusively yielded ketone (46%) and aldehyde (31%), as depicted in the accompanying scheme 5.6.
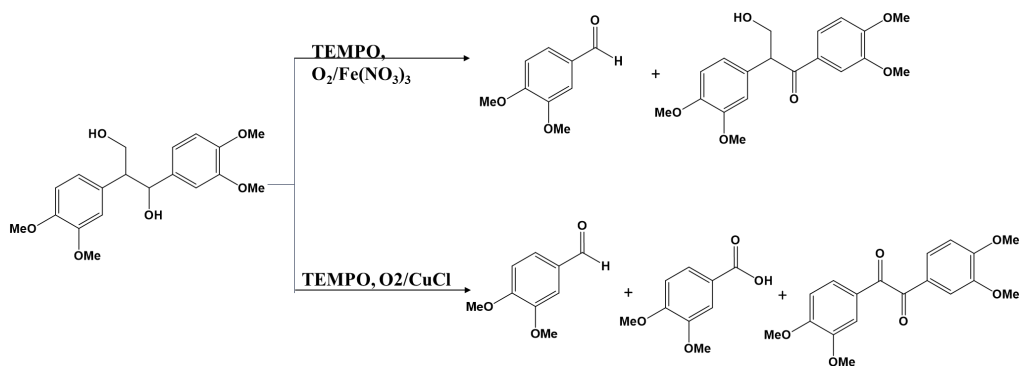


Scheme 5.6 Oxidation of (6) with TEMPO-based oxidation[13]

Wang et al.[230] conducted an extensive investigation into the catalytic depolymerization of a simplified lignin model compound using a $^t$BuOK-based catalytic

system devoid of transition metals. The study employed both β-O-4 and β-1 model compounds as substrates. Notably, the oxidation outcomes of the β-1 model compounds demonstrated the effective cleavage and depolymerization of the lignin model compound, as illustrated in Scheme 5.7 The experimental findings unequivocally establish the successful depolymerization of the β-1 model compound under these conditions, yielding a sole product, namely benzoic acid, in an approximate yield of 60%.
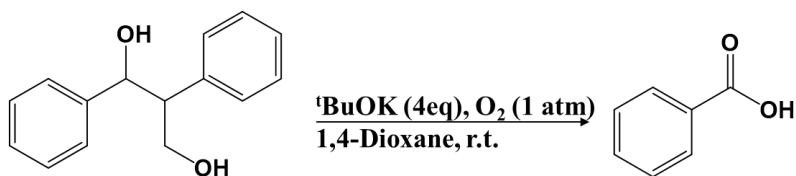


Scheme 5.7 Oxidation of β-1 model compound using a tBuOK-based oxidation system[230]

The oxidation and cleavage of the β-β linkages in lignin present a formidable challenge due to their robust chemical structure. Breaking these linkages can enhance lignin's reactivity, rendering it more amenable to conversion into valuable products. Therefore, in this study, we explored the potential of the $Au_1Pd_1$/Li-Al LDH catalytic system. We investigated its effectiveness in depolymerizing a β-β linked lignin model compound (12) under the same reaction conditions employed for the oxidation of (4). After the oxidation reaction, the mixture was extracted with ethyl acetate and the dissolved products were purified by column chromatography on silica gel and were analyzed using NMR spectroscopy and GC-MS. According to the results, the β-β model compound (12) underwent oxidation in the presence of the catalyst, achieving a 55% conversion within a 48-hour period. In this process, syringaldehyde was the sole identifiable product, yielding 45%, assuming a 1:2 molar ratio of the starting material to syringaldehyde, as demonstrated in Scheme 5.8. However, the fact that the yield is lower than the conversion suggests the potential formation of other aromatic ring-containing products that may not have been detected through NMR analysis or GC-MS analysis, possibly due to their low yield.

110
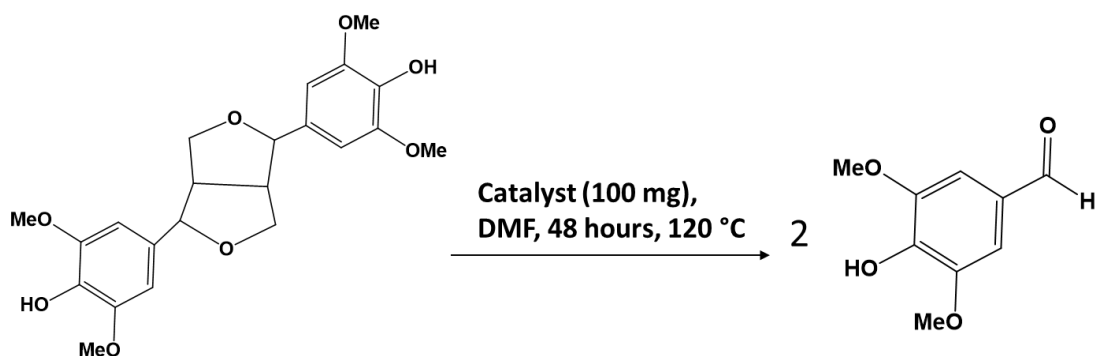
Scheme 5.8 Aerobic oxidation of lignin model dimer (12) using Au₁Pd₁/Li–Al LDH. Conditions: Substrate (0.5 mmol), catalyst (100 mg), dimethylformamide (10 mL), 120 °C, $p = 1$ atm. $O_2$ (10 mL min⁻¹)

The 2D HSQC NMR results obtained from the oxidation of GVL lignin (Chapter 4) provide valuable insights into the chemical transformations occurring during the reaction. Following the oxidation process, a significant observation was the absence of signals corresponding to the β-aryl ether (β-O-4) linkages in the aliphatic region of the GVL product. This absence of signals strongly indicates that the Au₁Pd₁/Li-Al LDH catalyst effectively cleaved the β-O-4 linkages within the lignin structure. Our findings, when considered alongside the results obtained from the oxidation of the β-O-4 lignin model compound, support the hypothesis that the β-aryl ether units in lignin may follow a reaction pathway similar to that illustrated in Figure 5.2. This pathway underscores the pivotal role of the Au₁Pd₁/Li-Al LDH catalyst in facilitating the cleavage of β-O-4 linkages in lignin, thus contributing to the depolymerization process. Conversely, when examining the residual β-β resinol units after the oxidation reaction, we observed weak signals corresponding to these units. This observation aligns with our understanding of the oxidation of β-β model compounds, where complete conversion is not typically achieved. It suggests that the β-β resinol units exhibit a different reactivity or stability during the

oxidation process. Furthermore, during the oxidation of GVL lignin, we were able to identify the formation of syringaldehyde as a reaction product. This finding raises the possibility that a portion of the syringaldehyde may originate from the oxidation of the β-β linkages within the lignin structure. This underscores the complexity of lignin depolymerization and the potential for generating valuable chemical products through selective reactions with specific lignin subunits. These results shed light on the intricate chemistry involved in lignin valorization and offer valuable insights for the development of sustainable and economically viable lignin conversion processes.

Westwood and colleagues conducted a comprehensive investigation into the selective modification of the β–β linkage in kraft lignin by means of oxidation.[231] They employed DDQ (2,3-dichloro-5,6-dicyano-1,4-benzoquinone) in DMF (dimethylformamide) for the treatment. To assess the impact of the oxidation, they subjected the lignin sample to thorough 2D-NMR analysis both before and after the oxidation process. Their analysis revealed a notable reduction in the presence of the β–β linkage in kraft lignin following the oxidation reaction. Motivated by the desire to elucidate the reaction pathways and products resulting from the oxidation of the β–β linkage, the researchers opted to employ a model compound to better understand the chemical reactions occurring in this context. The β–β model compound was treated with varying quantities of DDQ, specifically one mole equivalent and three mole equivalents (as illustrated in Scheme 5.9). Utilization of one mole equivalent of DDQ in DMF led to the formation of an alkene product with a conversion of 50%. Conversely, when the model compound was subjected to treatment with three mole equivalents of DDQ, a pyran-4-one product was obtained in an isolated yield of 45%. Furthermore, a mixture comprising the model compound and the alkene product generated from the β–β model compound with one mole equivalent of DDQ. The outcome of this experiment pointed to the formation of the pyran-4-one product suggesting that the alkene product serves as an intermediate in the conversion process, ultimately leading to the pyran-4-one product.
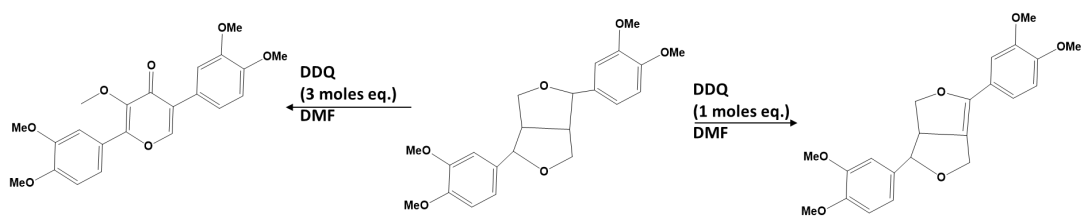
Scheme 5.9 Oxidation of a β-β model compound using DDQ according to Westwood et al.[231]

Samec and his research team explored the oxidation of a β–β model compound using Bobbitt's salt at room temperature in a methanol and water mixture.[227] Their investigation revealed a high selectivity of the oxidation system toward the production of 2,6-dimethoxybenzoquinone (DMBQ). Furthermore, they examined the impact of varying quantities of Bobbitt's salt on the β–β model compound. Specifically, they tested 0.175 mmol and 0.43 mmol of Bobbitt's salt in conjunction with 0.07 mmol of the model compound, as demonstrated in Scheme 5.10. The results of these oxidation reactions indicated a 75% yield of DMBQ when 0.175 mmol of Bobbitt's salt was used, and a significantly higher yield of 91% DMBQ when 0.43 mmol of Bobbitt's salt was employed.
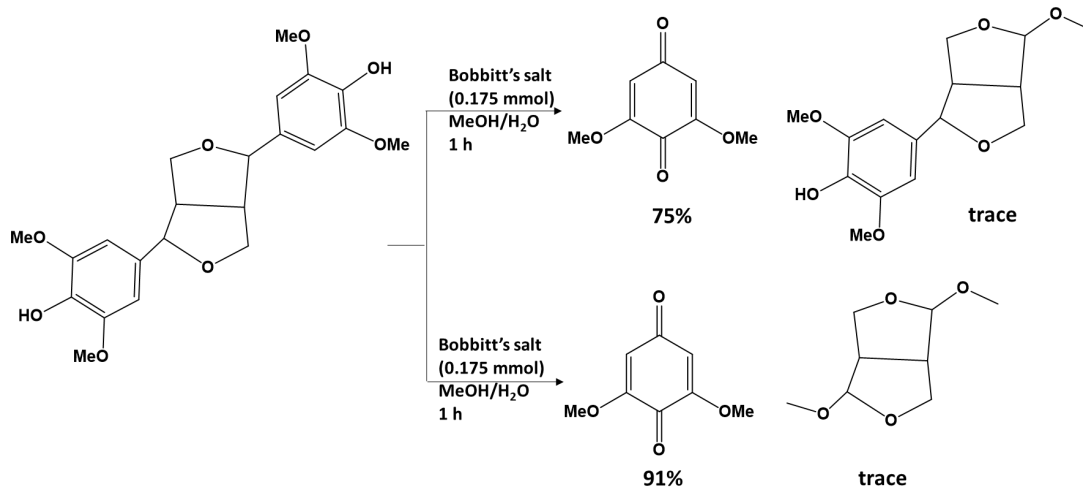
Scheme 5.10 Oxidation of β-β model compound using Bobbitt's salt according to Samec et al.[227]

**5.4     Conclusion**

As part of our research, we systematically prepared various lignin linkage models, including the β-O-4, β-1, and β-β linkages, with the aim of elucidating the intricate chemistry underlying the oxidation reactions facilitated by the $Au_1Pd_1$/Li-Al LDH catalyst under mild reaction conditions. Our investigation into these models yielded valuable insights into the reactivity of lignin subunits. In the case of the β-O-4 model compound, we observed successful oxidation reactions, leading to the cleavage of the β-O-4 linkage and the generation of cleaved products. Similarly, when exploring the β-1 model compound, we observed the direct cleavage of this linkage. These results showcase the $Au_1Pd_1$/Li-Al LDH catalyst's ability to induce selective cleavage of specific lignin linkages, contributing to our understanding of lignin depolymerization pathways. Furthermore, our investigation into the β-β compound revealed a different reactivity pattern. We observed the cleavage of the β-β linkage, accompanied by the formation of syringaldehyde. This observation indicates that the oxidation of the β-β linkage can lead to the generation of valuable chemical products, such as syringaldehyde, adding an intriguing dimension to our exploration of lignin conversion chemistry.

CHAPTER 6.  **CONCLUSION AND FUTURE WORK**

## 6.1    Conclusion

Lignin, a phenolic-rich biomass component, holds great potential for the production of value-added products. However, its complex structure and inherent resistance to breakdown pose substantial challenges in harnessing its full potential. In response to these challenges, we developed a bimetallic catalyst, namely AuPd/Li-Al layered double hydroxide (LDH), with the purpose of facilitating the depolymerization of lignin. To achieve this, a series of catalysts consisting of Au, Pd, and Au–Pd supported on Li-Al LDH was synthesized through a sol-immobilization method.

Our research began by examining the catalytic activity of these catalysts in the oxidation of simple benzylic alcohols. It was evident that among the catalysts tested, $Au_7Pd_3$/Li-Al LDH and $Au_1Pd_1$/Li-Al LDH displayed superior catalytic activity compared to $Au_3Pd_7$/Li-Al LDH, pure Au, and pure Pd catalysts. Encouraged by these results, we delved deeper into the properties of the $Au_7Pd_3$/Li-Al LDH and $Au_1Pd_1$/Li-Al LDH catalysts, focusing on their performance in the aerobic oxidation of benzylic alcohol groups in β–O–4 linked lignin model dimers, conducted under atmospheric pressure. What emerged was a sequential oxidation process, which led to the cleavage of the β-O-4 linkage, illustrating the remarkable potential of these catalysts in lignin depolymerization.

Subsequently, we extended our investigation to the oxidative deconstruction of γ-valerolactone (GVL) extracted maple lignin, conducted at 120 °C using $O_2$ as the oxidant. Of all the catalysts, $Au_1Pd_1$/Li-Al LDH proved to be the most effective, yielding a diverse range of aromatic monomers, including vanillin, vanillic acid, syringaldehyde, and syringic acid, among others, with an impressive 27% total monomer yield. These results strongly indicate that the $Au_1Pd_1$/Li–Al LDH catalyst system holds promise as an eco-friendly and efficient catalyst for lignin depolymerization under mild reaction conditions.

Inspired by the success of our lignin oxidation experiments, we embarked on a study of lignin linkage models, including the β-O-4, β-1, and β-β linkages. Our objective was to gain a deeper understanding of the intricate chemistry underlying the oxidation reactions facilitated by the $Au_1Pd_1$/Li-Al LDH catalyst under mild reaction conditions. These investigations yielded intriguing insights. For the β-O-4 model compound, we witnessed successful oxidation reactions leading to the cleavage of the β-O-4 linkage and the formation of cleaved products. Similarly, when exploring the β-1 model compound, we observed direct cleavage of this linkage. These findings underscore the remarkable ability of the $Au_1Pd_1$/Li-Al LDH catalyst to selectively cleave specific lignin linkages, enriching our understanding of lignin depolymerization pathways. Furthermore, our study of the β-β compound revealed a distinct reactivity pattern. Cleavage of the β-β linkage was accompanied by the formation of syringaldehyde, introducing a new dimension to our exploration of lignin conversion chemistry. In sum, these findings offer a improved understanding of lignin valorization and the potential for the $Au_1Pd_1$/Li-Al LDH catalyst system to pave the way for sustainable and economically viable lignin conversion processes.

## 6.2    Future Work

(1) During this research, we employed a suite of characterization techniques, including $N_2$ physisorption, ICP-MS, TEM, and XPS analysis, to attain a comprehensive understanding of our AuPd bimetallic catalyst system. These techniques have proven invaluable, shedding light on elemental composition, particle size distribution, electronic interactions between Au and Pd, and the catalyst's behavior with support materials. Looking ahead to future investigations, we recognize the paramount importance of incorporating in-situ studies to visualize the dynamic behavior of AuPd bimetallic catalysts under real experimental conditions.

The inclusion of in-situ characterization techniques in our research is imperative, given the intrinsically dynamic nature of AuPd bimetallic catalysts during catalytic reactions.[232] An in-depth comprehension of how these catalysts operate under actual operational conditions is central to optimizing their performance and uncovering the fundamental drivers of their catalytic activity.[233] In-situ techniques offer an invaluable avenue for obtaining real-time insights into the catalyst's dynamic structural and chemical transformations, the behavior of active sites, and the influence of varying reaction parameters.

(2) In our previous research, we conducted a comprehensive investigation into the oxidation of model compounds representing β-O-4, β-1, and β-β linkages. This inquiry was carried out utilizing the $Au_1Pd_1$/Li-Al LDH catalyst system, and it provided us with invaluable insights into the potential reaction pathways and transformations that occur during oxidative lignin depolymerization processes. Building on these findings, our future research endeavors will address an additional significant aspect of lignin chemistry, namely the presence of β-5 linkages, which are noteworthy components of lignin biomass. While our prior work shed light on the reactivity of specific lignin linkages, it is essential to recognize the substantial prevalence of the β-5 linkage within lignin biomass. Depending on the source of lignin and the methods employed for its processing, the β-5 linkage can constitute a significant portion, ranging from 2% to 9% of all linkages in the lignin structure.[23, 221] Consequently, our forthcoming research will extend its focus to encompass the study of model compounds representing the β-5 linked lignin structure. This study will employ the same $Au_1Pd_1$/Li-Al LDH catalyst system, which has demonstrated promise in our prior investigations with other model compounds.

This expanded research approach will enable us to thoroughly explore the reactivity, transformation pathways, and catalytic behavior of β-5 linked lignin model compounds under controlled conditions. By utilizing a consistent catalyst system across a range of model compounds, we aim to develop a comprehensive understanding of the catalyst's performance and its influence on the intricate processes involved in lignin depolymerization.

(3) A few research groups have studied supported AuAg and AuCu bimetallic catalysts mainly for oxidation of CO and benzyl alcohols.[112, 234, 235] These investigations have yielded promising results, demonstrating the high catalytic activity of both AuAg and AuCu bimetallic systems in these chemical transformations. The commonly employed supports in these studies have been $SiO_2$ and $TiO_2$. Looking ahead to future research directions, there is potential for extending these studies into a novel realm of catalysis. The focus would be on Li-Al layered double hydroxide (LDH)-supported Cu and Ag, in conjunction with Au bimetallic nanoparticles. This combination would be specifically tailored for oxidative lignin depolymerization.
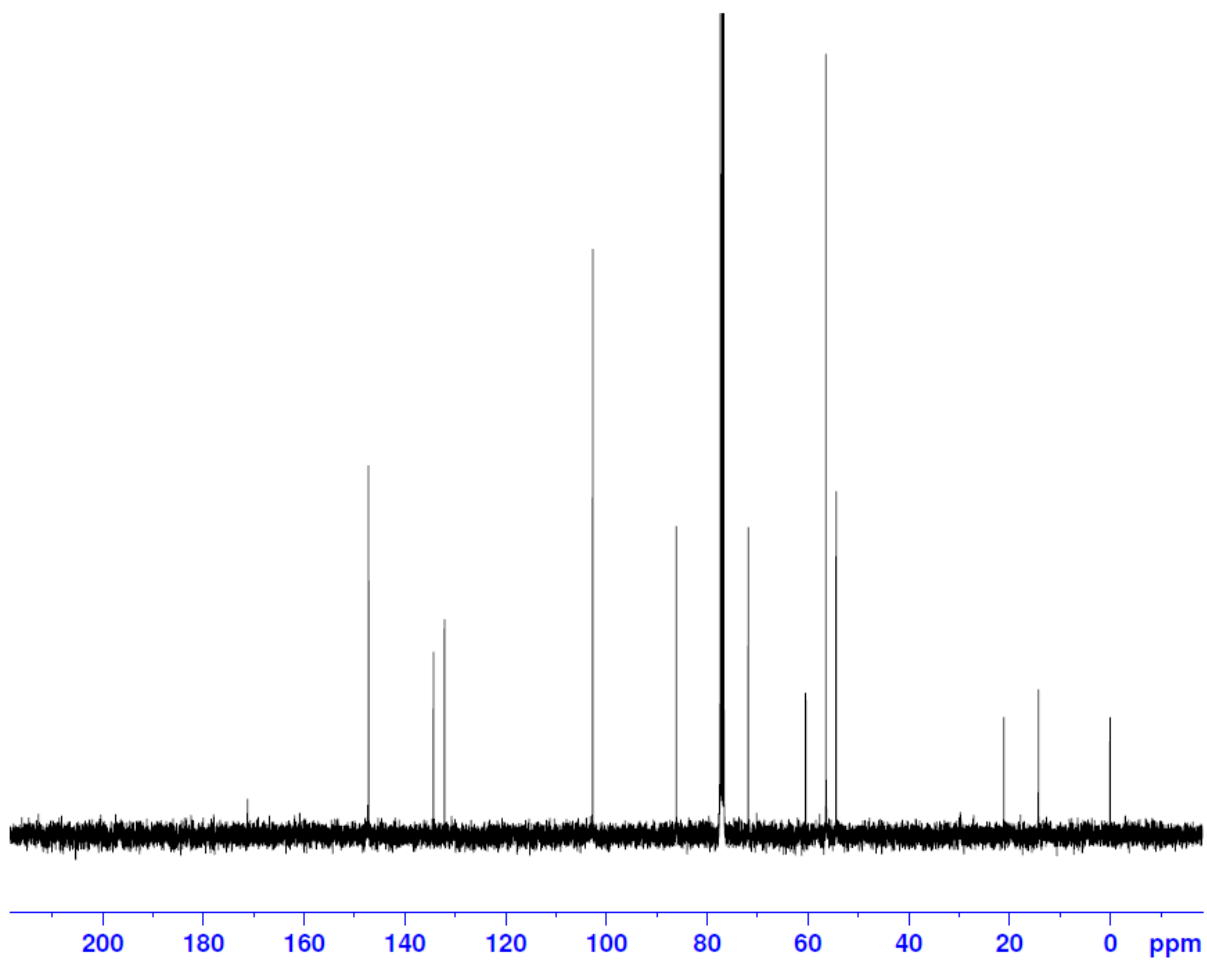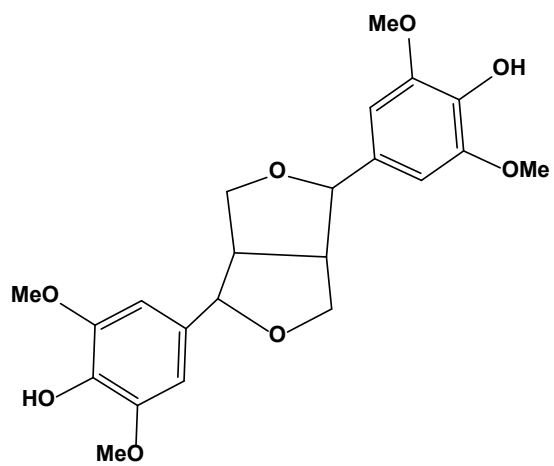
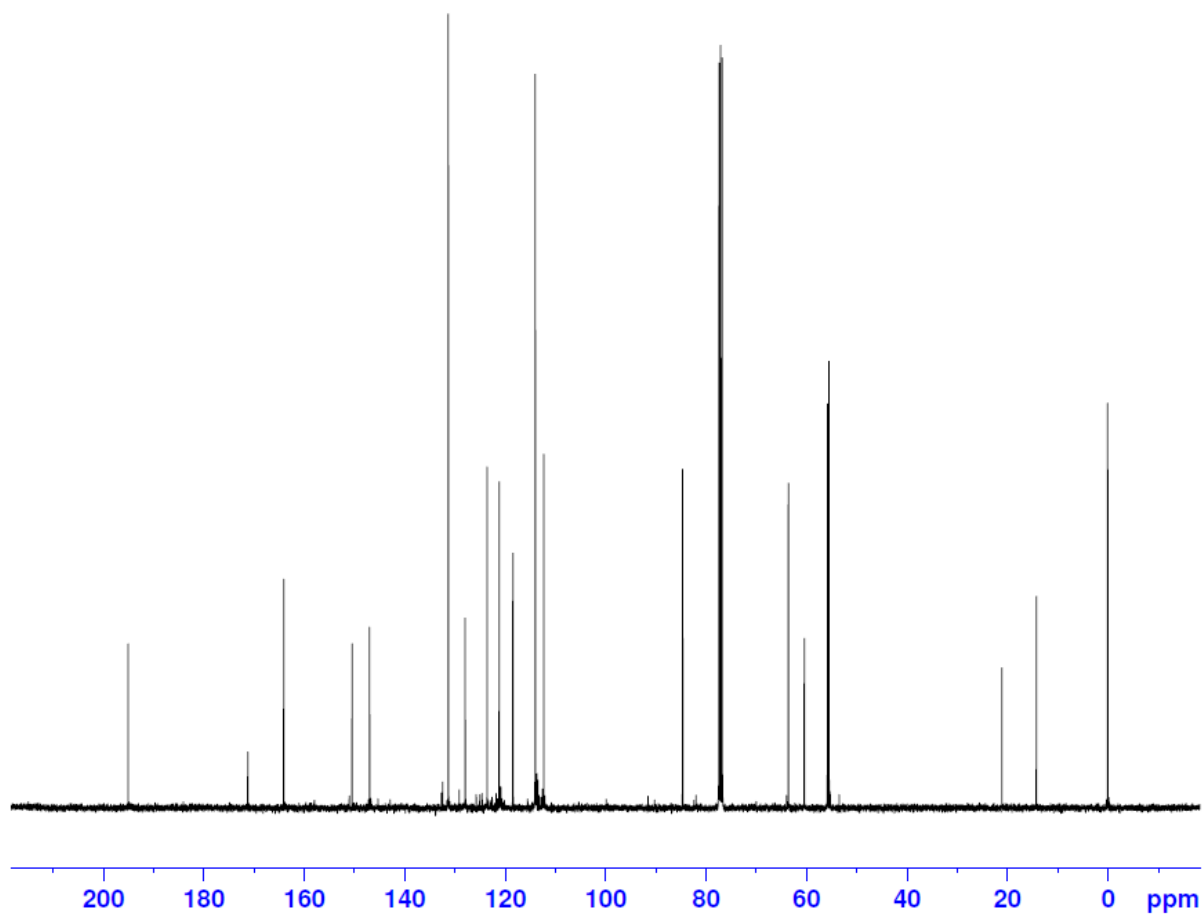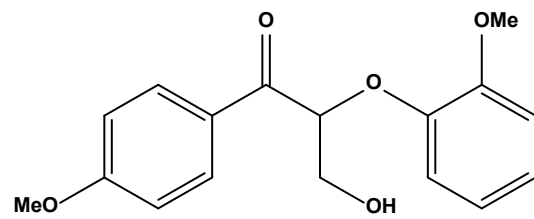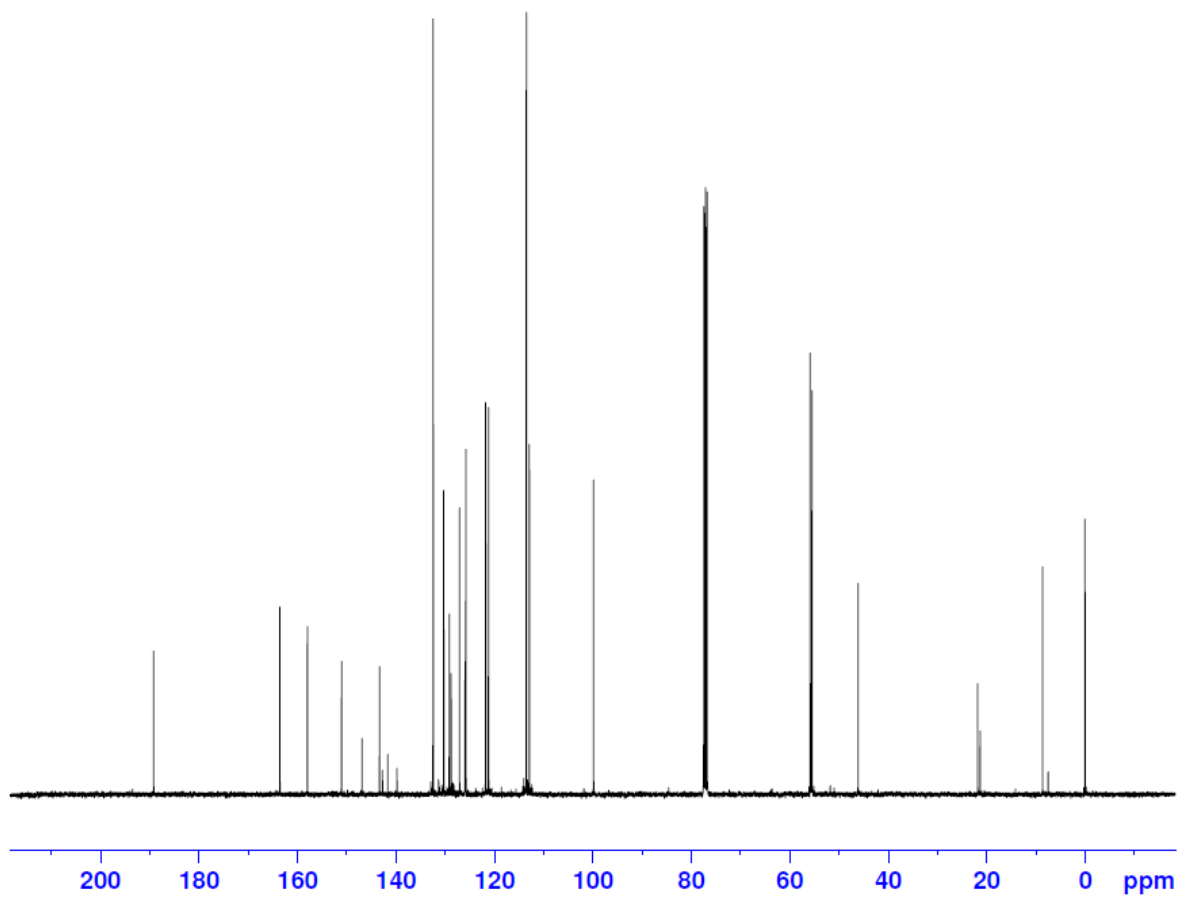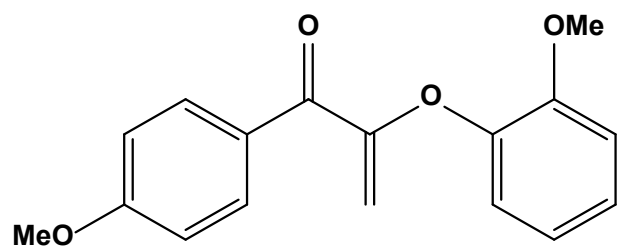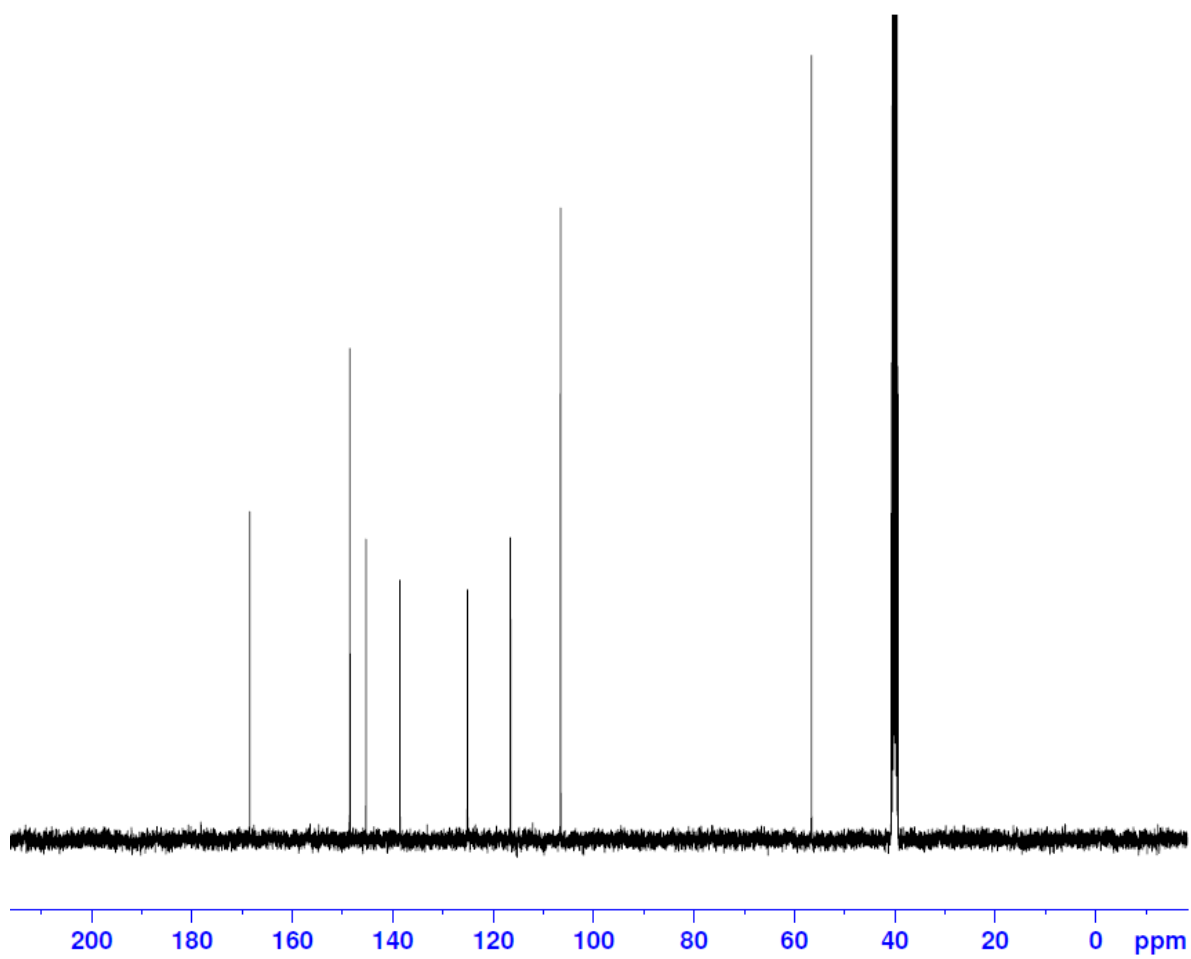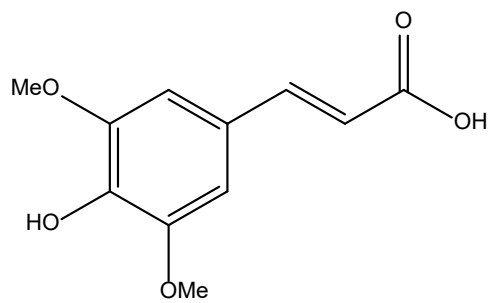$^{13}$CNMR spectra of synthesized lignin model compounds

125

126

130
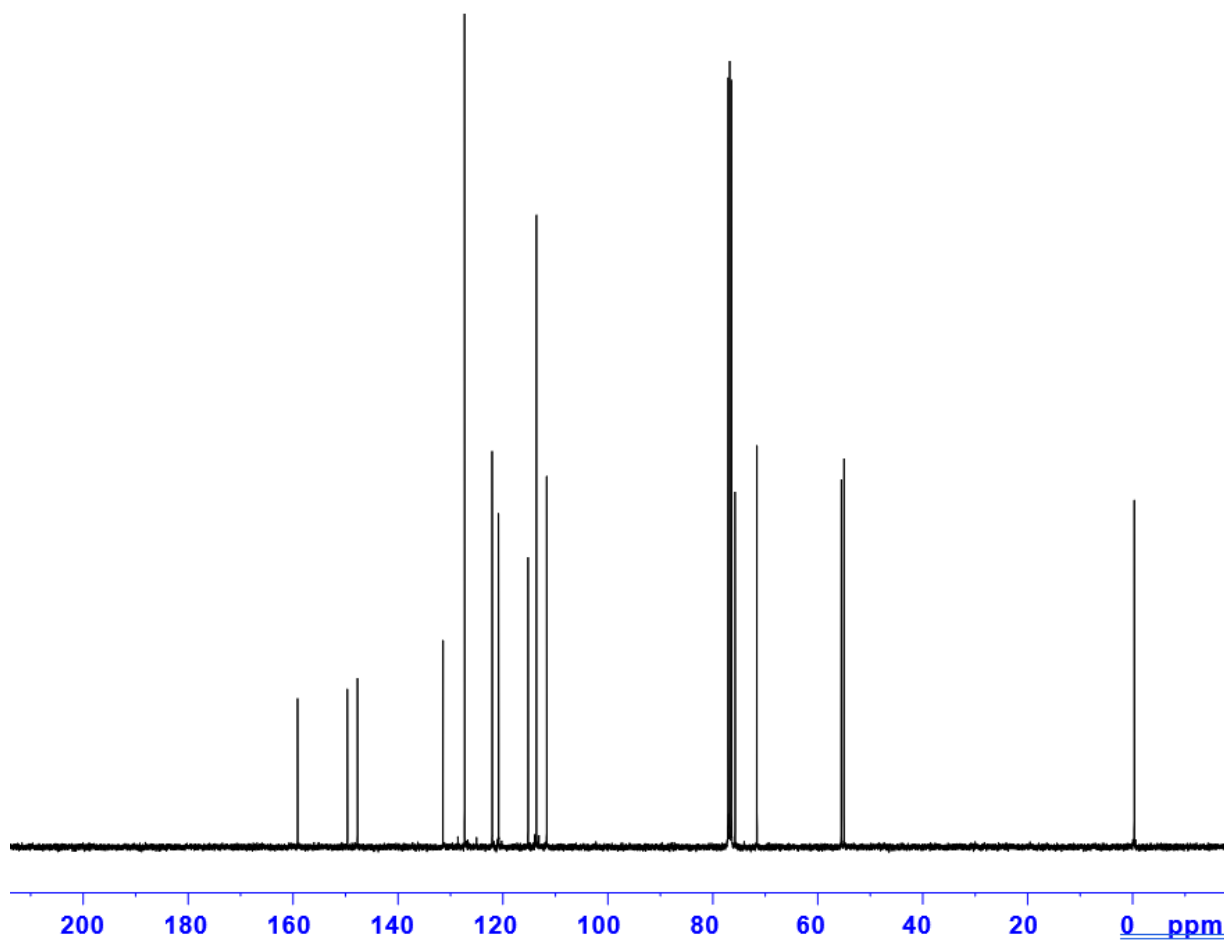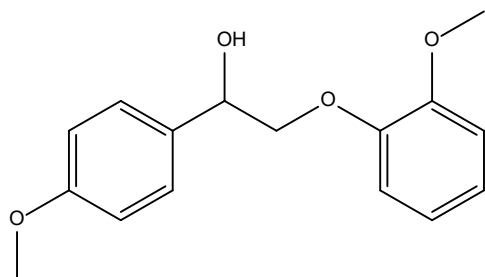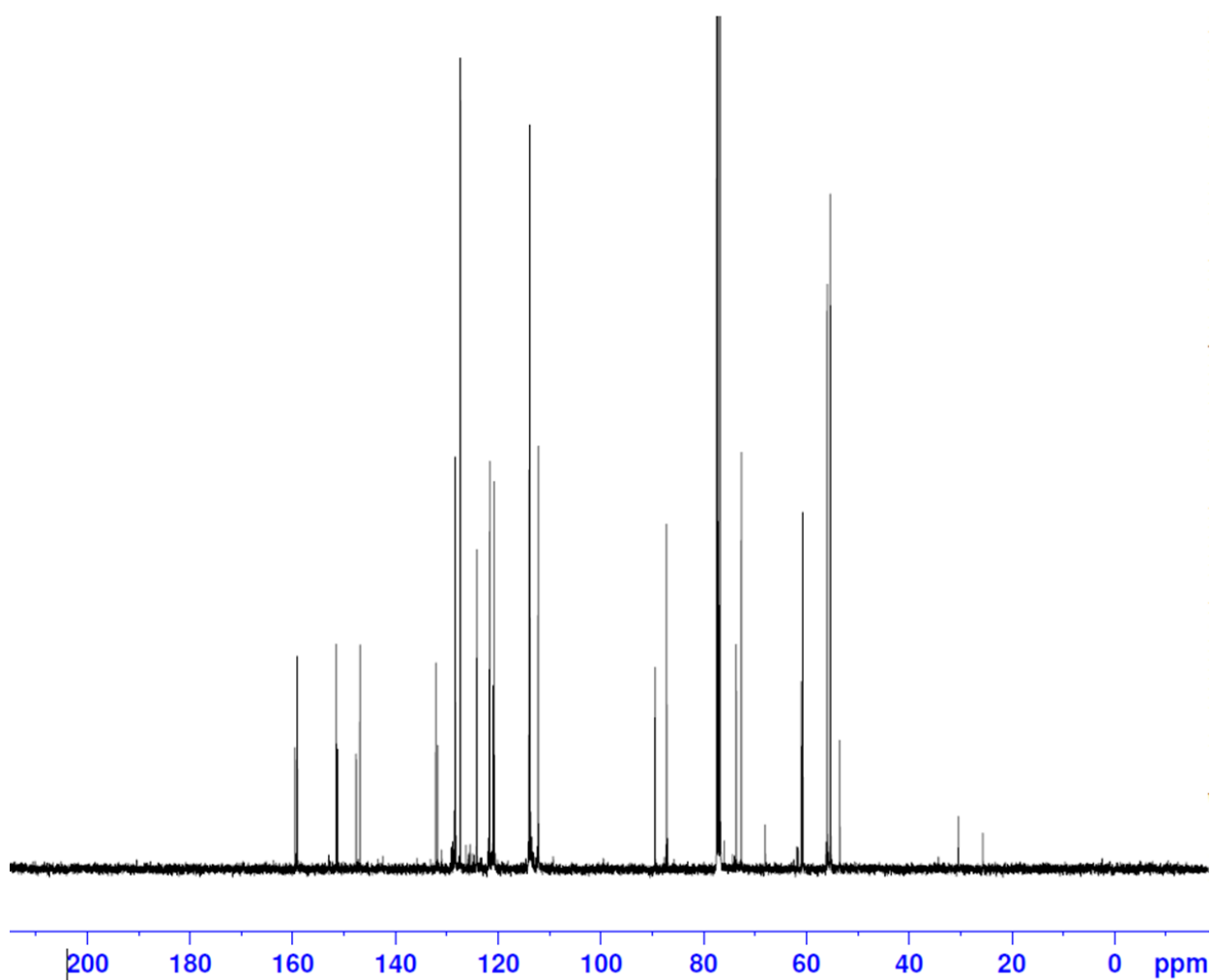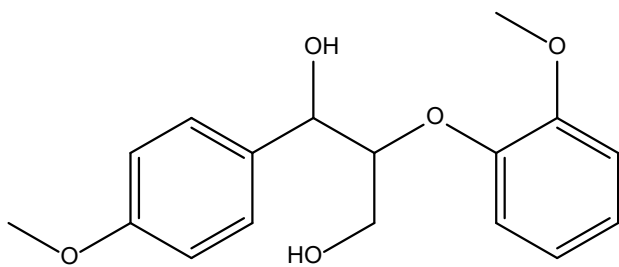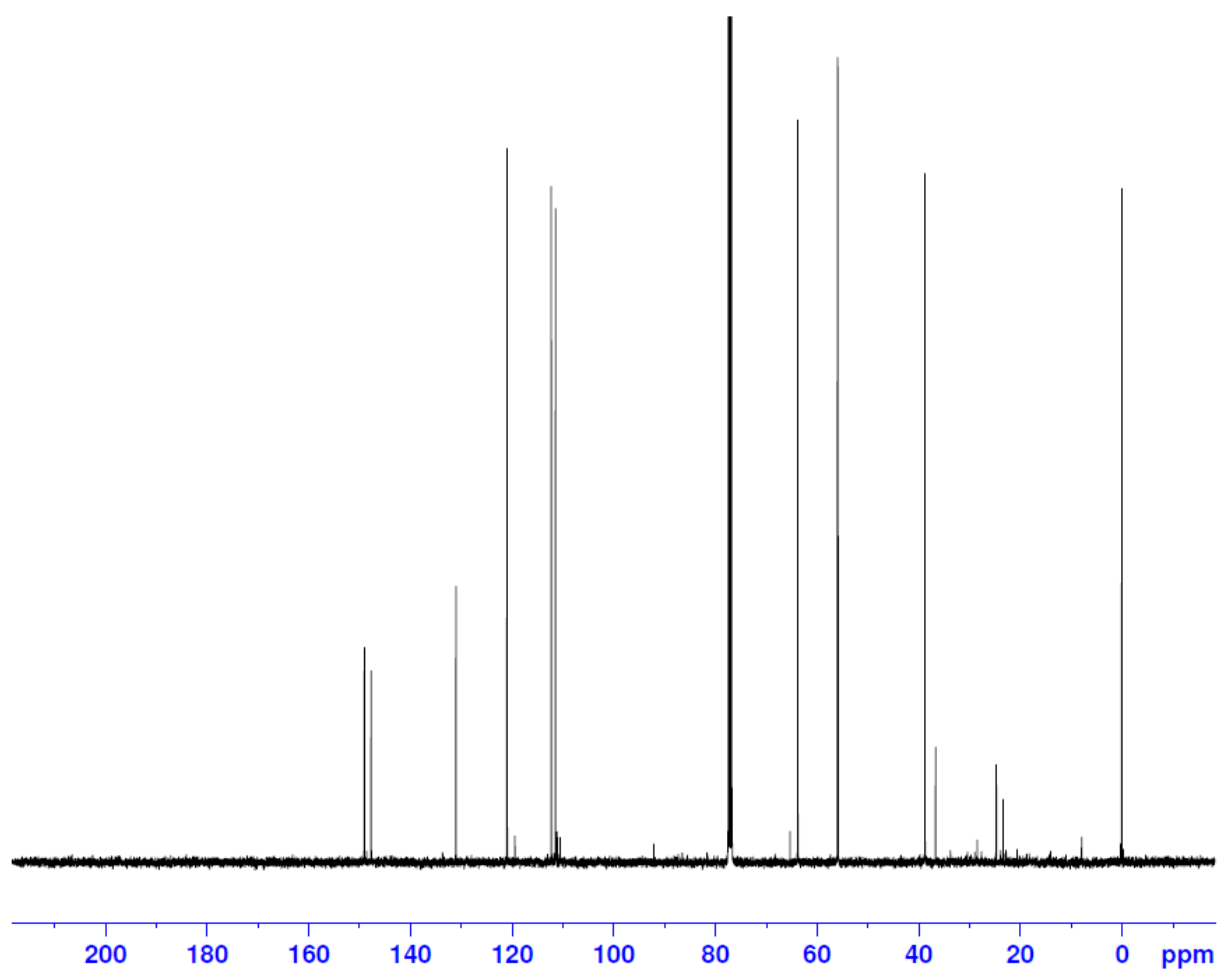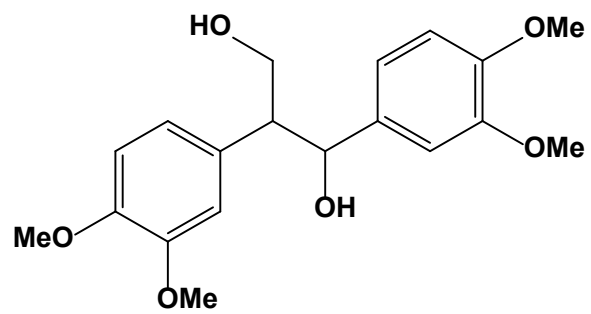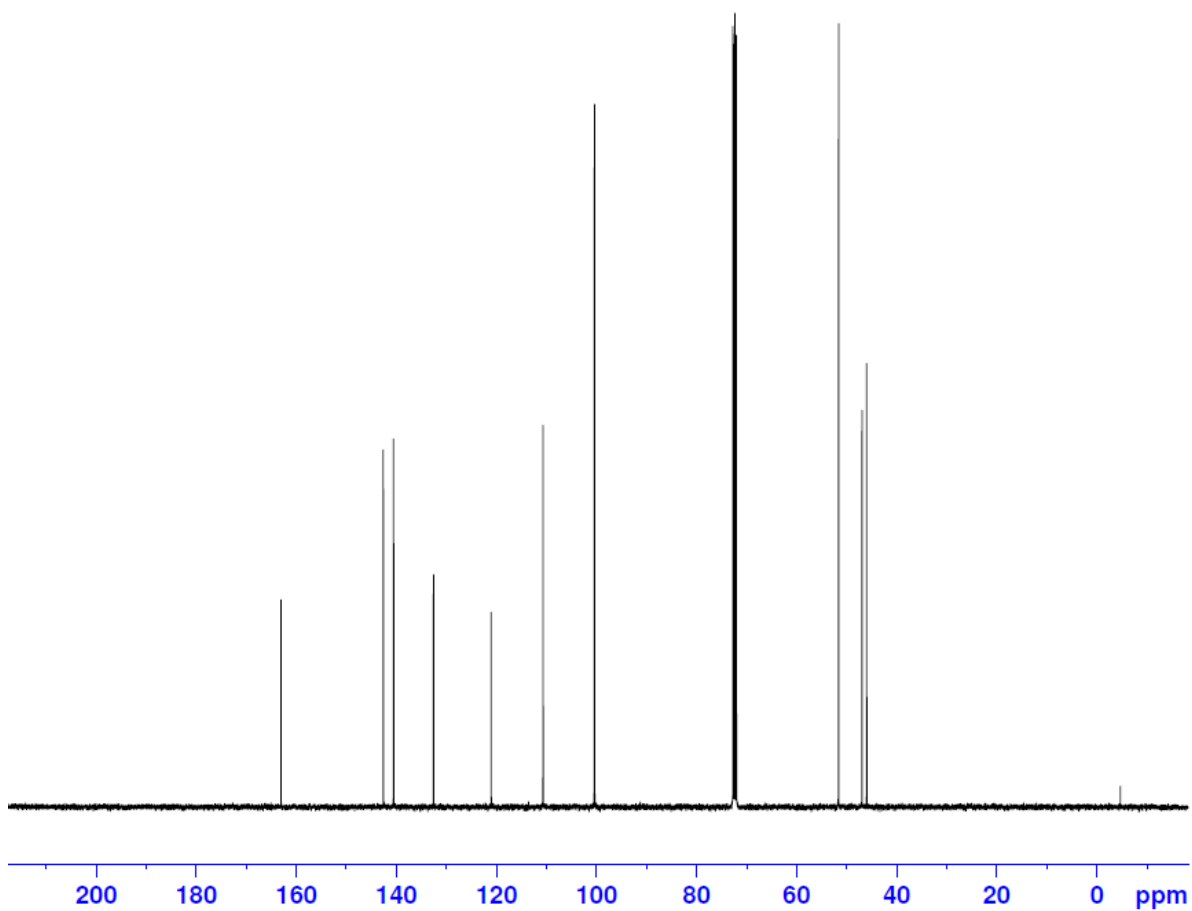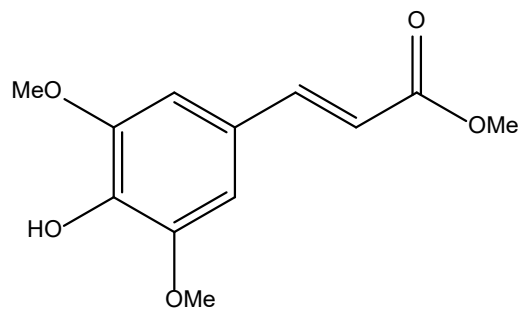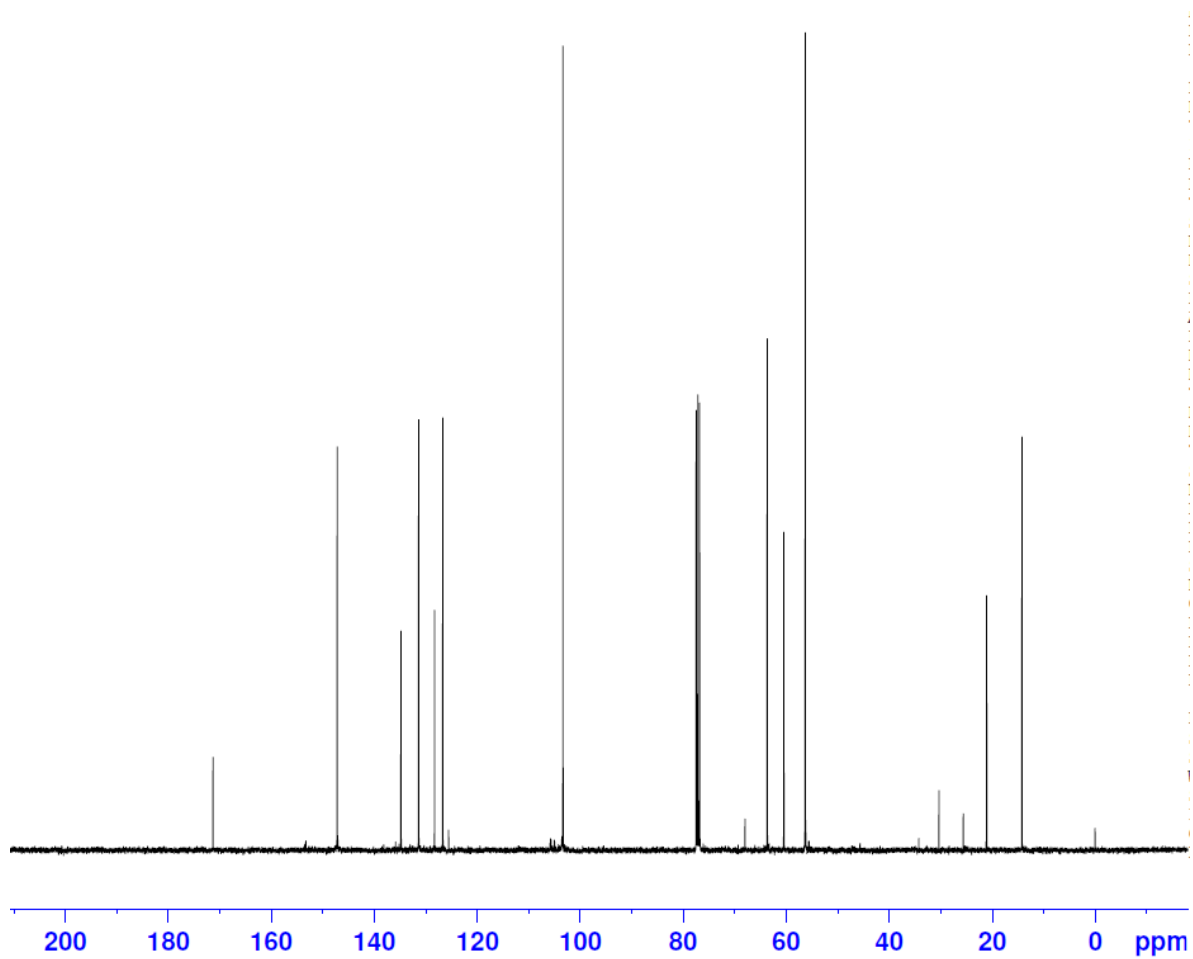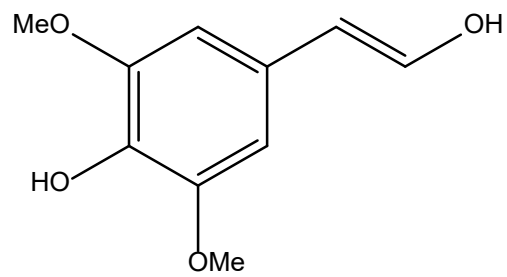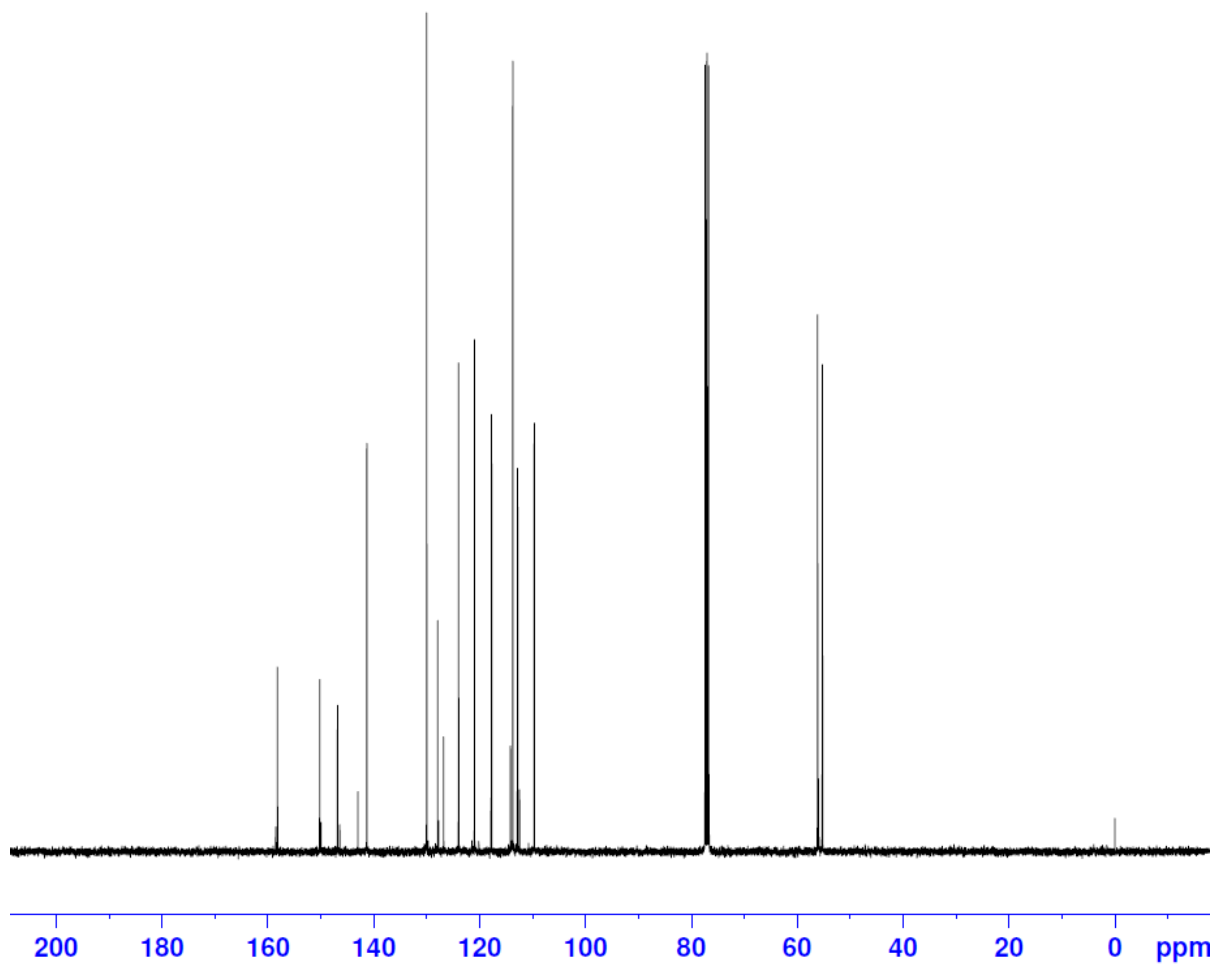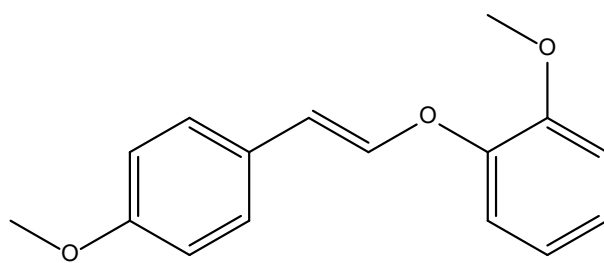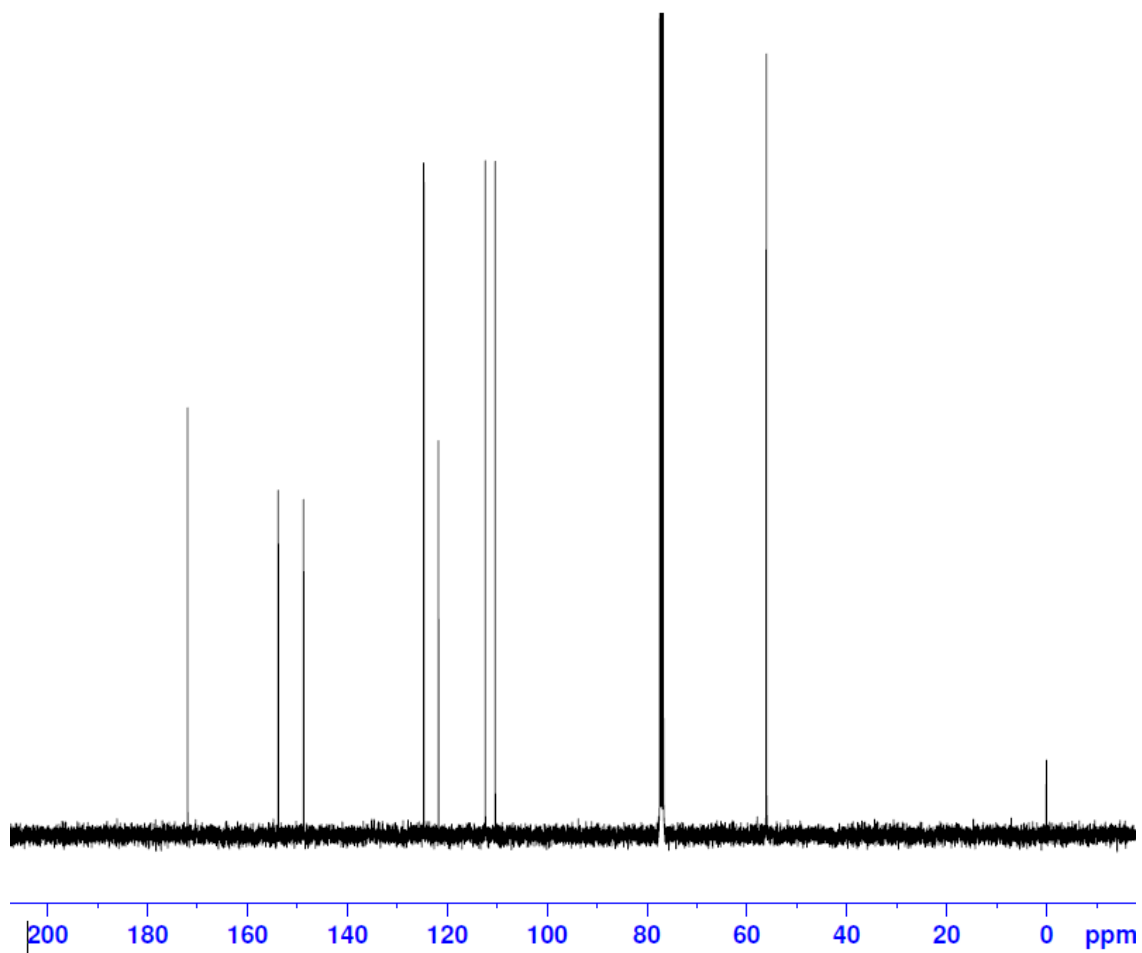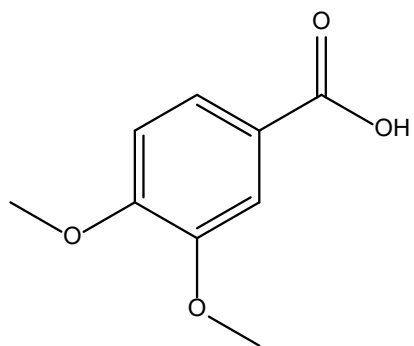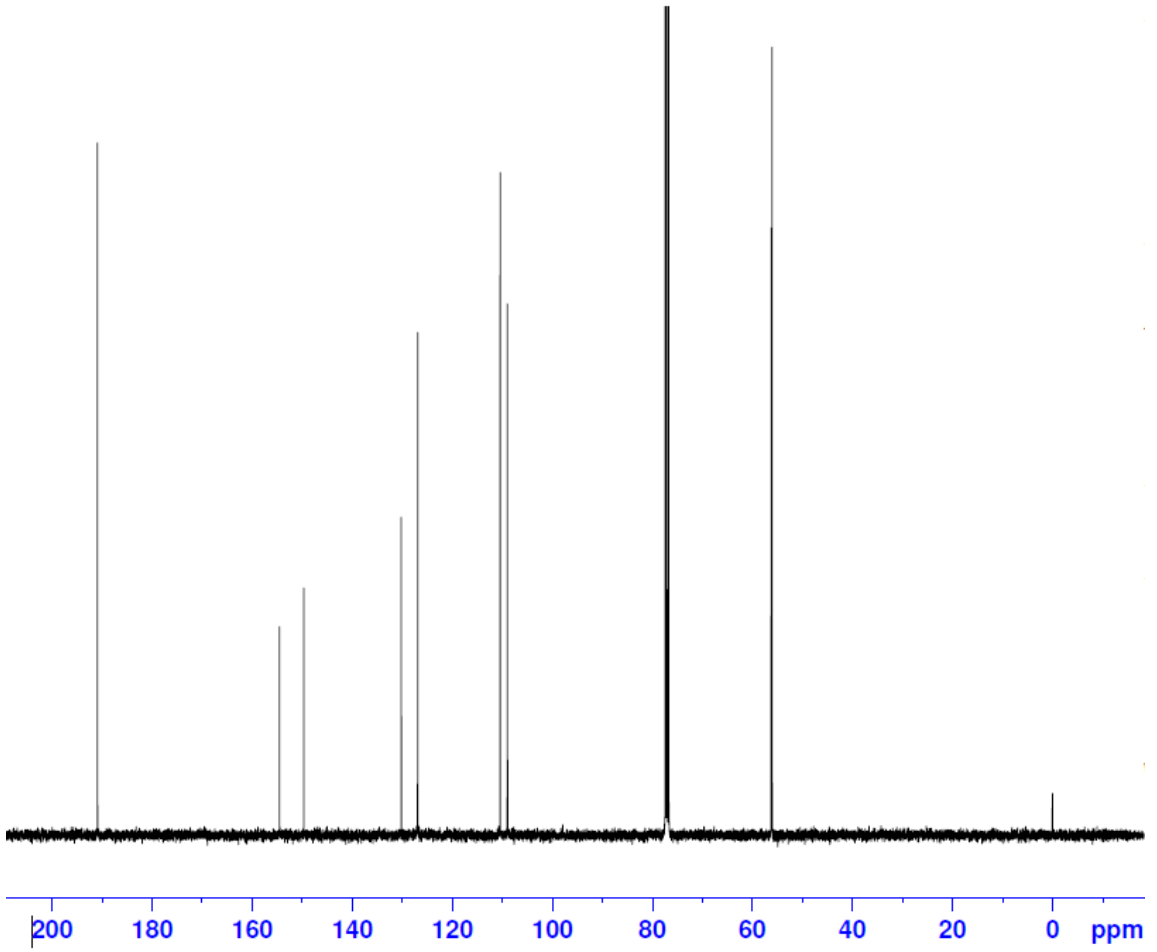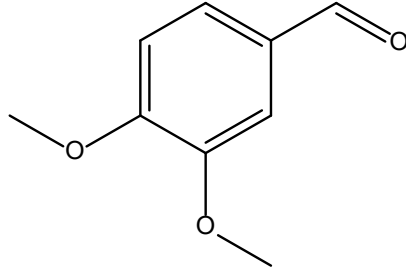
REFERENCES

1.       Schutyser, W.;  Renders, T.;  Van den Bosch, S.;  Koelewijn, S.-F.;  Beckham, G.; Sels, B., Chemicals from lignin: An interplay of lignocellulose fractionation, depolymerisation, and upgrading. *Chemical Society Reviews* **2018,** *47*.
2.       Upton, B. M.; Kasko, A. M., Strategies for the Conversion of Lignin to High-Value Polymeric Materials: Review and Perspective. *Chemical Reviews* **2016,** *116* (4), 2275-2306.
3.       Zakzeski, J.;  Jongerius, A. L.; Weckhuysen, B. M., Transition metal catalyzed oxidation of Alcell lignin, soda lignin, and lignin model compounds in ionic liquids. *Green Chemistry* **2010,** *12* (7), 1225-1236.
4.       Zhang, Y.-H. P., Reviving the carbohydrate economy via multi-product lignocellulose biorefineries. *Journal of Industrial Microbiology and Biotechnology* **2008,** *35* (5), 367-375.
5.       Bušić, A.;  Marđetko, N.;  Kundas, S.;  Morzak, G.;  Belskaya, H.;  Ivančić Šantek, M.;  Komes, D.;  Novak, S.; Šantek, B., Bioethanol Production from Renewable Raw Materials and Its Separation and Purification: A Review. *Food Technol Biotechnol* **2018,** *56* (3), 289-311.
6.       Sun, R.;  Sun, X. F.; Tomkinson, J., Hemicelluloses and Their Derivatives. In *Hemicelluloses: Science and Technology*, American Chemical Society: 2003; Vol. 864, pp 2-22.
7.       Hartman, J.;  Albertsson, A.-C.;  Lindblad, M.; Sjöberg, J., Oxygen barrier materials from renewable sources: Material properties of softwood hemicellulose-based films. *Journal of Applied Polymer Science* **2006,** *100*, 2985-2991.
8.       Zhao, Y.;  Deng, L.;  Liao, B.;  Fu, Y.; Guo, Q.-X., Aromatics Production via Catalytic Pyrolysis of Pyrolytic Lignins from Bio-Oil. *Energy & Fuels* **2010,** *24* (10), 5735-5740.
9.       Sharma, A.;  Kaur, P.;  Singh, G.; Arya, S. K., Economical concerns of lignin in the energy sector. *Cleaner Engineering and Technology* **2021,** *4*.
10.     Campbell, M. M.; Sederoff, R. R., Variation in lignin content and composition (mechanisms of control and implications for the genetic improvement of plants). *Plant physiology* **1996,** *110* (1), 3.
11.     Wang, H.;  Pu, Y.;  Ragauskas, A.; Yang, B., From lignin to valuable products–strategies, challenges, and prospects. *Bioresource Technology* **2019,** *271*, 449-461.
12.     Ralph, J.;  Lundquist, K.;  Brunow, G.;  Lu, F.;  Kim, H.;  Schatz, P.;  Marita, J.; Ralph, S.;  Christensen, J.; Boerjan, W., Lignins: Natural polymers from oxidative coupling of 4-hydroxyphenyl- propanoids. *Phytochemistry Reviews* **2004,** *3*, 29-60.
13.     Fang, Z.; Meier, M. S., Toward the oxidative deconstruction of lignin: oxidation of β-1 and β-5 linkages. *Organic & Biomolecular Chemistry* **2018,** *16* (13), 2330-2341.
14.     Achyuthan, K. E.;  Achyuthan, A. M.;  Adams, P. D.;  Dirk, S. M.;  Harper, J. C.; Simmons, B. A.; Singh, A. K., Supramolecular Self-Assembled Chaos: Polyphenolic Lignin's Barrier to Cost-Effective Lignocellulosic Biofuels. *Molecules* **2010,** *15*, 8641 - 8688.

15. Sturgeon, M. R.; Kim, S.; Lawrence, K.; Paton, R. S.; Chmely, S. C.; Nimlos, M.; Foust, T. D.; Beckham, G. T., A Mechanistic Investigation of Acid-Catalyzed Cleavage of Aryl-Ether Linkages: Implications for Lignin Depolymerization in Acidic Environments. *ACS Sustainable Chemistry & Engineering* **2014,** *2* (3), 472-485.

16. Boerjan, W.; Ralph, J.; Baucher, M., Lignin biosynthesis. *Annual review of plant biology* **2003,** *54* (1), 519-546.

17. Amiri, M. T.; Bertella, S.; Questell-Santiago, Y. M.; Luterbacher, J. S., Establishing lignin structure-upgradeability relationships using quantitative 1 H–13 C heteronuclear single quantum coherence nuclear magnetic resonance (HSQC-NMR) spectroscopy. *Chemical science* **2019,** *10* (35), 8135-8142.

18. Calvo-Flores, F. G.; Dobado, J. A., Lignin as Renewable Raw Material. *ChemSusChem* **2010,** *3* (11), 1227-1235.

19. Zhang, L.; Larsson, A.; Moldin, A.; Edlund, U., Comparison of lignin distribution, structure, and morphology in wheat straw and wood. *Industrial Crops and Products* **2022,** *187*, 115432.

20. Hirayama, H.; Akiyama, T.; Kimura, S.; Nawawi, D. S.; Syafii, W.; Yokoyama, T.; Matsumoto, Y., Influence of the p-hydroxyphenyl/guaiacyl ratio on the biphenyl and β-5 contents in compression wood lignins. *Holzforschung* **2019,** *73* (10), 923-935.

21. Demuner, I. F.; Colodette, J. L.; Demuner, A. J.; Jardim, C. M., Biorefinery Review: Wide-Reaching Products Through Kraft Lignin. *2019* **2019,** *14* (3), 39.

22. Zakzeski, J.; Bruijnincx, P. C. A.; Jongerius, A. L.; Weckhuysen, B. M., The Catalytic Valorization of Lignin for the Production of Renewable Chemicals. *Chemical Reviews* **2010,** *110* (6), 3552-3599.

23. Pandey, M. P.; Kim, C. S., Lignin depolymerization and conversion: a review of thermochemical methods. *Chemical Engineering & Technology* **2011,** *34* (1), 29-41.

24. Maurya, D. P.; Singla, A.; Negi, S., An overview of key pretreatment processes for biological conversion of lignocellulosic biomass to bioethanol. *3 Biotech* **2015,** *5* (5), 597-609.

25. Isikgor, F. H.; Becer, C. R., Lignocellulosic biomass: a sustainable platform for the production of bio-based chemicals and polymers. *Polymer Chemistry* **2015,** *6* (25), 4497-4559.

26. Hernández-Beltrán, J. U.; Hernández-De Lira, I. O.; Cruz-Santos, M. M.; Saucedo-Luevanos, A.; Hernández-Terán, F.; Balagurusamy, N., Insight into Pretreatment Methods of Lignocellulosic Biomass to Increase Biogas Yield: Current State, Challenges, and Opportunities. *Applied Sciences* **2019,** *9* (18), 3721.

27. Lobato-Peralta, D. R.; Duque-Brito, E.; Villafán-Vidales, H. I.; Longoria, A.; Sebastian, P. J.; Cuentas-Gallegos, A. K.; Arancibia-Bulnes, C. A.; Okoye, P. U., A review on trends in lignin extraction and valorization of lignocellulosic biomass for energy applications. *Journal of Cleaner Production* **2021,** *293*, 126123.

28. Obst, J. R.; Kirk, T. K., Isolation of lignin. In *Methods in Enzymology*, Academic Press: 1988; Vol. 161, pp 3-12.

29. Oliveira, R. C. P.; Mateus, M. M.; Santos, D. M. F., Editors' Choice—On the Oxidation of Kraft Black Liquor for Lignin Recovery: A Voltammetric Study. *Journal of The Electrochemical Society* **2019,** *166* (16), E547.

30.      Azadi, P.;  Inderwildi, O. R.;  Farnood, R.; King, D. A., Liquid fuels, hydrogen and chemicals from lignin: A critical review. *Renewable and Sustainable Energy Reviews* **2013,** *21*, 506-523.

31.      Rinaldi, R.;  Jastrzebski, R.;  Clough, M. T.;  Ralph, J.;  Kennema, M.;  Bruijnincx, P. C. A.; Weckhuysen, B. M., Paving the Way for Lignin Valorisation: Recent Advances in Bioengineering, Biorefining and Catalysis. *Angewandte Chemie International Edition* **2016,** *55* (29), 8164-8215.

32.      Cattelan, L., Green Reactions and Technologies for Biomass Valorisation. **2018**.

33.      White, J., Top Value-Added Chemicals from Biomass Volume II—Results of Screening for Potential Candidates from Biorefinery Lignin. *Biomass Fuels* **2007,** *2*.

34.      Chakar, F. S.; Ragauskas, A. J., Review of current and future softwood kraft lignin process chemistry. *Industrial Crops and Products* **2004,** *20* (2), 131-141.

35.      Jawjit, W.;  Kroeze, C.;  Soontaranun, W.; Hordijk, L., Options to reduce the environmental impact by eucalyptus-based Kraft pulp industry in Thailand: model description. *Journal of Cleaner Production* **2007,** *15* (18), 1827-1839.

36.      Rietzler, B.;  Karlsson, M.;  Kwan, I.;  Lawoko, M.; Ek, M., Fundamental Insights on the Physical and Chemical Properties of Organosolv Lignin from Norway Spruce Bark. *Biomacromolecules* **2022,** *23* (8), 3349-3358.

37.      Berg, A.;  Fuentealba, C.; Salazar, J., Separation of lignocellulosic components in acetic acid media and evaluation of applications. *J-FOR* **2013,** *3*, 27-32.

38.      Den, W.;  Sharma, V. K.;  Lee, M.;  Nadadur, G.; Varma, R. S., Lignocellulosic biomass transformations via greener oxidative pretreatment processes: access to energy and value-added chemicals. *Frontiers in chemistry* **2018,** *6*, 141.

39.      Hodásová, Ľ.;  Jablonsky, M.;  Butor Skulcova, A.; Haz, A., Lignin, potential products and their market value. *Wood Research* **2015,** *60*, 973-986.

40.      Wang, S.;  Cheng, A.;  Liu, F.;  Zhang, J.;  Xia, T.;  Zeng, X.;  Fan, W.; Zhang, Y., Catalytic conversion network for lignocellulosic biomass valorization: a panoramic view. *Industrial Chemistry & Materials* **2023,** *1* (2), 188-206.

41.      Khwanjaisakun, N.;  Amornraksa, S.;  Simasatitkul, L.;  Charoensuppanimit, P.;  Assabumrungrat, S., Techno-economic analysis of vanillin production from Kraft lignin: Feasibility study of lignin valorization. *Bioresource Technology* **2020,** *299*, 122559.

42.      Khan, R. J.;  Lau, C. Y.;  Guan, J.;  Lam, C. H.;  Zhao, J.;  Ji, Y.;  Wang, H.;  Xu, J.;  Lee, D.-J.;  Leu, S.-Y., Recent advances of lignin valorization techniques toward sustainable aromatics and potential benchmarks to fossil refinery products. *Bioresource Technology* **2022,** *346*, 126419.

43.      Ma, R.;  Guo, M.; Zhang, X., Recent advances in oxidative valorization of lignin. *Catalysis Today* **2018,** *302*, 50-60.

44.      Partenheimer, W., The Aerobic Oxidative Cleavage of Lignin to Produce Hydroxyaromatic Benzaldehydes and Carboxylic Acids via Metal/Bromide Catalysts in Acetic Acid/Water Mixtures. *Advanced Synthesis & Catalysis* **2009,** *351*, 456-466.

45.      Tarabanko, V. E.;  Fomova, N. A.;  Kuznetsov, B. N.;  Ivanchenko, N. M.;  Kudryashev, A. V., On the mechanism of vanillin formation in the catalytic oxidation of lignin with oxygen. *Reaction Kinetics and Catalysis Letters* **1995,** *55* (1), 161-170.

46.      Deng, H.;  Lin, L.; Liu, S., Catalysis of Cu-Doped Co-Based Perovskite-Type Oxide in Wet Oxidation of Lignin To Produce Aromatic Aldehydes. *Energy & Fuels* **2010,** *24* (9), 4797-4802.

47.     Kurek, B.; Gaudard, F., Oxidation of Spruce Wood Sawdust by MnO2 plus Oxalate: A Biochemical Investigation. *Journal of Agricultural and Food Chemistry* **2000,** *48* (7), 3058-3062.

48.     Alvarez-Vasco, C.; Ma, R.; Quintero, M.; Guo, M.; Geleynse, S.; Ramasamy, K. K.; Wolcott, M.; Zhang, X., Unique low-molecular-weight lignin with high purity extracted from wood by deep eutectic solvents (DES): a source of lignin for valorization. *Green Chemistry* **2016,** *18* (19), 5133-5141.

49.     Crestini, C.; Crucianelli, M.; Orlandi, M.; Saladino, R., Oxidative strategies in lignin chemistry: A new environmental friendly approach for the functionalisation of lignin and lignocellulosic fibers. *Catalysis Today* **2010,** *156* (1), 8-22.

50.     Al-Hussaini, L.; Launay, F.; Galvez, E., Vanadium-Substituted Phosphomolybdic Acids for the Aerobic Cleavage of Lignin Models—Mechanistic Aspect and Extension to Lignin. *Materials* **2020,** *13* (4), 812.

51.     Ma, R.; Guo, M.; Zhang, X., Selective conversion of biorefinery lignin into dicarboxylic acids. *ChemSusChem* **2014,** *7* (2), 412-415.

52.     DiCosimo, R.; Szabo, H. C., Oxidation of lignin model compounds using single-electron-transfer catalysts. *The Journal of Organic Chemistry* **1988,** *53* (8), 1673-1679.

53.     Hedges, J. I.; Ertel, J. R., Characterization of lignin by gas capillary chromatography of cupric oxide oxidation products. *Analytical Chemistry* **1982,** *54* (2), 174-178.

54.     Lequart, C.; Kurek, B.; Debeire, P.; Monties, B., MnO2 and Oxalate: An Abiotic Route for the Oxidation of Aromatic Components in Wheat Straw. *Journal of Agricultural and Food Chemistry* **1998,** *46* (9), 3868-3874.

55.     Yurdakal, S.; Palmisano, G.; Loddo, V.; Augugliaro, V.; Palmisano, L., Nanostructured rutile TiO2 for selective photocatalytic oxidation of aromatic alcohols to aldehydes in water. *Journal of the American Chemical Society* **2008,** *130* (5), 1568-1569.

56.     Linsebigler, A. L.; Lu, G.; Yates, J. T., Jr., Photocatalysis on TiO2 Surfaces: Principles, Mechanisms, and Selected Results. *Chemical Reviews* **1995,** *95* (3), 735-758.

57.     Ma, Y.-S.; Chang, C.-N.; Chiang, Y.-P.; Sung, H.-F.; Chao, A. C., Photocatalytic degradation of lignin using Pt/TiO2 as the catalyst. *Chemosphere* **2008,** *71* (5), 998-1004.

58.     Son, S.; Toste, F. D., Non-Oxidative Vanadium-Catalyzed C-O Bond Cleavage: Application to Degradation of Lignin Model Compounds. *Angewandte Chemie International Edition* **2010,** *49* (22), 3791-3794.

59.     Sedai, B.; Diaz-Urrutia, C.; Baker, R. T.; Wu, R.; Silks, L. P.; Hanson, S. K., Aerobic oxidation of β-1 lignin model compounds with copper and oxovanadium catalysts. *ACS Catalysis* **2013,** *3* (12), 3111-3122.

60.     Hanson, S. K.; Baker, R. T.; Gordon, J. C.; Scott, B. L.; Thorn, D. L., Aerobic oxidation of lignin models using a base metal vanadium catalyst. *Inorganic chemistry* **2010,** *49* (12), 5611-5618.

61.     Cui, Y.; Goes, S. L.; Stahl, S. S., Chapter Four - Sequential oxidation-depolymerization strategies for lignin conversion to low molecular weight aromatic chemicals. In *Advances in Inorganic Chemistry*, Ford, P. C.; van Eldik, R., Eds. Academic Press: 2021; Vol. 77, pp 99-136.

62.     Rahimi, A.; Ulbrich, A.; Coon, J. J.; Stahl, S. S., Formic-acid-induced depolymerization of oxidized lignin to aromatics. *Nature* **2014,** *515* (7526), 249-252.

63.     Sun, Z.; Li, G.; Liu, L.; Liu, H.-o., Au nanoparticles supported on Cr-based metal-organic framework as bimetallic catalyst for selective oxidation of cyclohexane to cyclohexanone and cyclohexanol. *Catalysis Communications* **2012,** *27*, 200-205.

64.     Zakzeski, J.; Dębczak, A.; Bruijnincx, P. C.; Weckhuysen, B. M., Catalytic oxidation of aromatic oxygenates by the heterogeneous catalyst Co-ZIF-9. *Applied catalysis A: general* **2011,** *394* (1-2), 79-85.

65.     Hu, X.; Yip, A. C., Heterogeneous catalysis: enabling a sustainable future. Frontiers Media SA: 2021; Vol. 1, p 667675.

66.     Bravo-Suárez, J. J.; Chaudhari, R. V.; Subramaniam, B., Design of Heterogeneous Catalysts for Fuels and Chemicals Processing: An Overview. In *Novel Materials for Catalysis and Fuels Processing*, American Chemical Society: 2013; Vol. 1132, pp 3-68.

67.     Pinna, F., Supported metal catalysts preparation. *Catalysis Today* **1998,** *41* (1), 129-137.

68.     Astruc, D.; Lu, F.; Aranzaes, J. R., Nanoparticles as recyclable catalysts: the frontier between homogeneous and heterogeneous catalysis. *Angewandte Chemie International Edition* **2005,** *44* (48), 7852-7872.

69.     Sankar, M.; He, Q.; Engel, R. V.; Sainna, M. A.; Logsdail, A. J.; Roldan, A.; Willock, D. J.; Agarwal, N.; Kiely, C. J.; Hutchings, G. J., Role of the Support in Gold-Containing Nanoparticles as Heterogeneous Catalysts. *Chemical Reviews* **2020,** *120* (8), 3890-3938.

70.     Liu, L.; Corma, A., Metal Catalysts for Heterogeneous Catalysis: From Single Atoms to Nanoclusters and Nanoparticles. *Chemical Reviews* **2018,** *118* (10), 4981-5079.

71.     Feng, J.; Ma, C.; Miedziak, P. J.; Edwards, J. K.; Brett, G. L.; Li, D.; Du, Y.; Morgan, D. J.; Hutchings, G. J., Au–Pd nanoalloys supported on Mg–Al mixed metal oxides as a multifunctional catalyst for solvent-free oxidation of benzyl alcohol. *Dalton Transactions* **2013,** *42* (40), 14498-14508.

72.     Neyman, K. M.; Kozlov, S. M., Quantifying interactions on interfaces between metal particles and oxide supports in catalytic nanomaterials. *NPG Asia Materials* **2022,** *14* (1), 59.

73.     Hutchings, G. J., Vapor phase hydrochlorination of acetylene: Correlation of catalytic activity of supported metal chloride catalysts. *Journal of Catalysis* **1985,** *96* (1), 292-295.

74.     Haruta, M.; Yamada, N.; Kobayashi, T.; Iijima, S., Gold catalysts prepared by coprecipitation for low-temperature oxidation of hydrogen and of carbon monoxide. *Journal of Catalysis* **1989,** *115* (2), 301-309.

75.     Redina, E. A.; Kirichenko, O. A.; Shesterkina, A. A.; Kustov, L. M., Unusual behavior of bimetallic nanoparticles in catalytic processes of hydrogenation and selective oxidation. *Pure and Applied Chemistry* **2020,** *92* (7), 989-1006.

76.     Jin, X.; Taniguchi, K.; Yamaguchi, K.; Mizuno, N., Au-Pd alloy nanoparticles supported on layered double hydroxide for heterogeneously catalyzed aerobic oxidative dehydrogenation of cyclohexanols and cyclohexanones to phenols. (2041-6520 (Print)).

77.     Sha, J.; Paul, S.; Dumeignil, F.; Wojcieszak, R., Au-based bimetallic catalysts: how the synergy between two metals affects their catalytic activity. *RSC advances* **2019,** *9* (51), 29888-29901.

78.     Venugopal, A.; Aluha, J.; Scurrell, M. S., The Water-Gas Shift Reaction Over Au-Based, Bimetallic Catalysts. The Au-M (M=Ag, Bi, Co, Cu, Mn, Ni, Pb, Ru, Sn, Tl) on Iron(III) Oxide System. *Catalysis Letters* **2003,** *90* (1), 1-6.

79.     Jiang, H.-L.; Xu, Q., Recent progress in synergistic catalysis over heterometallic nanoparticles. *Journal of Materials Chemistry* **2011,** *21* (36), 13705-13725.

80.     Prati, L.; Villa, A., Gold colloids: from quasi-homogeneous to heterogeneous catalytic systems. *Accounts of Chemical Research* **2014,** *47* (3), 855-863.

81.     Ferrando, R.; Jellinek, J.; Johnston, R. L., Nanoalloys: From Theory to Applications of Alloy Clusters and Nanoparticles. *Chemical Reviews* **2008,** *108* (3), 845-910.

82.     Sankar, M.; Dimitratos, N.; Miedziak, P. J.; Wells, P. P.; Kiely, C. J.; Hutchings, G. J., Designing bimetallic catalysts for a green and sustainable future. *Chemical Society Reviews* **2012,** *41* (24), 8099-8139.

83.     Zhang, J.; Post, M.; Veres, T.; Jakubek, Z. J.; Guan, J.; Wang, D.; Normandin, F.; Deslandes, Y.; Simard, B., Laser-Assisted Synthesis of Superparamagnetic Fe@Au Core−Shell Nanoparticles. *The Journal of Physical Chemistry B* **2006,** *110* (14), 7122-7128.

84.     Mariscal, M. M.; Dassie, S. A.; Leiva, E. P. M., Collision as a way of forming bimetallic nanoclusters of various structures and chemical compositions. *The Journal of chemical physics* **2005,** *123* (18), 184505-184505-6.

85.     Wei, X.; Zhou, R.; Lefebvre, W.; He, K.; Le Roy, D.; Skomski, R.; Li, X.; Shield, J. E.; Kramer, M. J.; Chen, S.; Zeng, X. C.; Sellmyer, D. J., Structural and Magnetic Evolution of Bimetallic MnAu Clusters Driven by Asymmetric Atomic Migration. *Nano Letters* **2014,** *14* (3), 1362-1368.

86.     Ferrer, D.; Torres-Castro, A.; Gao, X.; Sepulveda-Guzman, S.; Ortiz Mendez, U.; Yacaman, M., Three-Layer Core/Shell Structure in Au−Pd Bimetallic Nanoparticles. *Nano letters* **2007,** *7*, 1701-5.

87.     Wang, L.; Yamauchi, Y., Strategic synthesis of trimetallic Au@ Pd@ Pt core− shell Nanoparticles from poly (vinylpyrrolidone)-based aqueous solution toward highly active electrocatalysts. *Chemistry of Materials* **2011,** *23* (9), 2457-2465.

88.     Banadaki, A. D.; Kajbafvala, A., Recent advances in facile synthesis of bimetallic nanostructures: An overview. *Journal of Nanomaterials* **2014,** *2014*, 4-4.

89.     Louis, C., Chemical preparation of supported bimetallic catalysts. Gold-based bimetallic, a case study. *Catalysts* **2016,** *6* (8), 110.

90.     Alshammari, A.; Kalevaru, V. N.; Martin, A., Bimetallic Catalysts Containing Gold and Palladium for Environmentally Important Reactions. *Catalysts* **2016,** *6* (7), 97.

91.     Campisi, S.; Stucchi, M.; Dimitratos, N.; Villa, A., A Career in Catalysis: Laura Prati. *ACS Catalysis* **2023,** *13* (2), 1326-1348.

92.     Villa, A.; Wang, D.; Veith, G. M.; Vindigni, F.; Prati, L., Sol immobilization technique: a delicate balance between activity, selectivity and stability of gold catalysts. *Catalysis Science & Technology* **2013,** *3* (11), 3036-3041.

93.     Guczi, L.; Beck, A.; Horváth, A.; Koppány, Z.; Stefler, G.; Frey, K.; Sajó, I.; Geszti, O.; Bazin, D.; Lynch, J., AuPd bimetallic nanoparticles on TiO2: XRD, TEM, in situ EXAFS studies and catalytic activity in CO oxidation. *Journal of Molecular Catalysis A: Chemical* **2003,** *204-205*, 545-552.

94.     Bianchi, C. L.; Canton, P.; Dimitratos, N.; Porta, F.; Prati, L., Selective oxidation of glycerol with oxygen using mono and bimetallic catalysts based on Au, Pd and Pt metals. *Catalysis today* **2005,** *102*, 203-212.

95.     Munnik, P.; de Jongh, P. E.; de Jong, K. P., Recent Developments in the Synthesis of Supported Catalysts. *Chemical Reviews* **2015,** *115* (14), 6687-6718.

96.     Andreeva, D.; Tabakova, T.; Idakiev, V.; Christov, P.; Giovanoli, R., Au/α-Fe2O3 catalyst for water–gas shift reaction prepared by deposition–precipitation. *Applied Catalysis A: General* **1998,** *169* (1), 9-14.

97.     Calzada, L. A.; Louis, C.; Wan Han, C.; Ortalan, V.; Zanella, R., Au-Ru/TiO2 prepared by deposition-precipitation with urea: Relevant synthesis parameters to obtain bimetallic particles. *Applied Catalysis B: Environmental* **2020,** *264*, 118503.

98.     Hermans, S.; Devillers, M., Gold as a promoter for the activity of palladium in carbon-supported catalysts for the liquid phase oxidation of glyoxal to glyoxalic acid. *Catalysis Letters* **2005,** *99* (1), 55-64.

99.     Haruta, M., Catalysis of Gold Nanoparticles Deposited on Metal Oxides. *CATTECH* **2002,** *6* (3), 102-115.

100.    Prati, L.; Martra, G., New gold catalysts for liquid phase oxidation. *Gold Bulletin* **1999,** *32* (3), 96-101.

101.    Pan, F.; Zhang, W.; Ye, Y.; Huang, Y.; Xu, Y.; Yuan, Y.; Wu, F.; Li, J., Adsorption Synthesis of Iron Oxide-Supported Gold Catalyst under Self-Generated Alkaline Conditions for Efficient Elimination of Carbon Monoxide. *Catalysts* **2018,** *8* (9), 357.

102.    Carabineiro, S. A., Supported gold nanoparticles as catalysts for the oxidation of alcohols and alkanes. *Frontiers in Chemistry* **2019,** *7*, 702.

103.    Sandoval, A.; Aguilar, A.; Louis, C.; Traverse, A.; Zanella, R., Bimetallic Au–Ag/TiO2 catalyst prepared by deposition–precipitation: High activity and stability in CO oxidation. *Journal of Catalysis* **2011,** *281* (1), 40-49.

104.    Mimura, N.; Hiyoshi, N.; Daté, M.; Fujitani, T.; Dumeignil, F., Microscope Analysis of Au–Pd/TiO2 Glycerol Oxidation Catalysts Prepared by Deposition–Precipitation Method. *Catalysis Letters* **2014,** *144* (12), 2167-2175.

105.    Liu, X.; Wang, A.; Wang, X.; Mou, C.-Y.; Zhang, T., Au–Cu Alloy nanoparticles confined in SBA-15 as a highly efficient catalyst for CO oxidation. *Chemical Communications* **2008,** (27), 3187-3189.

106.    Liu, X.; Wang, A.; Yang, X.; Zhang, T.; Mou, C.-Y.; Su, D.-S.; Li, J., Synthesis of Thermally Stable and Highly Active Bimetallic Au−Ag Nanoparticles on Inert Supports. *Chemistry of Materials* **2009,** *21* (2), 410-418.

107.    Sharma, A. K.; Mehara, P.; Das, P., Recent Advances in Supported Bimetallic Pd–Au Catalysts: Development and Applications in Organic Synthesis with Focused Catalytic Action Study. *ACS Catalysis* **2022,** *12* (11), 6672-6701.

108.    Wang, H.; Zhang, D.; Zhang, R.; Ma, H.; Zhang, H.; Yao, R.; Liang, M.; Zhao, Y.; Miao, Z., Dealloying Synthesis of Bimetallic (Au–Pd)/CeO2 Catalysts for CO Oxidation. *ACS Omega* **2023,** *8* (13), 11889-11896.

109.    Ovchinnikov, A.; Smetana, V.; Mudring, A.-V., Metallic alloys at the edge of complexity: structural aspects, chemical bonding and physical properties*. *Journal of Physics: Condensed Matter* **2020,** *32* (24), 243002.

110. Villa, A.; Wang, D.; Su, D. S.; Prati, L., New challenges in gold catalysis: bimetallic systems. *Catalysis Science & Technology* **2015,** *5* (1), 55-68.

111. Centomo, P.; Canton, P.; Burato, C.; Meneghini, C.; Zecca, M., Resonant-XRD Characterization of Nanoalloyed Au-Pd Catalysts for the Direct Synthesis of H2O2: Quantitative Analysis of Size Dependent Composition of the Nanoparticles †. *Applied Sciences* **2019,** *9* (15), 2959.

112. Liu, X.; Wang, A.; Li, L.; Zhang, T.; Mou, C.-Y.; Lee, J.-F., Structural changes of Au–Cu bimetallic catalysts in CO oxidation: In situ XRD, EPR, XANES, and FT-IR characterizations. *Journal of Catalysis* **2011,** *278* (2), 288-296.

113. Pu, Y.; Zhang, J.; Wang, X.; Zhang, H.; Yu, L.; Dong, Y.; Li, W., Bimetallic Au–Ni/CSs catalysts for acetylene hydrochlorination. *Catalysis Science & Technology* **2014,** *4* (12), 4426-4432.

114. Xie, Z.; Winter, L. R.; Chen, J. G., Bimetallic-Derived Catalysts and Their Application in Simultaneous Upgrading of $CO_2$ and Ethane. *Matter* **2021,** *4* (2), 408-440.

115. Patterson, A., The Scherrer formula for X-ray particle size determination. *Physical review* **1939,** *56* (10), 978.

116. Su, D., Advanced electron microscopy characterization of nanomaterials for catalysis. *Green Energy & Environment* **2017,** *2* (2), 70-83.

117. Radnik, J.; Mohr, C.; Claus, P., On the origin of binding energy shifts of core levels of supported gold nanoparticles and dependence of pretreatment and material synthesis. *Physical Chemistry Chemical Physics* **2003,** *5* (1), 172-177.

118. Krishna, D. N. G.; Philip, J., Review on surface-characterization applications of X-ray photoelectron spectroscopy (XPS): Recent developments and challenges. *Applied Surface Science Advances* **2022,** *12*, 100332.

119. Chandler, B. D.; Pignolet, L. H., DRIFTS studies of carbon monoxide coverage on highly dispersed bimetallic Pt-Cu and Pt-Au catalysts. *Catalysis Today* **2001,** *65* (1), 39-50.

120. Calzada, L. A.; Collins, S. E.; Han, C. W.; Ortalan, V.; Zanella, R., Synergetic effect of bimetallic Au-Ru/TiO2 catalysts for complete oxidation of methanol. *Applied Catalysis B: Environmental* **2017,** *207*, 79-92.

121. Haruta, M.; Daté, M., Advances in the Catalysis of Au Nanoparticles. *Applied Catalysis A: General* **2001,** *222*, 427-437.

122. Hassan, J. Z.; Zaheer, A.; Raza, A.; Li, G., Au-based heterostructure composites for photo and electro catalytic energy conversions. *Sustainable Materials and Technologies* **2023,** *36*, e00609.

123. Liu, X.; He, L.; Liu, Y.-M.; Cao, Y., Supported Gold Catalysis: From Small Molecule Activation to Green Chemical Synthesis. *Accounts of Chemical Research* **2014,** *47* (3), 793-804.

124. Wang, A.; Liu, X. Y.; Mou, C.-Y.; Zhang, T., Understanding the synergistic effects of gold bimetallic catalysts. *Journal of Catalysis* **2013,** *308*, 258-271.

125. Chen, D.; He, X.; Chen, X.; Wang, Z.; Wang, X., Bimetallic Au-Ag catalysts in HCHO catalytic oxidation: No synergetic effect? *Separation and Purification Technology* **2022,** *301*, 121930.

126. Caridade Rodrigues, C.; de Carvalho, C., Process Development for Benzyl Alcohol Production by Whole-Cell Biocatalysis in Stirred and Packed Bed Reactors. *Microorganisms* **2022,** *10*, 966.

127. Laasri, L.; El Makhfi, M., Ecofriendly oxidation of benzyl alcohol to benzaldehyde using Zr-Ni/Natural phosphate as an efficient and recyclable heterogeneous catalyst. *Materials Today: Proceedings* **2020,** *31*, S156-S161.

128. Lukato, S.; Wendt, O. F.; Wallenberg, R.; Kasozi, G. N.; Naziriwo, B.; Persson, A.; Folkers, L. C.; Tebandeke, E., Selective oxidation of benzyl alcohols with molecular oxygen as the oxidant using Ag-Cu catalysts supported on polyoxometalates. *Results in Chemistry* **2021,** *3*, 100150.

129. Chan-Thaw, C. E.; Savara, A.; Villa, A., Selective benzyl alcohol oxidation over Pd catalysts. *Catalysts* **2018,** *8* (10), 431.

130. Liu, L.; Zhou, X.; Xin, C.; Zhang, B.; Zhang, G.; Li, S.; Liu, L.; Tai, X., Efficient oxidation of benzyl alcohol into benzaldehyde catalyzed by graphene oxide and reduced graphene oxide supported bimetallic Au–Sn catalysts. *RSC Advances* **2023,** *13* (34), 23648-23658.

131. Kodchasee, J.; Chanloi, C.; Khemthong, P.; Uapipatanakul, B.; Ehara, M.; Bobuatong, K., Catalytic Oxidation of Benzyl Alcohol to Benzaldehyde on Au8 and Au6Pd2 Clusters: A DFT Study on the Reaction Mechanism. *Catalysts* **2021,** *11*, 720.

132. Dimitratos, N.; Villa, A.; Wang, D.; Porta, F.; Su, D.; Prati, L., Pd and Pt catalysts modified by alloying with Au in the selective oxidation of alcohols. *Journal of Catalysis* **2006,** *244* (1), 113-121.

133. Nishimura, S.; Yakita, Y.; Katayama, M.; Higashimine, K.; Ebitani, K., The role of negatively charged Au states in aerobic oxidation of alcohols over hydrotalcite supported AuPd nanoclusters. *Catalysis Science & Technology* **2013,** *3* (2), 351-359.

134. Nagy, G.; Gál, T.; Srankó, D. F.; Sáfrán, G.; Maróti, B.; Sajó, I. E.; Schmidt, F. P.; Beck, A., Selective aerobic oxidation of benzyl alcohol on alumina supported Au-Ru and Au-Ir catalysts. *Molecular Catalysis* **2020,** *492*, 110917.

135. Al Soubaihi, R. M.; Saoud, K. M.; Dutta, J., Critical review of low-temperature CO oxidation and hysteresis phenomenon on heterogeneous catalysts. *Catalysts* **2018,** *8* (12), 660.

136. Freund, H. J.; Meijer, G.; Scheffler, M.; Schlögl, R.; Wolf, M., CO oxidation as a prototypical reaction for heterogeneous processes. *Angewandte Chemie International Edition* **2011,** *50* (43), 10064-10094.

137. Wang, Y.-G.; Cantu, D. C.; Lee, M.-S.; Li, J.; Glezakou, V.-A.; Rousseau, R., CO Oxidation on Au/TiO2: Condition-Dependent Active Sites and Mechanistic Pathways. *Journal of the American Chemical Society* **2016,** *138* (33), 10467-10476.

138. Casaletto, M. P.; Longo, A.; Venezia, A. M.; Martorana, A.; Prestianni, A., Metal-support and preparation influence on the structural and electronic properties of gold catalysts. *Applied Catalysis A: General* **2006,** *302* (2), 309-316.

139. Al Soubaihi, R. M.; Saoud, K. M.; Awadallah-F, A.; Elkhatat, A. M.; Al-Muhtaseb, S. A.; Dutta, J., Investigation of palladium catalysts in mesoporous silica support for CO oxidation and CO2 adsorption. *Heliyon* **2023,** *9* (7).

140. Li, H.; Yu, K.; Wan, C.; Zhu, J.; Li, X.; Tong, S.; Zhao, Y., Comparison of the nickel addition patterns on the catalytic performances of LaCoO3 for low-temperature CO oxidation. *Catalysis Today* **2017,** *281*, 534-541.

141. Cao, S.; Tao, F.; Tang, Y.; Li, Y.; Yu, J., Size- and shape-dependent catalytic performances of oxidation and reduction reactions on nanocatalysts. *Chemical Society Reviews* **2016,** *45* (17), 4747-4765.

142.    Gong, X.; Liu, B.; Kang, B.; Xu, G.; Wang, Q.; Jia, C.; Zhang, J., Boosting Cu-Ce interaction in CuxO/CeO2 nanocube catalysts for enhanced catalytic performance of preferential oxidation of CO in H2-rich gases. *Molecular Catalysis* **2017,** *436*, 90-99.

143.    Dey, S.; Mehta, N. S., Oxidation of carbon monoxide over various nickel oxide catalysts in different conditions: A review. *Chemical Engineering Journal Advances* **2020,** *1*, 100008.

144.    Dey, S.; Sun, S.; Mehta, N. S., Carbon monoxide catalytic oxidation over various iron-based nanoparticles at ambient conditions: A Review. *Carbon Capture Science & Technology* **2021,** *1*, 100013.

145.    Soliman, N. K., Factors affecting CO oxidation reaction over nanosized materials: A review. *Journal of Materials Research and Technology* **2019,** *8* (2), 2395-2407.

146.    Hutchings, G., New directions in gold catalysis. *Gold Bull.* **2004,** *37*, 3-11.

147.    Gaya, N. A.; Charles, V.; Joseph, I.; Louis, H., A review on CO oxidation, methanol synthesis, and propylene epoxidation over supported gold catalysts. **2019,** *6* (1), 13-37.

148.    Centeno, M. A.; Ramírez Reina, T.; Ivanova, S.; Laguna, O. H.; Odriozola, J. A. Au/CeO2 Catalysts: Structure and CO Oxidation Activity *Catalysts* [Online], 2016.

149.    Kozlov, A. I.; Kozlova, A. P.; Liu, H.; Iwasawa, Y., A new approach to active supported Au catalysts. *Applied Catalysis A: General* **1999,** *182* (1), 9-28.

150.    Zhang, L.; Kim, H. Y.; Henkelman, G., CO Oxidation at the Au–Cu Interface of Bimetallic Nanoclusters Supported on CeO2(111). *The Journal of Physical Chemistry Letters* **2013,** *4* (17), 2943-2947.

151.    Yen, C.-W.; Lin, M.-L.; Wang, A.; Chen, S.-A.; Chen, J.-M.; Mou, C.-Y., CO Oxidation Catalyzed by Au−Ag Bimetallic Nanoparticles Supported in Mesoporous Silica. *The Journal of Physical Chemistry C* **2009,** *113* (41), 17831-17839.

152.    Kirichenko, O. A.; Redina, E. A.; Davshan, N. A.; Mishin, I. V.; Kapustin, G. I.; Brueva, T. R.; Kustov, L. M.; Li, W.; Kim, C. H., Preparation of alumina-supported gold-ruthenium bimetallic catalysts by redox reactions and their activity in preferential CO oxidation. *Applied Catalysis B: Environmental* **2013,** *134-135*, 123-129.

153.    Venezia, A.; Liotta, L.; Pantaleo, G.; La Parola, V.; Deganello, G.; Beck, A.; Koppány, Z.; Frey, K.; Horvath, D.; Guczi, L., Activity of SiO2 supported gold-palladium catalysts in CO oxidation. *Applied Catalysis A: General* **2003,** *251* (2), 359-368.

154.    Wang, A.-Q.; Liu, J.-H.; Lin, S.; Lin, T.-S.; Mou, C.-Y., A novel efficient Au–Ag alloy catalyst system: preparation, activity, and characterization. *Journal of Catalysis* **2005,** *233* (1), 186-197.

155.    Liu, X.; Wang, A.; Zhang, T.; Su, D.-S.; Mou, C.-Y., Au–Cu alloy nanoparticles supported on silica gel as catalyst for CO oxidation: Effects of Au/Cu ratios. *Catalysis Today* **2011,** *160* (1), 103-108.

156.    Bernardotto, G.; Menegazzo, F.; Pinna, F.; Signoretto, M.; Cruciani, G.; Strukul, G., New Pd–Pt and Pd–Au catalysts for an efficient synthesis of H2O2 from H2 and O2 under very mild conditions. *Applied Catalysis A: General* **2009,** *358* (2), 129-135.

157.    Han, Y.-F.; Zhong, Z.; Ramesh, K.; Chen, F.; Chen, L.; White, T.; Tay, Q.; Yaakub, S. N.; Wang, Z., Au Promotional Effects on the Synthesis of H2O2 Directly from H2 and O2 on Supported Pd−Au Alloy Catalysts. *The Journal of Physical Chemistry C* **2007,** *111* (24), 8410-8413.

158. Pang, X.; Skillen, N.; Bahnemann, D. W.; Rooney, D. W.; Robertson, P. K. J., Photocatalytic $H_2O_2$ Generation Using Au-Ag Bimetallic Alloy Nanoparticles loaded on ZnO. *Catalysts* **2022,** *12* (9), 939.

159. García, T.; Agouram, S.; Dejoz, A.; Sánchez-Royo, J. F.; Torrente-Murciano, L.; Solsona, B., Enhanced $H_2O_2$ production over Au-rich bimetallic Au–Pd nanoparticles on ordered mesoporous carbons. *Catalysis Today* **2015,** *248*, 48-57.

160. Burch, R.; Ellis, P. R., An investigation of alternative catalytic approaches for the direct synthesis of hydrogen peroxide from hydrogen and oxygen. *Applied Catalysis B: Environmental* **2003,** *42* (2), 203-211.

161. Samanta, C.; Choudhary, V. R., Direct formation of $H_2O_2$ from $H_2$ and $O_2$ and decomposition/hydrogenation of $H_2O_2$ in aqueous acidic reaction medium over halide-containing $Pd/SiO_2$ catalytic system. *Catalysis Communications* **2007,** *8* (12), 2222-2228.

162. Edwards, J. K.; Freakley, S. J.; Carley, A. F.; Kiely, C. J.; Hutchings, G. J., Strategies for Designing Supported Gold–Palladium Bimetallic Catalysts for the Direct Synthesis of Hydrogen Peroxide. *Accounts of Chemical Research* **2014,** *47* (3), 845-854.

163. Gudarzi, D.; Ratchananusorn, W.; Turunen, I.; Heinonen, M.; Salmi, T., Promotional effects of Au in Pd–Au bimetallic catalysts supported on activated carbon cloth (ACC) for direct synthesis of $H_2O_2$ from $H_2$ and $O_2$. *Catalysis Today* **2015,** *248*, 58-68.

164. Sahin, O. G., Microwave-assisted synthesis of PtAu@C based bimetallic nanocatalysts for non-enzymatic H2O2 sensor. *Electrochimica Acta* **2015,** *180*, 873-878.

165. Landon, P.; Collier, P. J.; Carley, A. F.; Chadwick, D.; Papworth, A. J.; Burrows, A.; Kiely, C. J.; Hutchings, G. J., Direct synthesis of hydrogen peroxide from H2 and O2 using Pd and Au catalysts. *Physical Chemistry Chemical Physics* **2003,** *5* (9), 1917-1923.

166. Han, G.-H.; Kim, K.; Nam, H.; Kim, H.; Yoon, J.; Lee, J.-H.; Kim, H.-K.; Ahn, J.-P.; Lee, S.; Lee, K.-Y.; Yu, T., Facile Direct Seed-Mediated Growth of AuPt Bimetallic Shell on the Surface of Pd Nanocubes and Application for Direct H2O2 Synthesis. *Catalysts* **2020,** *10*, 650.

167. Song, Y.; Mobley, J. K.; Motagamwala, A. H.; Isaacs, M.; Dumesic, J. A.; Ralph, J.; Lee, A. F.; Wilson, K.; Crocker, M., Gold-catalyzed conversion of lignin to low molecular weight aromatics. *Chemical Science* **2018,** *9* (42), 8127-8133.

168. Song, Y., Oxidative Depolymerization of Lignin to Low Molecular Weight Aromatics. PhD. Thesis, University of Kentucky**, 2019.**

169. Mobley, J.; Crocker, M., Catalytic oxidation of alcohols to carbonyl compounds over hydrotalcite and hydrotalcite-supported catalysts. *Rsc Advances* **2015,** *5* (81), 65780-65797.

170. Sun, Y.; Yun, R.; Zang, Y.; Pu, M.; Xiang, X., Highly Efficient Lithium Recovery from Pre-Synthesized Chlorine-Ion-Intercalated LiAl-Layered Double Hydroxides via a Mild Solution Chemistry Process. *Materials* **2019,** *12* (12), 1968.

171. Olmos Carreño, C.; Chinchilla, L.; Delgado, J.; Hungria, A.; Blanco, G.; Calvino, J. J.; Chen, X., CO Oxidation over Bimetallic Au–Pd Supported on Ceria–Zirconia Catalysts: Effects of Oxidation Temperature and Au:Pd Molar Ratio. *Catalysis Letters* **2016,** *146*.

172. Tanner, R.; Enache, D.; Wells, R. P. K.; Kelly, G.; Casci, J.; Hutchings, G. J., Comments on the use of 2-methylbut-3-yn-2-ol decomposition as a probe reaction for the

potential reactivity Mg–Al hydrotalcites as base catalysts. *Catalysis Letters* **2005,** *100* (3), 259-265.

173.    Wang, D.; Villa, A.; Spontoni, P.; Su, D. S.; Prati, L., In situ formation of Au-Pd bimetallic active sites promoting the physically mixed monometallic catalysts in the liquid-phase oxidation of alcohols. *Chemistry* **2010,** *16 33*, 10007-13.

174.    Yin, Z.; Chi, M.; Zhu, Q.; Ma, D.; Sun, J.; Bao, X., Supported bimetallic PdAu nanoparticles with superior electrocatalytic activity towards methanol oxidation. *Journal of Materials Chemistry A* **2013,** *1* (32), 9157-9163.

175.    Gao, F.; Wang, Y.; Goodman, D. W., CO Oxidation over AuPd(100) from Ultrahigh Vacuum to Near-Atmospheric Pressures: The Critical Role of Contiguous Pd Atoms. *Journal of the American Chemical Society* **2009,** *131* (16), 5734-5735.

176.    Rucinska, E.; Pattisson, S.; Miedziak, P. J.; Brett, G. L.; Morgan, D. J.; Sankar, M.; Hutchings, G. J., Cinnamyl Alcohol Oxidation Using Supported Bimetallic Au–Pd Nanoparticles: An Optimization of Metal Ratio and Investigation of the Deactivation Mechanism Under Autoxidation Conditions. *Topics in Catalysis* **2020,** *63* (1), 99-112.

177.    Shumaker, J. L.; Crofcheck, C.; Tackett, S. A.; Santillan-Jimenez, E.; Morgan, T.; Ji, Y.; Crocker, M.; Toops, T. J., Biodiesel synthesis using calcined layered double hydroxide catalysts. *Applied Catalysis B: Environmental* **2008,** *82* (1), 120-130.

178.    Sissoko, I.; Iyagba, E. T.; Sahai, R.; Biloen, P., Anion intercalation and exchange in Al(OH)3-derived compounds. *Journal of Solid State Chemistry* **1985,** *60* (3), 283-288.

179.    Gao, H.; Cao, R.; Xu, X.; Xue, J.; Zhang, S.; Hayat, T.; Alharbi, N. S.; Li, J., Surface Area- and Structure-Dependent Effects of LDH for Highly Efficient Dye Removal. *ACS Sustainable Chemistry & Engineering* **2019,** *7* (1), 905-915.

180.    Valden, M.; Lai, X.; Goodman, D., Onset of Catalytic Activity of Gold Clusters on Titania With the Appearance of Nonmetallic Properties. *Science (New York, N.Y.)* **1998,** *281*, 1647-50.

181.    Wang, S.; Yin, S.; Chen, G.; Li, L.; Zhang, H., Nearly atomic precise gold nanoclusters on nickel-based layered double hydroxides for extraordinarily efficient aerobic oxidation of alcohols. *Catalysis Science & Technology* **2016,** *6* (12), 4090-4104.

182.    Wang, L.; Zhang, J.; Meng, X.; Zheng, D.; Xiao, F.-S., Superior catalytic properties in aerobic oxidation of alcohols over Au nanoparticles supported on layered double hydroxide. *Catalysis Today* **2011,** *175* (1), 404-410.

183.    Tsunoyama, H.; Ichikuni, N.; Sakurai, H.; Tsukuda, T., Effect of Electronic Structures of Au Clusters Stabilized by Poly(N-vinyl-2-pyrrolidone) on Aerobic Oxidation Catalysis. *Journal of the American Chemical Society* **2009,** *131* (20), 7086-7093.

184.    Wu, P.; Cao, Y.; Zhao, L.; Wang, Y.; He, Z.; Xing, W.; Bai, P.; Mintova, S.; Yan, Z., Formation of PdO on Au–Pd bimetallic catalysts and the effect on benzyl alcohol oxidation. *Journal of Catalysis* **2019,** *375*, 32-43.

185.    Thøgersen, A.; Mayandi, J.; Vines, L.; Sunding, M. F.; Olsen, A.; Diplas, S.; Mitome, M.; Bando, Y., Composition and structure of Pd nanoclusters in SiO x thin film. *Journal of Applied Physics* **2011,** *109* (8), 084329.

186.    Viswanathan, B. K., K R ; Saranya, A ; vivakandhan, G ; Thinauvkkarasu, K, Studies on palladium based bimetallic catalysts-Pd-M/TiO2 (M=Cu, Ag & Au): I-Selective hydrogenation of 1-heptyne. *Indian Journal of Chemistry* **2019,** *58* (2), 271-280.

187.    Yi, C. W.; Luo, K.; Wei, T.; Goodman, D. W., The Composition and Structure of Pd−Au Surfaces. *The Journal of Physical Chemistry B* **2005,** *109* (39), 18535-18540.

188.    Krivetskiy, V.; Zamanskiy, K.; Beltyukov, A.; Asachenko, A.; Topchiy, M.; Nechaev, M.; Garshev, A.; Krotova, A.; Filatova, D.; Maslakov, K.; Rumyantseva, M.; Gaskov, A., Effect of AuPd Bimetal Sensitization on Gas Sensing Performance of Nanocrystalline SnO(2) Obtained by Single Step Flame Spray Pyrolysis. *Nanomaterials (Basel)* **2019,** *9* (5), 728.

189.    Gao, F.; Goodman, D. W., Pd–Au bimetallic catalysts: understanding alloy effects from planar models and (supported) nanoparticles. *Chemical Society Reviews* **2012,** *41* (24), 8009-8020.

190.    Fang, W.; Chen, J.; Zhang, Q.; Deng, W.; Wang, Y., Hydrotalcite-supported gold catalyst for the oxidant-free dehydrogenation of benzyl alcohol: studies on support and gold size effects. *Chemistry–A European Journal* **2011,** *17* (4), 1247-1256.

191.    Chen, T.; Zhang, F.; Zhu, Y., Pd Nanoparticles on Layered Double Hydroxide as Efficient Catalysts for Solvent-Free Oxidation of Benzyl Alcohol Using Molecular Oxygen: Effect of Support Basic Properties. *Catalysis Letters* **2013,** *143* (2), 206-218.

192.    Yoon, B.; Häkkinen, H.; Landman, U.; Wörz, A. S.; Antonietti, J. M.; Abbet, S. p.; Judai, K.; Heiz, U., Charging Effects on Bonding and Catalyzed Oxidation of CO on Au8 Clusters on MgO. *Science* **2005,** *307*, 403 - 407.

193.    Yoon, B.; Häkkinen, H.; Landman, U., Interaction of O2 with Gold Clusters: Molecular and Dissociative Adsorption. *The Journal of Physical Chemistry A* **2003,** *107* (20), 4066-4071.

194.    Jia, Y.; Chen, H., Enhanced Selective Production of Carbonyl Products for Aerobic Oxidation of Benzylic Alcohols over Mesoporous Fe2O3 Supported Gold Nanoparticles. *Catalysts* **2019,** *9*, 754.

195.    Saleem, M., Possibility of utilizing agriculture biomass as a renewable and sustainable future energy source. *Heliyon* **2022,** *8* (2), e08905.

196.    Zeng, Y.; Himmel, M. E.; Ding, S.-Y., Visualizing chemical functionality in plant cell walls. *Biotechnol Biofuels* **2017,** *10*, 263-263.

197.    DeMartini, J. D.; Pattathil, S.; Miller, J. S.; Li, H.; Hahn, M. G.; Wyman, C. E., Investigating plant cell wall components that affect biomass recalcitrance in poplar and switchgrass. *Energy & Environmental Science* **2013,** *6* (3), 898-909.

198.    Karagoz, P.; Khiawjan, S.; Marques, M. P. C.; Santzouk, S.; Bugg, T. D. H.; Lye, G. J., Pharmaceutical applications of lignin-derived chemicals and lignin-based materials: linking lignin source and processing with clinical indication. *Biomass Conversion and Biorefinery* **2023**.

199.    Bampidis, V.; Azimonti, G.; Bastos, M. d. L.; Christensen, H.; Dusemund, B.; Kouba, M.; Kos Durjava, M.; López-Alonso, M.; López Puente, S.; Marcon, F.; Mayo, B.; Pechová, A.; Petkova, M.; Ramos, F.; Sanz, Y.; Villa, R. E.; Woutersen, R.; Aquilina, G.; Bories, G.; Gropp, J.; Nebbia, C.; Finizio, A.; Focks, A.; Teodorovic, I.; Innocenti, M. L.; Tarrés-Call, J., Safety of lignosulphonate for all animal species. *EFSA journal* **2020,** *18* (2), n/a.

200.    Ekielski, A.; Mishra, P. K., Lignin for Bioeconomy: The Present and Future Role of Technical Lignin. *International journal of molecular sciences* **2020,** *22* (1), 63.

201.    Kärkäs, M. D.; Bosque, I.; Matsuura, B. S.; Stephenson, C. R. J., Photocatalytic Oxidation of Lignin Model Systems by Merging Visible-Light Photoredox and Palladium Catalysis. *Organic Letters* **2016,** *18* (19), 5166-5169.

202.    Davis, K.; Rover, M.; Brown, R.; Bai, X.; Wen, Z.; Jarboe, L., Recovery and Utilization of Lignin Monomers as Part of the Biorefinery Approach. *Energies* **2016,** *9* (10), 808.

203.    Davis, R.; Tao, L.; Tan, E. C. D.; Biddy, M.; Beckham, G. T.; Scarlata, C. J.; Jacobson, J. J.; Cafferty, K. G.; Ross, J. A.; Lukas, J. C.; Knorr, D.; Schoen, P. In *Process Design and Economics for the Conversion of Lignocellulosic Biomass to Hydrocarbons: Dilute-Acid and Enzymatic Deconstruction of Biomass to Sugars and Biological Conversion of Sugars to Hydrocarbons*, 2013.

204.    Kautto, J.; Realff, M.; Ragauskas, A.; Kässi, T., Economic Analysis of an Organosolv Process for Bioethanol Production. *Bioresources* **2014,** *9*, 6041-6072.

205.    Partenheimer, W., The Aerobic Oxidative Cleavage of Lignin to Produce Hydroxyaromatic Benzaldehydes and Carboxylic Acids via Metal/Bromide Catalysts in Acetic Acid/Water Mixtures. *Advanced Synthesis & Catalysis* **2009,** *342* (8), 456-466.

206.    Luterbacher, J. S.; Azarpira, A.; Motagamwala, A. H.; Lu, F.; Ralph, J.; Dumesic, J. A., Lignin monomer production integrated into the γ-valerolactone sugar platform. *Energy & Environmental Science* **2015,** *8* (9), 2657-2663.

207.    Yoo, C. G.; Ragauskas, A. J., Opportunities and Challenges of Lignin Utilization. In *Lignin Utilization Strategies: From Processing to Applications*, American Chemical Society: 2021; Vol. 1377, pp 1-12.

208.    Zakzeski, J.; Jongerius, A.; Bruijnincx, P.; Weckhuysen, B., Catalytic Lignin Valorization Process for the Production of Aromatic Chemicals and Hydrogen. *ChemSusChem* **2012,** *5*, 1602-9.

209.    Yoo, C. G.; Ragauskas, A., Opportunities and Challenges of Lignin Utilization. 2021; pp 1-12.

210.    Kärkäs, M. D.; Matsuura, B. S.; Monos, T. M.; Magallanes, G.; Stephenson, C. R. J., Transition-metal catalyzed valorization of lignin: the key to a sustainable carbon-neutral future. *Organic & Biomolecular Chemistry* **2016,** *14* (6), 1853-1914.

211.    Grinshpan, D.; Savitskaya, T.; Tsygankova, N.; Makarevich, S.; Kimlenka, I.; Ivashkevich, O., Good real world example of wood-based sustainable chemistry. *Sustainable Chemistry and Pharmacy* **2017,** *5*, 1-13.

212.    Kleinert, M.; Barth, T., Phenols from lignin. *Chemical Engineering & Technology: Industrial Chemistry-Plant Equipment-Process Engineering-Biotechnology* **2008,** *31* (5), 736-745.

213.    Bajwa, D. S.; Pourhashem, G.; Ullah, A. H.; Bajwa, S. G., A concise review of current lignin production, applications, products and their environmental impact. *Industrial Crops and Products* **2019,** *139*, 111526.

214.    Nguyen, L. T.; Phan, D.-P.; Sarwar, A.; Tran, M. H.; Lee, O. K.; Lee, E. Y., Valorization of industrial lignin to value-added chemicals by chemical depolymerization and biological conversion. *Industrial Crops and Products* **2021,** *161*, 113219.

215.    Abdelaziz, O. Y.; Clemmensen, I.; Meier, S.; Costa, C. A. E.; Rodrigues, A. E.; Hulteberg, C. P.; Riisager, A., On the Oxidative Valorization of Lignin to High-Value Chemicals : A Critical Review of Opportunities and Challenges. *ChemSusChem* **2022,** *15* (20).

216.    Zhang, Y.; Huo, F.; Wang, Y.; Xia, Y.; Tan, X.; Zhang, S.; He, H., Theoretical Elucidation of β-O-4 Bond Cleavage of Lignin Model Compound Promoted by Sulfonic Acid-Functionalized Ionic Liquid. *Frontiers in Chemistry* **2019,** *7*, 78.

217.    Lu, F.; Ralph, J., Novel tetrahydrofuran structures derived from β–β-coupling reactions involving sinapyl acetate in Kenaf lignins. *Organic & Biomolecular Chemistry* **2008,** *6* (20), 3681-3694.

218.    G. Calvo-Flores, F.; Dobado, J., Lignin as Renewable Raw Material. *ChemSusChem* **2010,** *3*, 1227-35.

219.    Agarwal, A.;  Rana, M.; Park, J.-H., Advancement in technologies for the depolymerization of lignin. *Fuel Processing Technology* **2018,** *181*, 115-132.

220.    Zhang, Y.; Huo, F.; Wang, Y.; Xia, Y.; Tan, X.; Zhang, S.; He, H., Theoretical Elucidation of β-O-4 Bond Cleavage of Lignin Model Compound Promoted by Sulfonic Acid-Functionalized Ionic Liquid. *Frontiers in Chemistry* **2019,** *7*.

221.    Cui, F.; Dolphin, D., The biomimetic oxidation of β-1, β-0-4, β-5, and biphenyl lignin model compounds by synthetic iron porphyrins. *Bioorganic & Medicinal Chemistry* **1994,** *2* (7), 735-742.

222.    Lancefield, C. S.; Westwood, N. J., The synthesis and analysis of advanced lignin model polymers. *Green Chemistry* **2015,** *17* (11), 4980-4990.

223.    Song, Q.;  Cai, J.;  Zhang, J.;  Yu, W.;  Wang, F.; Xu, J., Hydrogenation and cleavage of the C-O bonds in the lignin model compound phenethyl phenyl ether over a nickel-based catalyst. *Chinese Journal of Catalysis* **2013,** *34* (4), 651-658.

224.    Roelofs, J. C. A. A.;  Lensveld, D. J.;  van Dillen, A. J.; de Jong, K. P., On the Structure of Activated Hydrotalcites as Solid Base Catalysts for Liquid-Phase Aldol Condensation. *Journal of Catalysis* **2001,** *203* (1), 184-191.

225.    Scimmi, C.;  Sancineto, L.;  Drabowicz, J.; Santi, C., New Insights into Green Protocols for Oxidative Depolymerization of Lignin and Lignin Model Compounds. *International Journal of Molecular Sciences* **2022,** *23* (8), 4378.

226.    Cui, T.;  Ma, L.;  Wang, S.;  Ye, C.;  Liang, X.;  Zhang, Z.;  Meng, G.;  Zheng, L.; Hu, H.-S.;  Zhang, J.;  Duan, H.;  Wang, D.; Li, Y., Atomically Dispersed Pt–N3C1 Sites Enabling Efficient and Selective Electrocatalytic C–C Bond Cleavage in Lignin Models under Ambient Conditions. *Journal of the American Chemical Society* **2021,** *143* (25), 9429-9439.

227.    Subbotina, E.;  Rukkijakan, T.;  Marquez-Medina, M. D.;  Yu, X.;  Johnsson, M.; Samec, J. S. M., Oxidative cleavage of C–C bonds in lignin. *Nature Chemistry* **2021,** *13* (11), 1118-1125.

228.    Guadix-Montero, S.; Sankar, M., Review on Catalytic Cleavage of C–C Inter-unit Linkages in Lignin Model Compounds: Towards Lignin Depolymerisation. *Topics in Catalysis* **2018,** *61* (3), 183-198.

229.    Liao, Y.;  Koelewijn, S.-F.;  Van den Bossche, G.;  Van Aelst, J.;  Van den Bosch, S.;  Renders, T.;  Navare, K.;  Nicolaï, T.;  Van Aelst, K.; Maesen, M., A sustainable wood biorefinery for low–carbon footprint chemicals production. *Science* **2020,** *367* (6484), 1385-1390.

230.    Wang, L.;  He, M.;  Liu, X.;  Zhai, L.;  Niu, L.;  Xue, Z.; Wu, H., t-BuOK promoted C–C bond oxidative cleavage of β-O-4 and β-1 lignin models to benzoic acids at room temperature. *Green Chemistry* **2023,** *25* (2), 550-553.

231.    Tran, F.;  Lancefield, C. S.;  Kamer, P. C. J.;  Lebl, T.; Westwood, N. J., Selective modification of the β–β linkage in DDQ-treated Kraft lignin analysed by 2D NMR spectroscopy. *Green Chemistry* **2015,** *17* (1), 244-249.

232.   Bukhtiyarov, A. V.;  Prosvirin, I. P.;  Saraev, A. A.;  Klyushin, A. Y.;  Knop-Gericke, A.; Bukhtiyarov, V. I., In situ formation of the active sites in Pd–Au bimetallic nanocatalysts for CO oxidation: NAP (near ambient pressure) XPS and MS study. *Faraday Discussions* **2018,** *208* (0), 255-268.

233.   Melián-Cabrera, I., Catalytic Materials: Concepts to Understand the Pathway to Implementation. *Industrial & Engineering Chemistry Research* **2021,** *60* (51), 18545-18559.

234.   Sandoval, A.;  Louis, C.; Zanella, R., Improved activity and stability in CO oxidation of bimetallic Au–Cu/TiO2 catalysts prepared by deposition–precipitation with urea. *Applied Catalysis B: Environmental* **2013,** *140-141*, 363-377.

235.   Wang, A.-Q.;  Chang, C.-M.; Mou, C.-Y., Evolution of Catalytic Activity of Au−Ag Bimetallic Nanoparticles on Mesoporous Support for CO Oxidation. *The Journal of Physical Chemistry B* **2005,** *109* (40), 18860-18867.

**Educational:**

| | |
|---|---|
| BSc: Chemistry, Botany, Zoology | 2013 |
| University of Ruhuna, Matara | Sri Lanka |
| | |
| MSc: Industrial Analytical Chemistry | 2017 |
| University of Sri Jayewardenepura, Nugegoda | Sri Lanka |

**Scholastic and professional honors:**

| | |
|---|---|
| Outstanding teaching assistant award | 2023 |
| | |
| Research challenge trust fund (RCTF) fellowship | Summer 2020 to Summer 2021 |
| | |
| Outstanding Oral Qualifier Award | 2020 |

**Professional publications:**

Karunasinghe, G.; Qian, D.; Crocker, M.; Meier, M.; Michela, M. Development of an effective Au:Pd bimetallic heterogeneous catalyst for oxidative lignin depolymerization to low molecular weight aromatics – In progress

Karunasinghe, G.; Qian, D.; Crocker, M.; Meier, M. Aerobic Oxidation of β-O-4, β-1, β-5 and β-β Lignin Model Compounds with an Au-Pd bimetallic heterogeneous catalyst - In progress.

Gayan Karunasinghe